Spring 2018

Service response and evaluation of prestressed concrete bridges through load testing

Eli Saul Hernandez Ramos

Department: Civil, Architectural and Environmental Engineering

SERVICE RESPONSE AND EVALUATION OF PRESTRESSED CONCRETE BRIDGES THROUGH LOAD TESTING

by

ELI SAUL HERNANDEZ RAMOS

A DISSERTATION

Presented to the Faculty of the Graduate School of the

MISSOURI UNIVERSITY OF SCIENCE AND TECHNOLOGY

In Partial Fulfillment of the Requirements for the Degree

DOCTOR OF PHILOSOPHY

in

CIVIL ENGINEERING

2018

Approved

John J. Myers, Advisor
Roger LaBoube
Mohamed ElGawady
Victor Birman
K. Chandrashekhara

PUBLICATION DISSERTATION OPTION

This dissertation consists of six articles, formatted using the publication option:

Paper I: Pages 12-41, have been accepted and published by the *ACI SP-304, Sustainable Performance of Concrete Bridges and Elements Subjected to Aggressive Environments: Monitoring, Evaluation and Rehabilitation*.

Paper II: Pages 42-69, have been accepted by the *ACI SP-323 Evaluation of Concrete Bridge Behavior Through Load Testing – International Perspective*.

Paper III, Pages 70-97, are intended for submission to the *ASCE Journal of Bridge Engineering*.

Paper IV, Pages 98-114, have been submitted and accepted for publication in the proceeding of the *9th International Conference on Bridge Maintenance, safety and Management (IABMAS 2018)*.

Paper V, Pages 115-140, are intended for submission to the *ASCE Journal of Bridge Engineering*.

Paper VI, Pages 141-176, are intended for submission to the *ASCE Journal of Bridge Engineering*.

ABSTRACT

During the last two decades, self-consolidating concrete (SCC) has emerged as an alternative to produce structures with longer life expectancy. Despite the advantages that come with using SCC, there are some concerns related to its structural and serviceability response. The effect of the larger paste content and smaller coarse aggregate size is of particular interest because this combination may inhibit the development of the SCC's target mechanical properties. Field tests are an effective method to monitor the service response of infrastructure. In addition, field tests have largely confirmed reserves of strength capacity in existing bridges despite their visual condition and age. Sources that explain the difference in the reported strength capacity are diverse and may be attributed to in-situ parameters that are not considered during the design or evaluation of a bridge. This study aimed at presenting an evaluation protocol using experimental data to obtain the load rating of prestressed concrete bridges in Load and Resistance Factor Rating (LRFR) format. The proposed experimental evaluation approach will enable bridge owners to estimate, isolate and remove the unreliable parameters' contribution from a bridge load rating. Bridge A7957 is the first implementation project executed by MoDOT using high-strength and normal-strength SCC in prestressed concrete members. In addition, Bridge A7957 was a unique opportunity to monitor and establish the baseline service response and strength capacity of its main supporting members. The proposed experimental data and evaluation methodology are expected to encourage more discussion among bridge evaluators to better understand and improve current bridge analysis and evaluation practices of prestressed concrete bridges.

ACKNOWLEDGMENTS

I would like to express my sincere and deepest gratitude to my advisor and mentor, Dr. John Myers, for his guidance, encouragement, motivation, and support during the completion of this degree. He has played an important influential role during this time of the greatest accomplishments in my life.

I would like to thank the members of my advisory committee: Dr. Roger LaBoube, Dr. Mohamed ElGawady, Dr. Victor Birman, and Dr. K. Chandrashekhara. Each of you provided a valuable source of technical experience, and advice. that continuously helped me improve my knowledge for the completion of this work.

Funding opportunities from the Missouri S&T Civil Engineering program are gratefully acknowledged. The support received from the Missouri Department of Transportation and the Tier 1 University Transportation Center RECAST at Missouri S&T to complete this research is also gratefully acknowledged. Thanks are due to the Highbay laboratory staff: Gary Abbott, Brian Swift, John Bullock and Greg Lekrone and to the staff from the Department of Civil Engineering, and Center for Infrastructure Engineering Studies (CIES) at Missouri S&T.

I would also like to acknowledge my fellow graduate students in the Civil Engineering Department; especially Hayder, Alexander, Zuhair, Saipavan, Kaylea, Wei, Michael, Zena, Benjamin, Alexis, and Russ for their assistance and friendship. Thanks to my friends in Rolla and back at home for accompanied me during this time.

From the bottom of my heart, I would like to acknowledge and thank my wife, Maria Alejandra, for her love, patience and pleasant company in all my adventures during these years. Finally, I would like to thank my family. Thanks to my parents Gisela y Eli Saul, Mariemma y Nelson, and my siblings Elixandro, Elis David, and Elis Alfredo for their continued support, encouragement, inspiration, and love. Without them, none of this would be possible.

TABLE OF CONTENTS

Page

PAPER

LIST OF ILLUSTRATIONS

Page

PAPER I

PAPER II

PAPER III

PAPER VI

LIST OF TABLES

Page

PAPER I

PAPER II

PAPER III

1. INTRODUCTION

1.1. BACKGROUND

Infrastructure facilities constitute a major part of the national asset. According to the National Bridge Inventory (NBI) database, reported by the Federal Highway Administration (FHWA) at the end of 2015, there are nearly 612,000 bridges. Approximately 9.6% of them (58,791) are structurally deficient and 13.7% of them (84,124) are functionally obsolete (FHWA 2017). In Missouri, there are 24,398 bridges; 13.2% of them (3,222) are considered structural deficient and 12.5% of them (3,059) have been labeled as functionally obsolete. Major decisions must be made to allocate dwindling funds for repairing, rehabilitating, and replacing this deficient or obsolete infrastructure. As infrastructure facilities continue to age and deteriorate, innovative concrete materials have been developed to increase their service life expectancy.

Since the early 1990s, the use of self-consolidating concrete (SCC) has emerged as an alternative to produce more durable and stronger infrastructure due to its inherent properties (Ouchi et al. 2003, Domone 2006, McSaveney et al. 2011, Keske et al. 2014, Hernandez and Myers 2015b). Some of the SCC's attributes include (1) a highly flowable characteristic that permits better consolidation and ease of concrete placement, resulting in fewer voids and honeycombing; (2) a more condensed microstructure that increases the concrete's durability properties; (3) reductions in labor and equipment costs; and (4) decreased maintenance expenses. In addition, high-strength self-consolidating concrete (HS-SCC) has added enhanced flexural performance to normal-strength NS-SCC's attributes as the result of increasing the normal compressive strength available in SCC

mixtures developed in the past two decades. This stronger flexural feature brings the possibility of reducing the number of the main supporting elements and interior supports of bridge superstructures.

Despite the advantages that come with using SCC, there is some reluctance to implement this novel material in highway infrastructure on a large scale due to the lack of test bed applications that may help extrapolate SCC's structural and service performance over the long term (WsDOT 2009). The effect of the larger paste content and the smaller coarse aggregate size utilized in the mixture is of particular interest (Myers et al. 2012). Some researchers have reported a lower expected modulus of elasticity (MOE) and higher prestress losses (e.g., shrinkage and creep) when SCC is used (Khayat and Mitchell 2009, Myers and Bloch 2011). Accordingly, it has been critical to monitor the initial and long-term service behavior, and to evaluate the available strength capacity of full-scale highway infrastructure employing SCC in PC/PS concrete members to validate and thus encourage the implementation of this material in highway projects.

1.2. OBJECTIVE AND SCOPE OF THE WORK

The objective of this research study was threefold: first, to provide an implementation test bed and showcase the use of NS-SCC and HS-SCC in infrastructure projects; second, to present a diagnostic test protocol using robust and reliable measurement devices (including noncontact laser technology) that allow recording the bridge's baseline service response and comparing the SCC versus conventional prestressed concrete girders' response when subjected to service loads; and third, to provide an experimental strength evaluation methodology to monitor changes in the

flexural strength of Bridge A7957's main carrying members during the service life of its structure. The monitoring program provided unique data on the service performance of these materials when exposed to the same field loading and environmental conditions. This evaluation protocol may be updated with in-situ data to estimate a more realistic live load capacity of the prestressed concrete bridge structures. The following scope of work was implemented to attain these goals: (1) literature review; (2) development of the instrumentation and load testing program to be executed in Bridge A7957, object of this study (Papers I and II); (3) experimentally characterization of the mechanical properties of the bridge superstructure elements (Paper I); (4) execution of first series of static and dynamic diagnostic load tests (Papers II, III, IV and VI); (5) development of finite element analysis (FEA) simulations of the bridge structure and static load cases applied during the static tests (Papers II and IV); and (6) development and implementation of the experimental strength evaluation methodology through load testing to establish the main carrying members' baseline flexural strength (Papers V and VI).

1.3. DISSERTATION OUTLINE

This dissertation includes three sections. Section 1 provides a brief introduction to the research topic and presents background information for this study. In addition, the objective and scope of the work, and a detailed literature review that establishes the state-of-the-art on the topic of this study is presented in this section.

Section 2 contains five journal articles and one conference paper that discuss (1) the instrumentation and monitoring program; (2) mechanical characterization of the materials employed in the fabrication of all the bridge's components; (3) details of the

diagnostic load test conducted to obtain the bridge's baseline static and dynamic service response and strength capacity; (4) details on finite element modeling; and (5) proposed systematic experimental evaluation methodology to obtain the load rating capacity of prestressed SCC Bridge A7957.

Section 3 summarizes the work that was accomplished in this dissertation and the key findings of the load testing and strength evaluation implemented on the bridge's superstructure and conducted during the research study.

2. REVIEW OF RELEVANT LITERATURE

Load rating is the strength evaluation procedure employed to estimate the allowable in-service load that a bridge structure can withstand without suffering damage and the maximum load that the structure can carry without undergoing collapse or failure. This evaluation is a major basis in prioritizing maintenance operations, allocating economic resources, and making decisions concerning load posting and permit decisions. Traditionally, bridge evaluation standards (AASHTO 2010) provide two approaches to load rating: analytical calculations and field testing. Analytical ratings are based on simplifying assumptions and may not closely reflect a realistic response of a bridge due to its current physical condition. Conversely, field testing presents a more realistic visualization of the live-load capacity of a bridge because it provides an in-service, as-built characterization of its performance. Field testing permits the verification of design and analysis assumptions such as actual lateral load distribution, dynamic load allowance (impact factor), influence line position, degree of composite action, and unintended support restraint. Although field testing applications may sometimes be hindered by costs, time, test truck requirements, traffic interruptions, safety, difficulty to access a bridge structure, and difficulty to install sensors, it is the most accurate approach. Load testing permits (1) better understanding of the response of bridges fabricated with innovative designs and new construction technologies; (2) evaluation of the response of posted and deteriorated bridges; and (3) evaluation of a bridge's response to permit and nonstandard vehicles (ACI 2016). In general, the American Association of State Highway and Transportation Officials (AASHTO) Manual for Bridge Evaluation (MBE) defines

two different options for load testing: diagnostic load tests and proof load tests (AASHTO 2010). Independent of the method employed to conduct a strength evaluation (analytical or experimental), load rating a bridge structure involves good "engineering judgment" to guarantee that the rating results minimize the economic impacts on the community served by the bridge without sacrificing the public's safety at the same time.

2.1. AASHTO GUIDELINES FOR BRIDGE EVALUATION

Throughout the years, design and evaluation techniques have been proposed by engineers to dispense satisfactory safety margins. The first approaches were based on the engineers' judgment and confidence in the analysis of the load effects and the strength of the materials employed. As analysis and evaluation methods advanced and the quality control for materials was refined, the design procedures were improved. To better understand the differences between current load rating practices, the following discussion presents a summary of AASHTO analytical and experimental guidelines for bridge design and evaluation.

2.1.1. Analytical Load Rating. The AASHTO MBE (AASHTO 2010) is currently consistent with three AASHTO design philosophies, namely allowable stress design (ASD), load factor design (LFD), and load and resistance factor design (LRFD). Three theoretical load rating methods are presented in chronological order as adopted by AASHTO.

2.1.1.1. Allowable stress rating (ASR). The first national highway design specification, which was adopted by AASHTO in 1931, was based on the ASD until the beginning of 1970s. In the AASHTO ASD method, an allowable or admissible stress is

defined as a fraction of the strength capacity of a structural component. The structural effect resulting from the applied loads may not exceed this allowable limit to ensure the structural member safety. Procedures to conduct load rating of existing bridges based on the ASD approach were presented in the AASHTO Manual for Maintenance Inspection of Bridges (AASHTO 1970). The resulting strength evaluation procedure is referred to as the allowable stress rating (ASR).

2.1.1.2. Load factor rating (LFR). At the beginning of the 1970s, as the design of reinforced concrete and steel structures were presented in terms of "ultimate strength" and "plastic design", respectively, the load analysis employed in the AASHTO ASD design specifications was improved. Adjustments were made by adding load factors as an attempt to represent the relative uncertainty in predicting different actions such as vehicle loads and earthquake effects. These specifications also introduced a "capacity reduction" factor to downgrade the theoretical strength of an element to account for uncertainties in the predictability of its capacity. The resulting design and strength evaluation methodologies were referred to as the load factor design (LFD) and load factor rating (LFR), respectively.

In 1994, the LFR approach was included in the Manual for Condition Evaluation of Bridges (AASHTO 1994), which allows strength evaluations to be determined by either ASR or LFR. Both approaches rate bridge components at two levels: operating and inventory. The operating rating level reflects the maximum permissible live load to which a structure may be subjected during a period of time. Conversely, load ratings based on the inventory rating level compare the estimated capacity of an existing bridge with that

of a new bridge. The rating factor of a bridge component in ASR and LFR (AASHTO 1994) is computed by

$$RF = \frac{C - A_1 D}{A_2 L(1 + I)} \quad (1)$$

where RF = rating factor (expressed as a ratio of the design live load effect); C = member capacity; D = dead load effects; $L(1+I)$ = live load and impact factor; and A_1 and A_2 = factors for dead and live load, respectively. In Equation (1), $A_1 = A_2 = 1$ (ASR's operating and inventory levels); $A_1 = 1.3$ (LFR's operating and inventory levels); $A_2 = 1.3$ (LFR's operating level); and $A_2 = 2.16$ (LFR's inventory level).

2.1.1.3. Load and resistance factor rating (LRFR). In 1998, the AASHTO LRFD bridge design specifications were proposed as the primary design method for highway bridges. These specifications represented the first AASTHO effort to integrate modern principles of structural reliability and probabilistic models of loads and resistance into the design of highway bridges. In addition, these specifications introduced reliability-based limit states concepts into the design philosophy through the use of calibrated load and resistance factors that satisfy uniform safety levels corresponding to each limit state. The approach was extended to the evaluation of bridges with the completion of the Manual for Condition Evaluation and Load and Resistance Factor Rating (LRFR) of Highway Bridges (MCE) published in 2003 (AASHTO 2003). The MCE is the first bridge strength evaluation approach in the United States presenting a structural reliability format (LRFR). A more recent update of the LRFR procedure is found in the AASHTO Manual for Bridge Evaluation (MBE) updated in 2010 (AASHTO

2010). The rating factor of a bridge component in the LRFR approach is obtained (Minervino et al. 2004, AASHTO 2010) by

$$RF = \frac{C - \gamma_{DC} DC - \gamma_{DW} DW \pm \gamma_P P}{\gamma_L LL(1 + IM)} \quad (2)$$

where RF = rating factor; C = capacity = $\varphi\varphi_C\varphi_S R_n \geq 0.85\varphi R_n$ (strength limit states); C = f_R (service limit states); f_R = allowable stress specified in LRFD specifications (Minervino et al. 2004, AASHTO 2012); φ = LRFD resistance factor; φ_C = condition factor; φ_S = system factor; R_n = nominal member resistance; DC = dead load effect due to structural components and attachments; DW = dead load effect due to wearing surface and utilities; P = permanent loads other than dead loads (e.g., post-tensioning); LL = live load effect; IM = dynamic load allowance (impact factor); γ_{DC} = LRFD load factor for structural component and attachments; γ_{DW} = LRFD load factor for wearing surfaces and utilities; γ_P = LRFD load factor for permanent loads other than dead loads; and γ_L = evaluation live load factor.

2.1.2. Experimental Load Rating (Load Rating through Load Testing). Load rating of bridges through load testing includes the observation of a bridge's response measurement when it is subjected to predetermined loadings that do not alter the elastic response of the structure. The principle of load testing is the comparison of the field response of the bridge under test loads with its theoretical performance as predicted by the analysis (TRB 1998). In general, there are two types of nondestructive tests: diagnostic and proof load tests.

2.1.2.1 Diagnostic load tests. Diagnostic load tests use service level loads and are performed to determine certain response characteristics of the bridge (e.g., lateral load distribution, dynamic load allowance, and longitudinal load distribution). After conducting a diagnostic load test, the experimental data is used to modify the bridge's analytical load rating, which reflects a more realistic response of the structure. This is achieved through a simple rating adjustment factor applied to the calculated ratings (AASHTO 2010).

2.1.2.2. Proof load tests. Proof load tests allow verifying the maximum safe load safe load capacity of a bridge. In proof load tests, higher loads are applied to the bridge structure than in diagnostic load tests. The MBE (AASHTO 2010) presents a procedure for determining a target live load factor suitable for a specific bridge. This live load factor is multiplied by the rating vehicle weight (RVW) to determine the test load that must be applied for a valid proof test. The target live load factor accounts for the live load uncertainties that are not evaluated by the test.

2.2. RESEARCH JUSTIFICATION

Currently, the analytical strength evaluation procedures adopted by the AASHTO MBE (AASHTO 2010) tend to be overly conservative due to simplified assumptions made to represent a bridge response. Analytical load ratings underestimate the real bridge response, particularly in the case of PC/PS concrete bridges. Field testing has proven that bridges possess additional strength compared to what analytical methods predict. The most predominant parameters that explain the increment in capacity have been largely investigated (Stallings and Yoo 1993, TRB 1998, Barker 1999, 2001, Cai and Shahawy

2003) and defined as (1) actual lateral live load distribution; (2) actual dynamic load allowance (impact factor); (3) unaccounted section stiffness, such as in curbs and railings; (4) actual longitudinal live load distribution; (5) actual section dimensions; (6) bearing restrain effects; and (7) unintended or additional composite action. A bridge structure response obtained by means of load testing contains a combination of these factors. Contributing factors such as the lateral load distribution or the dynamic load allowance are considered welcome benefits that improve a bridge's load rating and may be relied on during the service life of a bridge. Conversely, factors such as unintended composite action and bearing restraining forces are unreliable because their contribution may not be present when service loads exceed certain levels (TRB 1998, Barker 1999, 2001, Cai and Shahawy 2003). Accordingly, it is critical to provide bridge authorities with an experimental bridge evaluation methodology that enables removing unreliable contributing factors from a strength evaluation conducted by means of load testing.

PAPER

I. USE OF SELF-CONSOLIDATING CONCRETE AND HIGH-VOLUME FLY ASH CONCRETE IN MISSOURI BRIDGE A7957

E.S. Hernandez[1] and J.J. Myers[2]

[1]Ph.D. Candidate of the Civil, Architectural & Environmental Engineering Department, Missouri University of Science and Technology, 205 Pine Building, 1304 N Pine St, Rolla, MO 65409; email: ehd36@mst.edu

[2]Associate Dean, Professor of the Civil, Architectural & Environmental Engineering Department; Missouri University of Science and Technology; 325 Butler-Carlton Hall, 1401 N Pine St., Missouri University of Science and Technology, Rolla, MO 65409; email: jmyers@mst.edu

ABSTRACT

Self-consolidating concrete (SCC), as defined by ACI 237R-07, is a very flowable, non-segregating concrete that can spread into placed, fill the formwork and encapsulate the reinforcement without any mechanical consolidation. SCC, compared to traditional concrete mixtures, has primary benefits that include a reduction in equipment and labor associated costs as well as higher construction effectiveness. Innovative materials such as high volume fly ash concrete (HVFAC), represent a substantial advantage to producing stronger, more durable cast-in-place (CIP) concrete members. A level of 50% fly ash to cement proportion, as well as both normal strength self-consolidating concrete (NS-SCC) and high strength self-consolidating concrete (HS-

SCC), were employed in the implementation project for Missouri Bridge A7957. The objective of this research was to provide an implementation test bed and showcase for the use of these materials. The serviceability and structural performance, both short-term and long-term, of the concrete members within the bridge were monitored in an effort to investigate the in-situ performance of not only SCC but also HVFAC. The initial instrumentation program consisted of obtaining the temperature, strain, and deflection data for the different components within the bridge's structure, from casting through service conditions. The results obtained from this two-year monitoring program will lead to propose certain specification requirements that can be used for future project implementations.

Keywords: Bridge superstructure, extended service life, high-volume fly ash concrete, long-term monitoring, self-consolidating concrete**.**

1. INTRODUCTION

One of the advantages of using high-strength self-consolidating concrete (HS-SCC) is the possibility to place additional mild or prestressing steel within a reinforced concrete (RC) or precast, prestressed (PC/PS) concrete member. This benefit comes with a strength gain that reduces the number of longitudinal members and/or interior supports of a structure in transportation infrastructure. HS-SCC reduces labor and equipment costs, maintenance expenses, and, thus, the overall project costs. Furthermore, the flowable characteristic of SCC produces better consolidation and placement, with fewer voids and honeycombing problems as compared to conventional concrete mixtures (ACI 2007). A more condensed microstructure increases the concrete durability properties,

leading to a longer service life. Despite all these benefits, several concerns are related to HS-SCC's mechanical behavior due to its constituent materials and proportions. Myers et al. (2012) reported that the effect of the larger paste content and the smaller coarse aggregate size employed in the mixture is of particular interest. The effects of using HS-SCC in PC/PS girders must be monitored by examining its response to prestress losses, shear capacity, creep, shrinkage, thermal gradients, mechanical properties development, and serviceability in full-scale infrastructures under varying loads (Myers and Bloch 2010).

High volume fly ash concrete (HVFAC) offers an alternative to typical concrete mixtures, producing stronger, more durable, and, therefore, longer lasting structures. Material specifications have typically restricted the amount of fly ash to 25 or 30 percent of portland cement replacement. Volz et al. (Volz et al. 2012) demonstrated that higher cement replacement percentages, even up to 75 percent, can produce an enhanced concrete in terms of strength and durability. Several limitations and concerns, however, are related to the application of HVFACs in full-scale structures. When the fly ash replacement content is increased, it generally slows down the setting time and hardening rates of concrete at early ages. This is especially important in the presence of cold weather conditions, and when less reactive fly ashes are used.

An instrumentation plan was designed and implemented during the construction stage to investigate the previously mentioned concerns and structural performance, both short-term and long-term, associated with several of the RC and PC/PS members within Bridge A7957. This plan included the monitoring of strains and stress variations at critical locations of selected PC/PS members. In addition, temperature changes of some

PC/PS girders, CIP RC deck, and bents from casting through service life were monitored during the same stage. This project enabled comparing the behavior of the three different concrete mixtures used to fabricate the PC/PS girders. The behavior of the two different concrete mixtures employed in the bents of Bridge A7957 under the same environmental conditions was also compared.

2. RESEARCH SIGNIFICANCE

During the last two decades, self-consolidating concrete (SCC) has grown in use in infrastructure projects around the world because of its primary benefits to produce stronger and longer lasting infrastructure. Similarly, within very recent years, high volume fly ash concrete (HVFAC) has seen its initial transformation from the laboratory to the field. In the United States, important efforts have been made by the Federal Highway Administration (FHWA) and their respective department of Transportation (DOT's) to implement these materials in infrastructure projects. The results presented with this paper are part of an on-going research program whose main objective was to provide an implementation test bed and showcase for the use of SCC, HS-SCC and HVFAC. This stage of the study investigated the in-situ performance of both SCC and HVFAC employed in Missouri Bridge A7957, the first implementation project, built by the Missouri Department of Transportation (MoDOT) using these innovative type of materials. The study also included monitoring the serviceability and structural performance both short-term and long-term of the concrete members of Bridge A7957. The results from this stage of the research are being utilized to establish a load rating of the bridge through diagnostic field load testing.

3. BRIDGE DESCRIPTION

The Missouri Department of Transportation (MoDOT) built Bridge A7957 during the summer and fall of 2013. This bridge, located on Highway 50 in Osage County, Missouri, is a three-span, PC/PS concrete bridge made continuous via a CIP deck (Figures 1 and 2). The PC/PS concrete NU53 girders in each span were designed with concrete mixtures of different compressive strength (Hernandez et al. 2014).

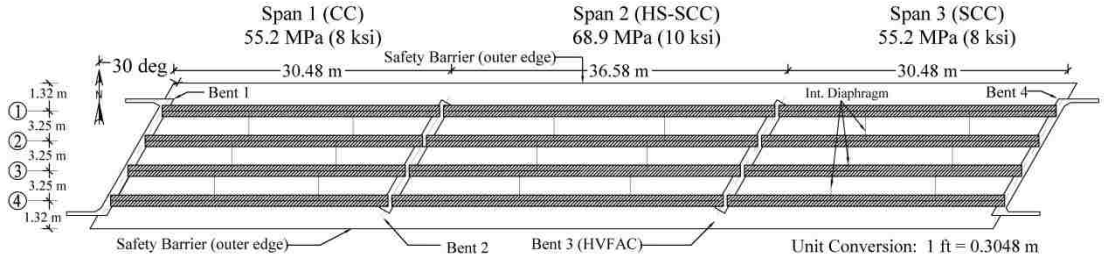

Figure 1. Bridge A7957 plan view.

The first span (between bents 1 and 2) is 30.48 m [100 ft.] long, and the PC/PS girders are comprised of a conventional concrete (CC) mixture designated by MoDOT as Class A-1. The target 28-day compressive strength was 55.2 MPa (8,000 psi), and the specified release strength was 44.8 MPa (6,500 psi). The second span (between bents 2 and 3) is 36.58 m (120 ft.) long. Girders on the second span were fabricated with HS-SCC with a target 28-day compressive strength of 68.9 MPa (10,000 psi) and a release compressive strength of 55.2 MPa (8,000 psi). The third span (between bents 3 and 4) measures 30.48 m (100 ft.) long. It contains girders fabricated with NS-SCC with target 28-day design strength of 55.2 MPa (8,000 psi) and release strength of 44.8 MPa (6,500 psi). The girders of the first and third spans were prestressed with thirty 15 mm (0.6 in.)

diameter Grade 270 low-relaxation prestressing strands of twenty straight strands and ten strands harped at double harping points as shown in Figures 3(a) and 4(a).

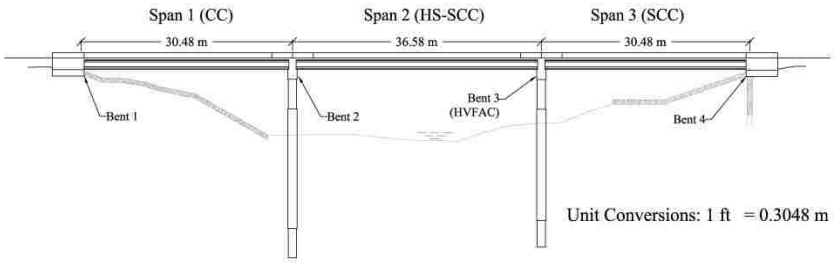

Figure 2. Bridge A7957 elevation.

The girders of the second span were prestressed with the same type of prestressing strands; however, twenty-eight straight strands and tend strands harped at double harping points were used as illustrated in Figures 3(b) and 4(b). Within the top flange of each girder (spans 1 through 3), four additional 9 mm [3/8 in.] diameter prestressing strands were added for crack control.

The mixture proportions employed in the fabrication of the PC/PS girders of each span are listed in Table 1. PC/PS concrete panels, were fabricated of conventional concrete (MoDOT's Class A-1) with a target compressive strength of 41.4 MPa (6,000 psi). These panels extend between the top flanges of the girders in the transverse direction of the bridge and underneath a CIP RC deck (Figure 5). The CIP deck was cast from a conventional concrete mix (MoDOT modified Class B-2) using a 25 % fly ash replacement of portland cement. The target design strength of this concrete mix was 27.6 MPa (4,000 psi).

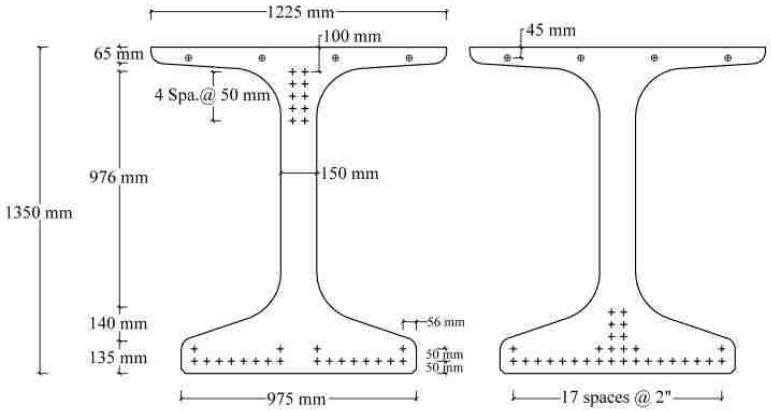

(a) Spans 1 and 3. Note: 1mm = 0.03937in

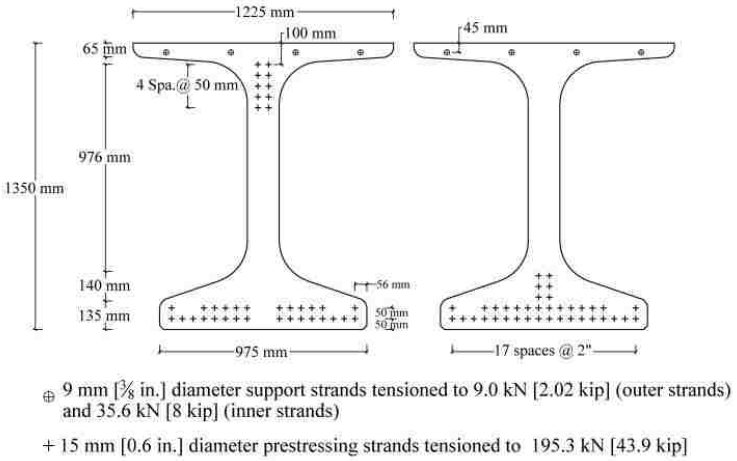

(b) Span 2. Note: 1mm = 0.03937in

Figure 3. NU53 PC/PS girder strand arrangement.

Two intermediate bents and two abutments support the superstructure (Figure 2). Both abutments and intermediate bent 2 were built with a conventional concrete mixture (MoDOT Class B) using a 20% fly ash replacement of portland cement with a design compressive strength of 20.7 MPa (3,000 psi). Intermediate bent 3 was cast from HVFAC with a 50% fly ash replacement of portland cement; it was designed with a specified compressive strength of 20.7 MPa (3,000 psi).

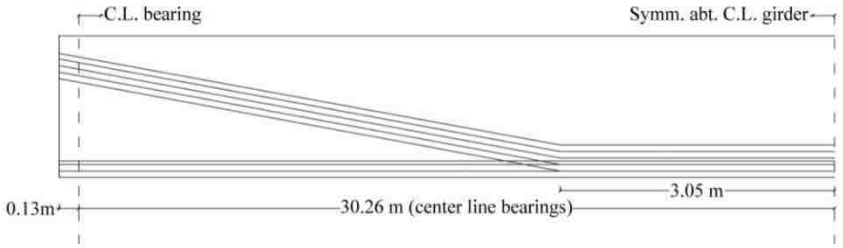

(a) Spans 1 & 3

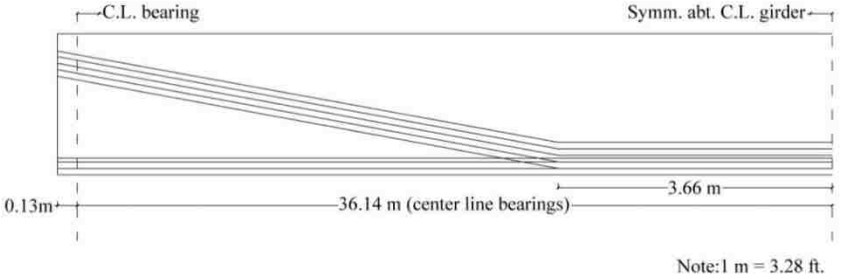

(b) Span 2

Figure 4. Half elevation of PC/PS girders.

Table 1. Summary of PC/PS girders' mixture proportions.

Component	CC (Span 1)	HS-SCC (Span 2)	SCC (Span 3)
Cement, kg/m^3	474.6	504.3	445.0
Water, kg/m^3	151.9	166.1	154.3
Water-cement ratio (w/c)	0.32	0.33	0.35
Coarse aggregate, kg/m^3	1056.0	795.0	875.7
Fine aggregate, kg/m^3	643.7	850.2	850.2
Air-entraining admixture, g/m^3	296.6	630.4	630.4
Type D water-reducing admixture and retardant, g/m^3	341.1	945.5	945.5
Water-reducing admixture, g/m^3	637.8	2836.6	2502.9
Air content (design), percentage	5.5	5.0	5.0

Notes: 1 kg/m^3 = 1.686 lb. / yd^3; 1 g/m^3 = 0.02697 oz./yd^3; 1 m^3 = 1.308 yd^3.

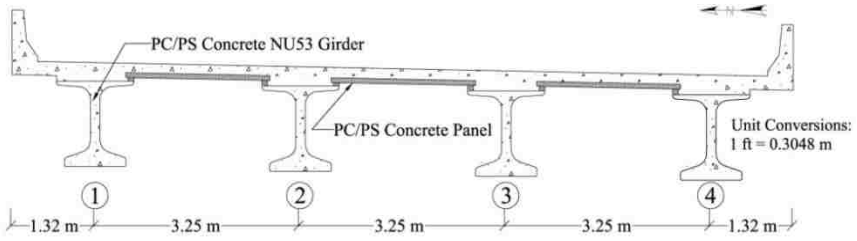

Figure 5. Bridge A7957 cross section.

The mixture proportions employed in the supports and CIP deck of Bridge A7957 are listed in Table 2.

Table 2. Summary of bents and CIP deck's mixture proportions.

Component	Bent 2 (CC)	Bent 3 (HVFAC)	CIP deck
Cement, kg/m^3	252.1	192.8	267.0
Fly ash (Class C), kg/m^3	62.3	192.8	89.0
Water, kg/m^3	147.1	126.4	130.5
Water-cementitious materials ratio (w/cm)	0.47	0.33	0.37
Coarse aggregate, kg/m^3	1091.6	1038.2	1124.3
Fine aggregate, kg/m^3	726.8	736.8	694.1
Air-entraining admixture, g/m^3	222.5	241.0	166.9
Water-reducing admixture, g/m^3	407.9	482.0	445.0
Air content (design), percentage	6.0	6.0	6.0

Notes: 1 kg/m^3 = 1.686 lb. / yd^3; 1 m^3 = 1.308 yd^3; 1 g/m^3 = 0.02697 oz./yd^3.

4. MONITORING PLAN

During the preconstruction of Bridge A7957, structural elements instrumented included: intermediate bents (Figure 6), two PC/PS NU53 girders per span, and two PC/PS panels located at mid-span (Figures 7 and 8). These two instrumented PC/PS panels were set in span 2, between girder lines 2 and 3, and girder lines 3 and 4, respectively.

A high-performance automated total station (ATS) was employed at the precast plant so that the girder's camber could be obtained immediately after the prestressing force was transferred to the PC/PS girders (Figure 9).

The type of sensors employed and details on their installation are described in the following subsections.

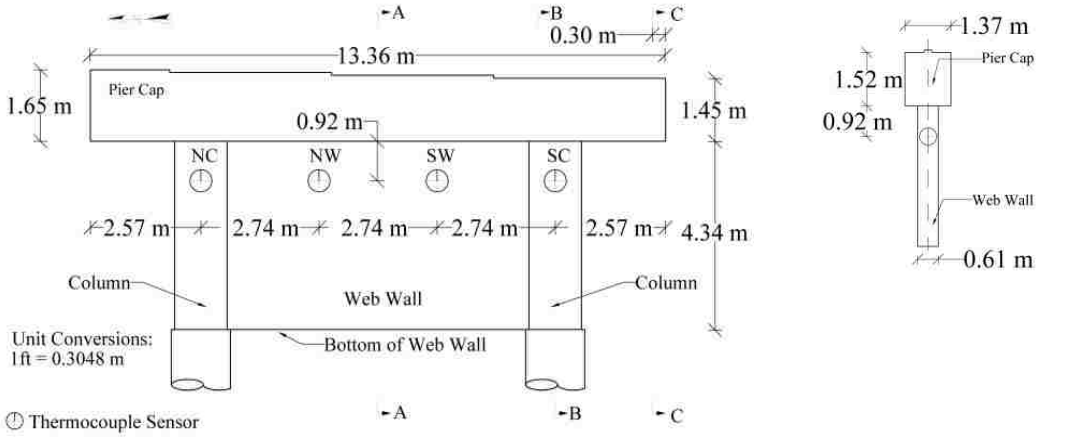

(a) Elevation (b) Section A-A

(c) Section B-B (d) Section C-C

Figure 6. Thermocouple installation details.

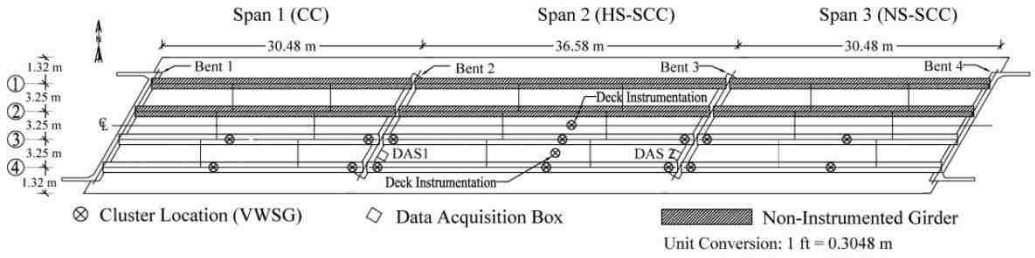

Figure 7. Bridge A7957 instrumentation layout.

4.1. INTERMEDIATE BENTS

Thermocouple sensors were installed within bents 2 and 3 so that the temperature and thermal gradients could be obtained once casting was complete. The bent sections at which these sensors were located are illustrated in Figure 6.

The ambient temperature was measured to adjust for any difference between concrete mixtures under similar exposure conditions. One thermocouple was placed within each bent at the center line of each column 0.92 m (3 ft.), from the bottom edge of the pier cap [sensors NC and SC in Figures 6(a) and 6(c)].

A second set of thermocouples was installed in the web wall, 2.74 m (9 ft.) from the center line of each column [sensors NW and SW in Precast Prestressed Girders in Figures 6(a) and 6 (b)] within the same horizontal plane. One exterior and three interior thermocouples were placed at section C [Figure 6(a)], located 0.30 m [1ft.] from the pier cap's south end according to the detail illustrated in Figure 6(d).

4.2. PRECAST PRESTRESSED GIRDERS

4.2.1. Vibrating Wire Strain Gauges (VWSG). A total of 86 vibrating wire strain gauges (VWSG) with built-in thermistors (type EM-5) were used to monitor the strain and stress variations, as well as temperature changes in the PC/PS girders, and the RC deck from fabrication through service life. A total of 62 VWSGs were installed in all spans within the PC/PS girders of lines 3 and 4 before the casting was begun. The PC/PS girder's cluster locations at which the VWSG were placed are illustrated in Figure 7. Within each girder of span 1 and span 3, the instrumentation clusters were located at two cross-sections. One section was located at mid-span, and the other section was placed at

approximately 0.61 m [2 ft.] from the support centerline of bents 2 and 3. The instrumentation clusters for span 2 were arranged at three different cross-sections: one at the mid-span and two at approximately 0.61 m [2 ft.] from each support centerline. Several details on VWSGs installed at the girders' near-support and mid-span sections before concrete was cast are illustrated in Figure 8. The following notation was used to identify the layers at which the VWSG sensors were set:

TD: Top deck (150 mm [6 in.] above the bottom fiber of deck)

BD: Bottom deck (50 mm [2 in.] above the bottom fiber of deck; mid-span only)

TF: Top flange (50 mm [2 in.] below its top fiber)

CGC: Center of gravity of composite beam section

CGU/CGI: Center of gravity of the non-composite beam section (mid-span only)

CGS: Center of gravity of prestressed strands

BF: Bottom flange (50 mm [2 in.] above the bottom fiber)

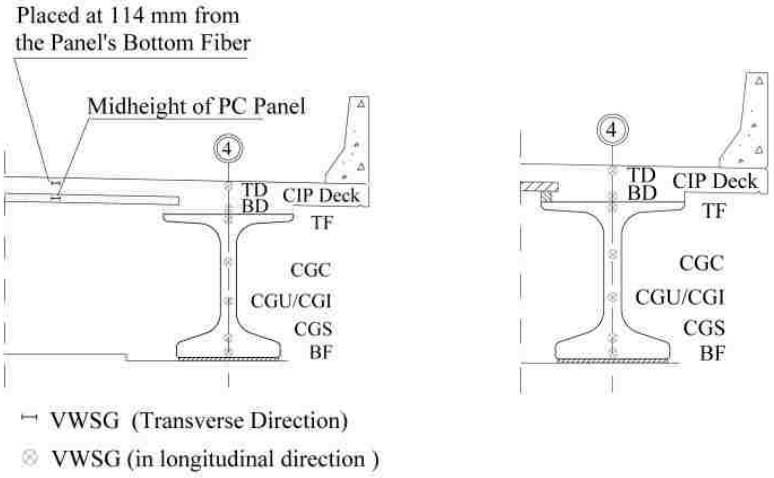

(a) Mid-span (b) Near support

Figure 8.VWSG installation details (PC/PS girders).

4.2.2. Automated Total Station. A high-performance automated total station (ATS) was utilized to obtain the instrumented girder's camber before and after the tendons were released. The ATS was set atop a secure tripod. Five prisms (targets) were placed at several locations of the girders' top flange (Figure 9).

(a) Total station

b) Prisms set on top flange

Figure 9. Automated total station recording camber deflection.

The prisms were set on steel plates that had been installed previously atop the girder's flange of the girders at the following locations: 0.30m (1.0 ft.) from each end, and sections located at L/4, L/2, and 3/4L. The spatial coordinates of these prisms were recorded by the ATS; they were used to compute the PC/PS girders' camber that was produced by the compression force the tendons transferred to the girders. Two prisms were also set atop secure tripods located between the PC/PS girder and the ATS. These additional prisms were utilized as reference points that helped verify whether or not the ATS experienced additional relative movements either before or after the strands were released.

4.3. PRECAST PRESTRESSED PANELS AND CAST-IN-PLACE DECK

A VWSG was set at the mid-height within two selected PC/PS panels [Figure 10(a)]. The VWSG installed within the CIP deck (mid-span section) is illustrated in [Figure 10(b)]. Twenty two VWSGs were placed within the CIP RC deck. Twenty VWSGs were installed along the girder's longitudinal direction (Sensors TD and TB in Figures 8 and 10). The last two VWSGs were set along the bridge's transverse direction between girder lines 2 and 3 and girder lines 3 and 4 [Figures 7 and 8(a)]. These two VWSGs were placed directly above the sensor that was installed within the panels, separated 114 mm [4.5 in.] from the top fiber of the panels [Figure 8(a)].

(a) PC/PS panels (b) CIP deck

Figure 10. VWSG installation details.

5. DATA COLLECTION

Three data acquisition systems (DAS) were used to record data while Bridge A7957 was being fabricated and constructed. A compact RIO system with an NI9214 High Accuracy Thermocouple module was employed to collect the temperature within the bents. A 90-watt solar panel was employed to power the DAS during the construction of the CIP bents [Figure 11(a)]. The VWSGs were connected to one of two Campbell Scientific CR800s while the girders were fabricated and erected [Figure 11(b)].

(a) Compact RIO and solar panel (b) CR800 DAS box

Figure 11. Data Acquisition Systems (DAS).

5.1. INTERMEDIATE BENT CONSTRUCTION

Temperature data were recorded while each of the two intermediate bents was cast. This data included the following: (1) bent 3 columns and web wall, (2) bent 2 columns and web wall, (3) bent 3 pier cap, and (4) bent 2 pier cap.

(a) Bent construction (thermocouples) (b) Girders fabrication (VWSGs)

Figure 12. DAS recording data during concrete placement.

The thermocouple wires were connected to the Compact RIO system after sensors were installed (as illustrated in Figure 6). Data were recorded for approximately 24-48 hours; it started right before concrete placement began. The CR800 DAS gathering data during concrete placement at the pier cap is illustrated in [Figure 12(a)].

5.2. GIRDERS AND PRECAST PRESTRESSED PANELS FABRICATION

Two CR800 DAS were employed at the precast plant so that data could be gathered from the VWSGs. After the VWSGs were installed at the different girders' sections (Figure 8), they were connected to the CR800 DAS [Figure 11(b)]. The CR800 DAS started collecting temperature and strain readings right before concrete casting until after the PC/PS girders' strands were released. Both strain and temperature data were also obtained from the two instrumented PC/PS panels during this time. The CR800 DAS were installed to collect data while the PC/PS girders were being fabricated [Figure 12(b)].

5.3. GIRDERS ERECTION

Two instrumented girders (identified as S2-G4 and S3-G4; span 2, girder 4 and span 3, girder 4, respectively) were monitored during their erection. One CR800 DAS was fixed to the girder's top, and the

Figure 13. Girders erection.

VWSGs were connected. Connecting the DAS during this process allowed the strain profile at the mid-span not only to be analyzed but also obtained to both the SCC and the HS-SCC mixture (S3-G4 and S2-G4, respectively). The VWSG remained fixed for an additional 30 minutes after the girder was placed atop the bents. Representative images of this phase of construction are given in Figure 13.

6. MONITORING RESULTS TO DATE

Temperature profile comparisons recorded at an early age from the sensors placed within the pier caps (top and middle sensors) of both bents are illustrated in (Figure 14).

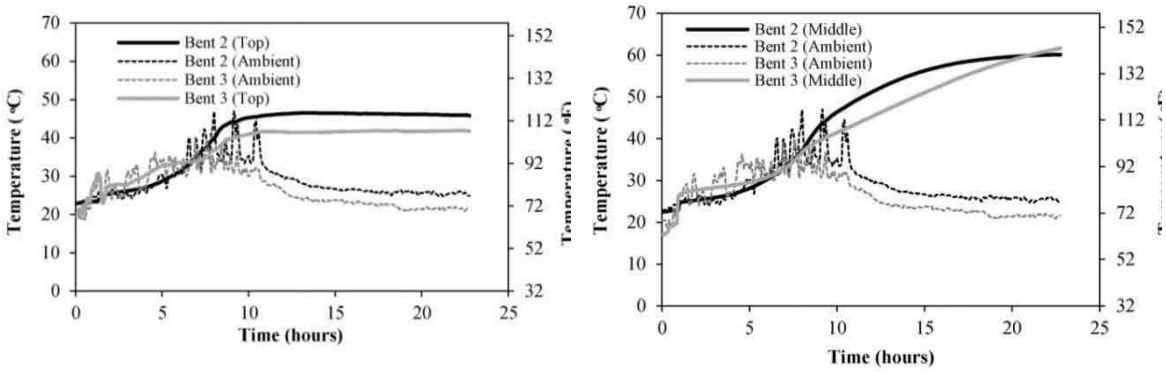

(a) Top sensor (b) Middle sensor

Figure 14. Bent hydration profile comparisons (pier cap).

As expected, an increment of the Class C fly ash content in the HVFAC mixtures (bent 3) helped reduce the heat release and delayed the peak of the hydration curve in comparison to the mixture employed in bent 2 and the abutments. This effectively retarded the set of the HVFAC mixture. For each bent, a minimum of twenty four 100 x 200 mm [4 x 8 in.] cylinders were prepared to obtain the compressive strength of the web

walls and pier caps at different ages. The specimens were match cured with the bents and were kept in the jobsite for 24 or 48 hours.

Table 3. Bents' compressive strength test results (MPa).

Member (Span-Girder)	Concrete Age (days)						
	1	3	7	14	28	56	365
Bent 2 (Web wall)	19.7*	22.0	29.9	29.5	29.9	38.7	40.3
	19.4*	22.2	31.1	32.0	30.3	35.4	41.2
	21.0*	22.8	30.3	32.5	32.5	35.8	—
Bent 2 (Pier cap)	14.0*	18.9	22.5	26.4	25.4	29.7	31.6
	14.1*	18.1	22.3	24.5	25.7	30.1	33.6
	14.1*	17.3	21.2	23.6	24.2	31.0	35.0
Bent 3 (Web wall)	17.8	19.1	27.0	28.5	32.6	32.9	40.0
	16.7	18.9	23.6	30.8	33.0	32.9	43.7
	17.8	18.5	26.3	26.7	34.6	30.5	—
Bent 3 (Pier cap)	18.5*	20.0	21.0	25.5	26.9	29.2	28.5
	17.8*	20.3	23.4	24.3	26.8	27.0	31.8
	17.4*	19.3	21.0	24.3	27.9	27.0	—

Notes: 1 MPa = 145 psi. *Tests were conducted after 2 days of concrete placement.

Afterwards, the specimens were transported to the research lab and stored outside to keep them under weather conditions similar to the existing on the bridge site. Before testing, the specimens were capped at the two bases to ensure parallel surfaces according to ASTM (2012b). The specimens were tested at 1, 3, 7, 28, 56, and 365 days according to (ASTM 2012a). The compressive strengths of the web walls and pier caps of both bents are listed in Table 3. A comparison between the compressive strength development for both mixtures used to cast bents 2 and 3 is given in Figure 15. The specified compressive strength of 20.7 MPa [3,000 psi] was exceeded at 7 days for both concrete mixtures. This early strength gain is in agreement with results reported by Naik et al. (2003). Naik et al. (2003) reported that Class C fly ashes perform well at early age strength gains due to the pozzolanic activity given by their higher calcium content.

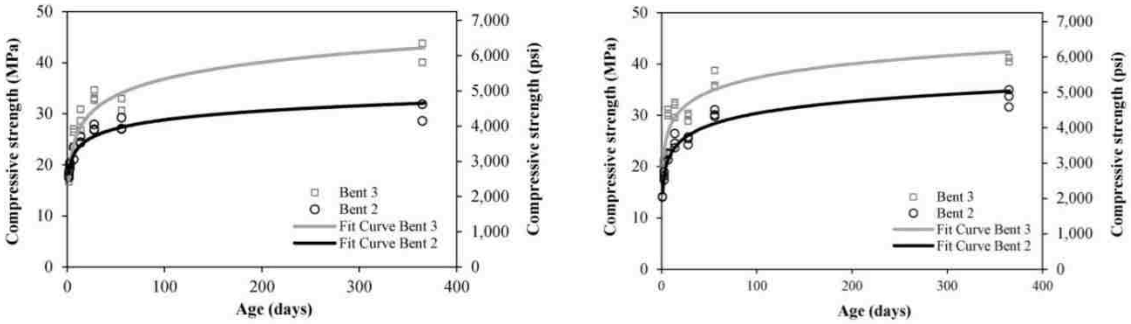

(a) Pier caps (b) Web walls

Figure 15. Bents compressive strength development.

The HVFAC mixture developed a larger compressive strength than the control mixture (MoDOT Class B mixture with 20 % fly ash replacement) employed at the abutments and intermediate bent 2. A substantial strength gain, approximately 25 %, occurred on the compressive strength of bent 3's web wall after one year. In the case of bent 3's pier cap, the compressive strength gain was closed to 35 %.

Table 4. Summary of the PC/PS girders' measured hydration temperatures.

Girder	S1-G3 (CC)	S1-G4 (CC)	S2-G3 (HS-SCC)	S2-G4 (HS-SCC)	S3-G3 (NS-SCC)	S3-G4 (NS-SCC)
Casting date	8/1/13	7/29/13	8/13/13	8/8/13	8/6/13	8/3/13
Placement time	12:00 pm	12:00 pm	2:30 pm	12:30 pm	12:00 pm	12:30 pm
Ambient temp., °C	22	22	26	24	23	26
Avg. placement temperature, °C	22	22	29	28	27	28
Avg. temp at end of dormant phase, °C	26	—	26	27	—	25
Peak hydration temperature, °C	61	—	59	56	57	64
Location of peak hydration temperature	CGS (mid-span)	—	CGS (east end)*	CGS, TF (mid-span)	CGS (mid-span)	TF (mid-span)
Max. temperature rise after dormant, °C	35	—	33	29	—	39

Notes: *Temperature data were only recorded by the sensors installed closed to the east-end section. °F = 1.8 x °C + 32.

A summary of the temperature values recorded by the VWSGs installed within the Precast, prestressed girders is presented in Table 4. The maximum temperature was

recorded by the VWSG installed at the CGS or TF location for most of the girders. A temperature profile comparison obtained at sensors CGS (Figure 8) during the first 24 hours, after concrete placement, in girder 3 of span 1 and girder 4 of spans 2 and 3, respectively is presented in Figure 16. A peak temperature value of 62 °C [143 °F] was recorded by the sensor installed in girder 4 of span3 (NS-SCC). Myers and Carrasquillo (1998) found that hydration temperatures above 77 °C [170 °F] can trigger microcracking within the concrete which adversely affects the strength and durability properties of the cast member. In addition, Khayat and Mitchell (2009) reported to limit the temperature rise during the steam-curing operation of PC/PS elements to 65 °C [150 °F]. Sensor TF installed at girder 4 of span 3 recorded a maximum temperature value of 64 °C [147 °F].

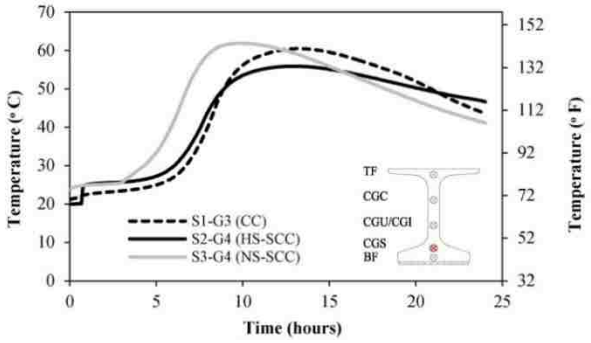

Figure 16. Girder hydration profile comparison (CGS location).

The peak hydration temperatures recorded in all the girders did not exceed the critical hydration temperature reported by Myers and Carrasquillo (1998) or the limit temperature recommended by Khayat and Mitchell (2009) indicating that the strength and durability properties of the three concrete mixtures employed have not been hindered during the steam-curing stage of the girders.

The fresh properties of the concrete mixtures were collected before casting each instrumented girder and are summarized in Table 5. For each girder, thirty 100 x 200 mm [4 x 8 in.] cylinders and six 150 x 150 x 545 mm [6 x 6 x 21 in.] beams were cast.

The specimens were prepared with the first concrete batch used to cast the instrumented girders shown in Figure 7. The cylinder and beam specimens were match cured with the girders and were kept together with the girders while they were being steam-cured. Once the concrete reached the release specified compressive strengths, 44.8 MPa (6,500 psi) (spans 1 and 3), and 55.2 MPa (8,000 psi) (span 2), prestressing tendons were released. Afterwards, the girders were moved to the yard, and the specimens were stored in an opened area located in the research lab. This was done to assure that the specimens and girders were exposed to similar weather conditions. Before testing, specimens were ground at the two bases to ensure parallel surfaces.

Table 5. Fresh properties of girder's concrete mixtures.

Member (Span-Girder)	S1-G3 (CC)	S1-G4 (CC)	S2-G3 (HS-SCC)	S2-G4 (HS-SCC)	S3-G3 (NS-SCC)	S3-G4 (NS-SCC)
Slump, mm	229	229	—	—	—	—
Air Content, %	6.9	6.9	7.9	8.3	5.4	8.3
Slump Flow, mm	—	—	686	584	635	686
J-Ring, mm	—	—	673	610	610	635

Notes: °F = 1.8 x °C + 32; 1 mm = 0.03937 in.

The specimens were tested at 1, 3 7, 28, 56 days of age, first part of load test 1 (April 2014), and second part of load test 1 (August 2014). The values of the compressive strength test results, obtained in accordance with ASTM (2012a), are presented in Table 6.

Table 6. Girders' compressive strength test results (MPa).

Member (Span-Girder)	Concrete Age (days)							
	1	3	7	14	28	56	T1D1	T1D3
S1-G3 (CC)	49.2	53.0	59.4	68.8	75.4	75.5	71.2	69.4
	51.3	52.5	56.8	66.0	75.8	74.6	70.9	77.9
	—	46.8	62.5	64.8	71.7	—	—	—
S1-G4 (CC)	54.1	53.8	54.9	62.0	69.8	71.0	73.7	84.0
	51.2	51.2	51.4	65.3	64.3	67.0	75.8	75.5
	—	50.7	60.3	67.0	67.2	69.8	70.7	—
S2-G3 (HS-SCC)	62.3*	64.1	65.4	80.4	74.7	81.2	79.6	89.6
	61.2*	64.5	75.5	82.0	85.8	74.9	73.8	87.6
	—	69.5	73.4	72.8	—	81.2	—	81.0
S2-G4 (HS-SCC)	—	58.1†	70.1	70.1	76.6	71.5	78.8	86.7
	—	61.8†	62.9	69.3	66.9	71.4	83.7	90.1
	—	—	63.5	76.4	72.3	70.9	76.5	78.3
S3-G3 (SCC)	46.7	60.2	61.3	64.9	67.0	71.0	69.5	81.1
	49.4	54.7	60.7	70.5	66.7	72.7	66.3	86.3
	47.2	55.6	64.5	66.7	72.4	71.5	62.9	—
S3-G4 (SCC)	47.6*	47.7	45.4	52.2	59.2	55.2	58.1	63.6
	46.3*	46.5	48.2	62.0	61.1	64.3	61.1	61.3
	—	—	—	—	—	—	—	—

Notes: 1 MPa = 145 psi. * Tests were conducted after 2 days of concrete placement. † Test were conducted after 4 days of concrete placement. Column T1D1 lists results of tests conducted on April 22nd, 2014. Column T1D3 presents results of tests conducted on August 12th, 2014.

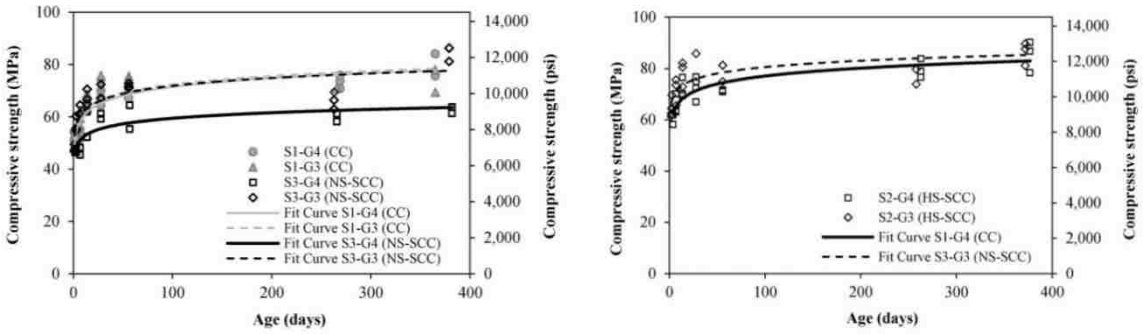

(a) Spans 1 and 3 (b) Span 2

Figure 17. PC/PS girders compressive strength development.

A comparison of the compressive strengths obtained for the concrete used to fabricate span 1 and span 3's girders is shown in Figure 17(a). The 28-day target strength of 55.2 MPa [8,000 psi] was reached by the girders after 7 days except for girder 4 of span 3 (S3-G4) that exceeded the compressive strength at 14 days. The strength

developed by girder S3-G4 was less than the strength gain achieved by the rest of the girders. A similar trend was observed in the compressive strength results obtained from the specimens of the girders of span 2 [Figure 17(b)] as a result of a slightly larger amount of air-entraining admixture added to the mixtures (see Table 5). Modulus of elasticity tests were conducted in accordance with ASTM (2010), and the results are listed in Table 7. The results obtained from the specimens of spans 1 and 3's girders are compared in Figure 18. In the case of the girder S3-G4, a reduction of the modulus of elasticity was observed [Figure 18(a)].

Table 7. Girders' modulus of elasticity test results (GPa).

Member (Span-Girder)	Concrete Age (days)							
	1	3	7	14	28	56	T1D1	T1D3
S1-G3 (CC)	30.0 31.4	31.4 31.0	32.8 34.5	35.2 35.5	36.2 35.9	36.5 35.9	39.6 38.3	40.7 40.7
S1-G4 (CC)	30.0 35.2	30.3 29.3	— —	— —	35.9 35.2	34.1 37.2	39.0 38.3	42.4 41.0
S2-G3 (HS-SCC)	36.2* 37.2*	34.1 36.2	36.9 36.5	37.6 36.9	38.3 40.3	35.9 39.0	36.2 40.7	44.5 41.0
S2-G4 (HS-SCC)	— —	32.1† 32.8†	33.8 34.5	33.8 35.9	34.5 35.9	34.8 36.9	38.6 41.7	42.1 41.4
S3-G3 (SCC)	33.4 31.4	33.4 32.8	34.1 33.8	37.2 35.2	35.5 37.2	35.2 36.9	41.7 37.9	41.0 43.4
S3-G4 (SCC)	30.7* 27.2*	29.0 32.1	— —	35.9 33.8	32.4 33.8	32.1 35.2	36.9 38.3	40.0 35.2

Notes: 1 GPa = 145 ksi. *Tests were conducted after 2 days of concrete placement (time of initial prestress). †Tests were conducted after 4 days of concrete placement (time of initial prestress). Column T1D1 lists test results of April 22nd, 2014. Column T1D3 presents test results of August 12th, 2014.

Table 5 lists the air content of all the instrumented girders. In the case of S3-G4, the air content value was 8.3 % which was greater than (approximately 20% and 50%) the air content value measured for the rest of the girders of spans 1 and 3. The extra amount of air-entraining admixture added to the concrete of girder S3-G4 caused a

reduction on the hardened properties of this girder, namely compressive strength and modulus of elasticity.

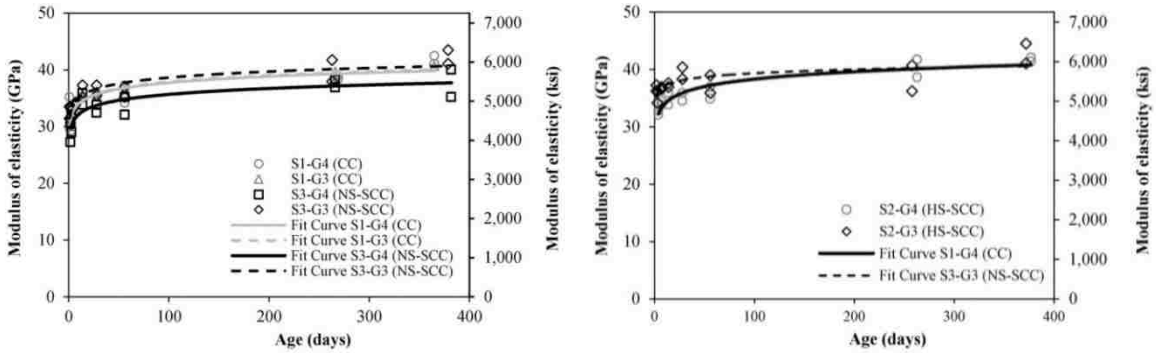

(a) Spans 1 and 3 (b) Span 2

Figure 18. PC/PS girders' modulus of elasticity.

This result implies that a strict control has to be followed when the constituents of a mixture are being proportioned. Slight variations of the mixture proportions adversely affect the mechanical properties of the concrete mixture as reported by Khayat and Mitchell (2009). A comparison of the girders strain developed at the time of prestress release is illustrated in Figure 19.

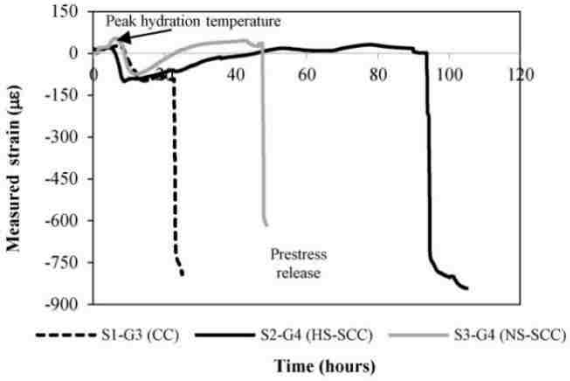

Figure 19. Girders strain comparison (BF).

These values were recorded by the BF sensor (Figure 8) at the girders' mid-span section. The values obtained for the three girders, span 1 girder 3 (CC), span 2 girder 4 (HS-SCC) and span 3 girder 4 (NS-SCC), are plotted.

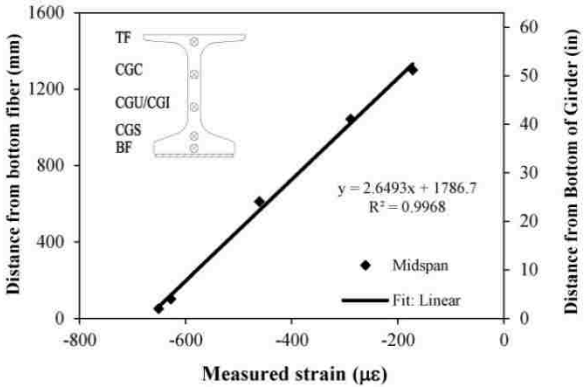

Figure 20. S3-G4 mid-span strain profile.

The strain profile of girder S3-G4 was obtained at mid-span and is shown in Figure 20. Furthermore, this profile shows that the section remained plane after the initial prestress force is transferred to the girder. Similar results were obtained for the rest of the girders. The compressive stress at the bottom layer of the girders was computed with Equation (1):

$$\sigma_c = E_{ci}\varepsilon_{bot} \tag{1}$$

where E_{ci} is the modulus of elasticity of concrete at prestress release and ε_{bot} is the compression strain at the girder's bottom fiber right after the strands were released. The permissible compressive stress of the extreme fiber at mid-span was computed with Equation (2) according to ACI (2014):

$$f_c = 0.60 f'_{ci} \tag{2}$$

where f_c is the permissible compressive stress and f_{ci} is the compressive strength of concrete at the time of initial prestress. The maximum compression stress and allowable stress limits for all girders are presented in Table 8.

Table 8. Compressive stress and permissible compressive stress limits at mid-span.

Member (Span-Girder)	ε_{bot} ($\mu\varepsilon$)	E_{ci} (GPa)	σ_{bot} (MPa)	f_c (MPa)
S1-G3 (CC)	719	30.7	22.1	30.1
S2-G4 (HS-SCC)	778	32.5	25.2	35.9
S3-G3 (NS-SCC)	672	32.4	21.8	28.6
S3-G4 (NS-SCC)	674	29.0	19.6	28.2

Notes: 1 MPa = 145 psi. The values of ε_{bot} and σ_{bot} correspond to compressive strain and stress, respectively. E_{ci} is the average of the modulus of elasticity values reported in Table 7 at the time of initial prestress.

The ε_{bot} values used to compute f_c corresponds to the maximum compressive stress estimated at the bottom fiber of the girder. It should be noted that the compressive stress in the girders' extreme fiber, computed from experimental data, were below the design limits for all of the girders. Therefore, these results confirmed that the girders remained uncracked at the time of prestress release and support that the assumptions made during the design were valid. A comparison between the girders camber measured with the ATS is presented in Figure 21. Girder S3-G4 (NS-SCC) exhibited a larger camber than girder S1-G3 (CC) at the time of the prestress release. The camber difference was approximately 20% and can be related to the lower elastic modulus of the NS-SCC girder. As reported by Khayat and Mitchell (2009), the use of a smaller volume and maximum size of coarse aggregate in the NS-SCC concrete mixture affects the mechanical properties of SCC mixtures. As mentioned previously, girder S3-G4 reported greater air content than girder S1-G3 which also might have contributed to a lower development of the mechanical properties of the mixture.

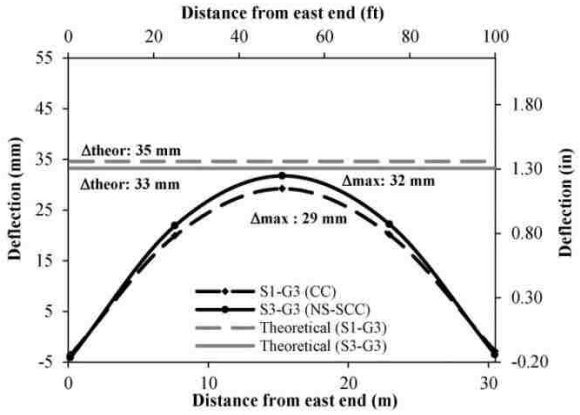

Figure 21. Camber at the time of prestress transfer (S1-G3 and S3-G3).

This variation in the hardened properties of the NS-SCC girder suggests that any improvised change in the mix design can result in a SCC mixture with unexpected mechanical properties and performance. A proper selection of materials constituents and proportions has to be conducted carefully to assure that the desire performance of SCC mixtures (Khayat and Mitchell 2009). Maturity studies are currently being undertaken on the different concrete mixtures implemented in Bridge A7957. These results will aid in analyzing the development of mechanical properties within the mixtures, such as creep, shrinkage, thermal gradients, time dependent behavior, and serviceability. Continuous monitoring has also been undertaken on Bridge A7957. This monitoring is scheduled to continue until the end of December 2015. The structure's static behavior has been and will continuously be evaluated during several series of live load tests to provide a basis benchmark of its response under live loads. The results obtained will be used to calibrate, improve and validate bridge models based on finite element analysis. In addition, these initial monitoring stage results will be used to establish a response baseline to detect and evaluate any changes in the structure's response in the short and long term

7. SUMMARY AND CONCLUSIONS

The Missouri Department of Transportation has conducted the first full-scale structure implementation of high-strength self-consolidating concrete (HS-SCC) and high volume fly ash concrete (HVFAC) on Bridge A7957.

The instrumentation phase of the project was conducted effectively. Maturity studies are currently being performed on the different concrete mixtures utilized in Bridge A7957. These studies will be used to compare the differences among the mechanical properties development including: creep, shrinkage, thermal gradients, time dependent behavior and serviceability in the long term.

High volume fly ash concrete, a sustainable material, was employed at a 50% replacement level within one of the bridge's interior supports. Coupled with the use of SCC, Bridge A7957 is expected to have a longer service life than traditional prestressed and reinforced concrete structures.

The maximum hydration temperature peak recorded during the steam-curing stage satisfied the maximum temperature limit reported in NCHRP Report 628 (ASTM 2010). Proper selection of material constituents and proper proportion is fundamental to ensure that SCC mixtures perform as expected and similarly as their conventional concrete mixtures counterparts.

The first series of live load tests was conducted at the initial stage of this project to establish a benchmark. These initial results will be used to monitor any trend in the structure's response and will be used to validate design assumptions used during the design stage of Bridge A7957. The load test results will also be employed to conduct an initial load rating of Bridge A7957 based on the experimental data.

AUTHOR CONTRIBUTIONS

ACI member Eli S. Hernandez is a Ph.D. Candidate at Missouri University of Science and Technology, Rolla, Missouri. He received both his BS and MS from the Universidad de los Andes, Merida, Venezuela. His research interests include advanced concrete materials for for prestressed and reinforced concrete structures, fiber-reinforced polymers for strengthening applications, and the performance evaluation of existing bridge structures.

John J. Myers, FACI, is a Professor at Missouri University of Science and Technology, Rolla, MO. He received his BAE from Pennsylvania State University, University Park, PA. He earned both his MS and his PhD from the University of Texas at Austin, Austin, TX. He is the current Chair of ACI Subcommittee 440-L, FRP-Durability and Past Chair of ACI Committee 363, High-Strength Concrete among involvement in numerous other ACI technical and educational committees. His research interests include advanced concrete materials for structural applications and fiber-reinforced polymers in strengthening applications.

ACKNOWLEDGEMENTS

The authors gratefully acknowledge the financial support provided by the Missouri Department of Transportation (MoDOT) and the National University Transportation Center (NUTC) at Missouri University of Science and Technology.

REFERENCES

American Concrete Institute. (ACI). (2007). "Self-Consolidating Concrete." ACI 237, Farmington Hills, MI.

American Concrete Institute. (ACI). (2014). "Building Code Requirements for Structural Concrete and Commentary." ACI 318-14, Farmington Hills, MI.

American Society for Testing and Materials. (ASTM). (2010). ASTM C469/C469M-10 “Standard Test Method for Static Modulus of Elasticity and Poisson’s Ratio of Concrete in Compression”, West Conshohocken, PA.

American Society for Testing and Materials. (ASTM). (2012a). ASTM C39/C39M-12a “Standard Test Method for Compressive Strength of Cylindrical Concrete Specimens.”, West Conshohocken, PA.

American Society for Testing and Materials. (ASTM). (2012b). ASTM C617/C617M-12 “Standard Practice for Capping Cylindrical Concrete Specimens”, West Conshohocken, PA.

Hernandez, E. S., Griffin, A., and Myers, J. J. (2014). "Balancing extended service life and sustainable concrete material usage in Missouri Bridge A7957." Proc., Struct. Faults & Repair: European Bridge Conference (SF&R), London, England, UK.

Khayat, K. H., and Mitchell, D. (2009). "Self-consolidating concrete for precast, prestressed concrete bridge elements." National Cooperative Highway Research Program Report 628, NCHRP 628, Transportation Research Board, Washington, DC, 2009, pp. 99.

Myers, J. J., and Bloch, K. (2010). "Innovative Concrete Bridging Systems for Pedestrian Bridges: Implementation and Monitoring." CIES Report for City of Rolla, Missouri University of Science and Technology, Rolla, Missouri, December, 2010, pp. 294.

Myers, J. J., and Carrasquillo, R. (1998). "Production and Quality Control of High Performance Concrete in Texas Bridge Structures." University of Texas at Austin, Austin, Texas, pp.

Myers, J. J., Volz, J., Sells, E., Porterfield, K., Looney, T., Tucker, B., and Holman, K. (2012). "Self-consolidating concrete (SCC) for infrastructure elements." cmr 13-003_A, Missouri University of Science and Technology, Rolla, Missouri, Aug. 2012, pp. 219.

Naik, T. R., Ramme, B. W., Krauss, R. N., and Siddique, R. (2003). "Long-term performance of high-volume fly ash concrete pavements." ACI Mater J, 100 (2), 150-155.

Volz, J. S., Myers, J. J., Richardson, D. N., Arezoumandi, M., Beckemeier, K., Davis, D., Holman, K., Looney, T., and Tucker, B. (2012). "Design and evaluation of high-volume fly ash (HVFA) concrete mixes." Report cmr 13-008, Missouri University of Science and Technology, Rolla, Missouri, October 2012, pp. 40.

II. DIAGNOSTIC TEST FOR LOAD RATING OF A PRESTRESSED SCC BRIDGE

E.S. Hernandez[1] and J.J. Myers[2]

[1]Ph.D. Candidate of the Civil, Architectural & Environmental Engineering Department, Missouri University of Science and Technology, 205 Pine Building, 1304 N Pine St, Rolla, MO 65409; email: ehd36@mst.edu

[2]Associate Dean, Professor of the Civil, Architectural & Environmental Engineering Department; Missouri University of Science and Technology; 325 Butler-Carlton Hall, 1401 N Pine St., Missouri University of Science and Technology, Rolla, MO 65409; email: jmyers@mst.edu

ABSTRACT

Self-consolidating concrete (SCC) has emerged as an alternative to build stronger structures with longer service life. Despite the advantages of using SCC, there are some concerns related to its service performance. The effect of a smaller coarse aggregate size and larger paste content is of special interest. It is fundamental to monitor the response to service loads of infrastructure employing SCC in prestressed concrete members. Bridge A7957 was built employing normal-strength and high-strength self-consolidating concrete in its main supporting members. The diagnostic test protocol implemented in this research included static and dynamic tests and the calibration of refined finite element models simulating the static loads acting on the structure during the first series of diagnostic tests. The main objective of this study centered on (a) presenting a diagnostic

test protocol using robust and reliable measurement devices (including noncontact laser technology) to record the bridge's initial service response; and (b) obtaining the initial spans' performance to evaluate and compare the SCC versus conventional concrete girders' response when subjected to service loads. The initial response of the end spans (similar geometry and target compressive strength, but with girders fabricated using concrete of different rheology) was compared, and no significant difference was observed.

Keywords: Assessment of bridge structures, diagnostic load tests, long-term monitoring, service evaluation of bridges.

1. INTRODUCTION

Since the late 1980s, self-consolidating concrete (SCC), a high-performance material that can flow easily into tight and constricted spaces without segregating, has been successfully employed for infrastructure projects in Europe, Japan, and Australia. The highly flowable feature of SCC results in better consolidation and placement, and fewer voids and honeycombing that creates a more condensed microstructure. For these reasons, SCC has become an effective alternative to build stronger infrastructure with longer service life (Ouchi et al. 2003, McSaveney et al. 2011, Keske et al. 2014, Hernandez and Myers 2015b). Despite these main advantages of SCC, several concerns are related to its mechanical properties. The effect of the smaller coarse aggregate proportion and size in addition to a larger paste content employed to attain a flowable mixture is of special interest. Prestressed concrete (PC) members fabricated with SCC are expected to develop higher prestress losses (creep and shrinkage) and to undergo an

increased in-service response due to its lower modulus of elasticity (Khayat and Mitchell 2009, Myers et al. 2012). Consequently, it is fundamental to monitor the in-service response of full-scale highway infrastructure employing self-consolidating concrete.

Field tests have largely demonstrated reserves of strength capacity of in-service bridges despite their visual condition and age. Sources that explain the difference are diverse and may be attributed to several in-situ parameters that are not considered during the design or strength evaluation of a bridge's structure. Load testing is a powerful approach used to assess the structural performance of bridges because it provides an in-service, as-built characterization of the bridge's performance. The AASHTO Manual for Bridge Evaluation (AASHTO 2010) presents two test options: proof load tests and diagnostic load tests. Proof load tests are employed to obtain the maximum safe live load a bridge can withstand without undergoing inelastic deformations, while diagnostic load tests are used to better understand the service response of a bridge. Diagnostic tests are also employed to validate design assumptions and to corroborate the structure's response improvements due to field factors deemed as beneficial for the bridge's performance (Cai and Shahawy 2003). These factors have a direct influence in the estimation of the dynamic load allowance (impact factor) and lateral load distribution of a bridge, which affects its load rating.

The tasks conducted on this research included (1) static load tests; (2) dynamic load tests; and (3) the calibration of refined finite element models (FEM) simulating the static loads acting on the bridge superstructure during the first series of diagnostic tests. The main objective of this study centered on (a) presenting a diagnostic test protocol using robust and reliable measurement devices (including noncontact laser technology) to

record the bridge's benchmark in-service response; and (b) obtaining the spans' performance to evaluate and compare the SCC girders' response to the conventional concrete girder's behavior when subjected to service loads

2. RESEARCH SIGNIFICANCE

In the United States, the Federal Highway Administration and some State Departments of Transportation have made important efforts to employ self-consolidating concrete in infrastructure projects. Bridge A7957 was the first implementation project built by the Missouri Department of Transportation using normal-strength and high-strength self-consolidating concrete (NS-SCC and HS-SCC) in its main supporting members. The results presented herein are part of an ongoing research program whose main objective was to provide an implementation test bed and showcase the use of SCC in a field project. This stage of the research focused on monitoring and comparing the initial in-service response of the different spans of the bridge. It is hoped that the results presented herein can be used by researchers and engineers to further understand the initial in-service behavior of prestressed SCC members. In addition, it is expected that these results will help establish an experimental load rating benchmark of the PC girders to monitor changes in the long-term as their different concrete mixtures are exposed to the same environmental conditions and loads.

3. BRIDGE DESCRIPTION

Bridge A7957 is a three-span, continuous bridge with a 30-degree skew angle and a smooth surface condition (Figure 1), fabricated with PC girders. The Nebraska University (NU) 53 PC girders [Figure 1(c)] in each span were designed with concrete

mixtures of different compressive strength (Hernandez et al. 2014, Hernandez and Myers 2015b). The girders in the first span are 30.48 m (100 ft) long and made of conventional concrete (MoDOT's Class A mixture) with a nominal compressive strength of 55.2 MPa (8,000 psi). Girders in the second span are 36.58 m (120 ft) long and were fabricated with a high-strength self-consolidating concrete (HS-SCC) mixture of 68.9 MPa (10,000 psi). The third span measures 30.48 m (100 ft) and employed normal-strength self-consolidating concrete (NS-SCC) with a target compressive strength of 55.2 MPa (8,000 psi).

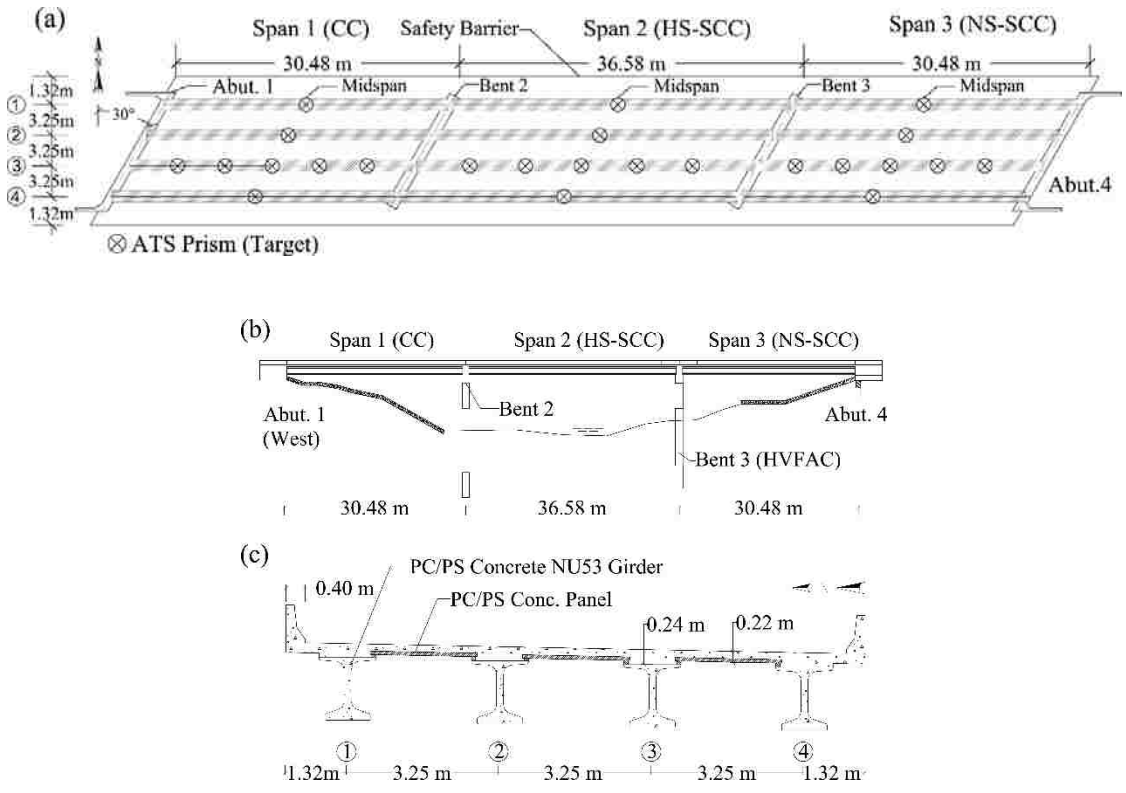

Figure 1. Bridge A7957.
(a) Plan view and ATS target (prism) locations; (b) elevation; (c) cross section.
Conversion factor: 1 m = 3.28 ft.

PC panels with a specified compressive strength of 41.4 MPa (6,000 psi) extend between the top flanges of the girders in the transverse direction and underneath a cast-in-place (CIP) reinforced concrete (RC) deck [Figure 1(c)]. The CIP deck was cast with a 25% fly ash replacement mixture of portland cement concrete having a design strength of 27.6 MPa (4,000 psi). Two intermediate bents and two abutments support the superstructure [Figs. 1(a) and 1(b)]. The abutments and the second intermediate bent were cast with a concrete mixture using a 20% fly ash replacement of portland cement with a nominal compressive strength of 20.7 MPa (3,000 psi). The third intermediate bent was built using high-volume fly ash concrete (HVFAC) with a 50% fly ash replacement of portland cement and a specified compressive strength of 20.7 MPa (3,000 psi). Complete details about the girders production and the mixtures employed on this bridge have been documented elsewhere (Hernandez and Myers 2015b, Myers et al. 2016).

4. TEST EQUIPMENT

The instrumentation was designed to collect (a) the static vertical deflection at midspan of girders 1–4 (spans 1–3) as shown in Figure 1(a); (b) the static vertical deflection at several sections along girder 3 (spans 1–3); and (c) the vertical dynamic deflection at girder 3's midspan (only spans 1 and 3). The next sections present details about the non-contact laser equipment employed to collect data described in (a)–(c).

4.1. AUTOMATED TOTAL STATION

An automated total station (ATS), Leica TCA2003 (Figure 2) with an accuracy of 1 mm (0.039 in.) ± 1 ppm (parts per million) for distance measurements and 0.5 arc-seconds (angular measurements) was employed to record the girders' vertical deflection

along girder 3's critical sections and at each girders' midspan during the first series of diagnostic tests. The ATS obtains three-dimensional (3D) coordinates of every target by measuring the horizontal and vertical angle as well as the distance between the ATS and target prisms. The instrument was configured to take three readings per target. This is done by four internal diodes installed to optically read a fine bar code set on a glass ring inside the Leica TCA2003. During monitoring, the equipment continuously read the bar codes on the horizontal and vertical planes by sending a laser ray that reflects on the targets mounted on the structure.

The accuracy of the ATS has been reported to be ±0.1 mm (0.004 in.) in vertical deflection measurements (Merkle and Myers 2004). Twenty-four critical locations were selected to monitor the superstructure response. Fifteen ATS prisms were deployed along the third girder at 1/6L, 1/3L, 1/2L, 2/3L, and 5/6L of each span. Three additional prisms were placed at the rest of the girders' midspan (1/2L) for each span [Figure 1 (a)]. MoDOT H20 dump trucks loaded the bridge superstructure (Hernandez and Myers 2016a) during the static tests as shown in Figure 2(a).

(a) (b) (c)

Figure 2. Automated total station.
(a) Leica TCA 2003; (b) target (prism); (c) reference target.

The prisms [Figure 2(b)] have an internal magnet that keep them fixed to steel plates that were previously attached to the girders' bottom flange with an epoxy adhesive.

4.2. REMOTE SENSING VIBROMETER

A remote sensing vibrometer (RSV-150) (Figure 3) was utilized to collect the dynamic bridge response (vertical deflection) of the exterior spans' girder 3 (midspan sections). The RSV-150 has a bandwidth up to 2 MHz for nondestructive test (NDT) measurements and can detect the vibration and displacement of distant structures with limited access. The accuracy of the RSV-150 is ±0.025 mm (0.001 in.) when it records the dynamic response of a member.

Figure 3. Remote sensing vibrometer (RSV-150).

5. DIAGNOSTIC TEST

Static and dynamic tests were performed on the superstructure of Bridge A7957. The static load tests were performed on three different dates (days 1-3 in Table 1) due to

time restrictions. The dynamic tests were performed on day 3 (see Table 1). The following subsections describe the test procedures and load configurations planned to obtain the maximum static and dynamic response of the bridge superstructure the authors have reported elsewhere (Hernandez and Myers 2016a, Hernandez and Myers 2016c, 2016b, Hernandez and Myers 2017).

5.1. STATIC LOAD TESTS

Figure 4 presents the average trucks' dimensions and Figures 5–6 show details of the static load configurations used to obtain the maximum bridge's response when a single lane or two lanes were loaded. For load stops 1–3, two lanes of trucks were driven from east to west.

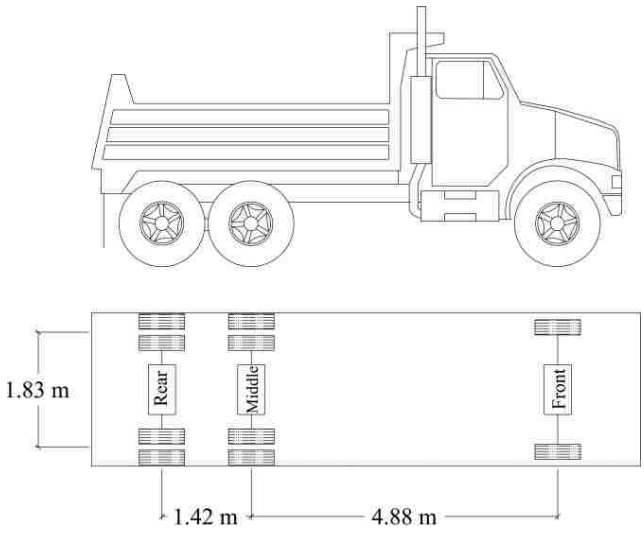

Figure 4. MoDOT's H20 dump truck employed during diagnostic test.
Conversion factor: 1 m = 3.28 ft.

The trucks were parked separately at the center of spans 3, 2 and 1 [Figure 5 (a)–5(c)]. For stops 4–6 [Figure 5(d)–5(f)], the trucks were driven from west to east, and

parked separately at the center of spans 1, 2, and 3. For these first six load stops, the center of the trucks' exterior wheels was separated 3.25 m (10.67 ft) from the safety barrier's edge, as illustrated in Figure 6(a). For stops 7–9, the trucks were driven from west to east, as illustrated in Figure 5(g)–5(i).

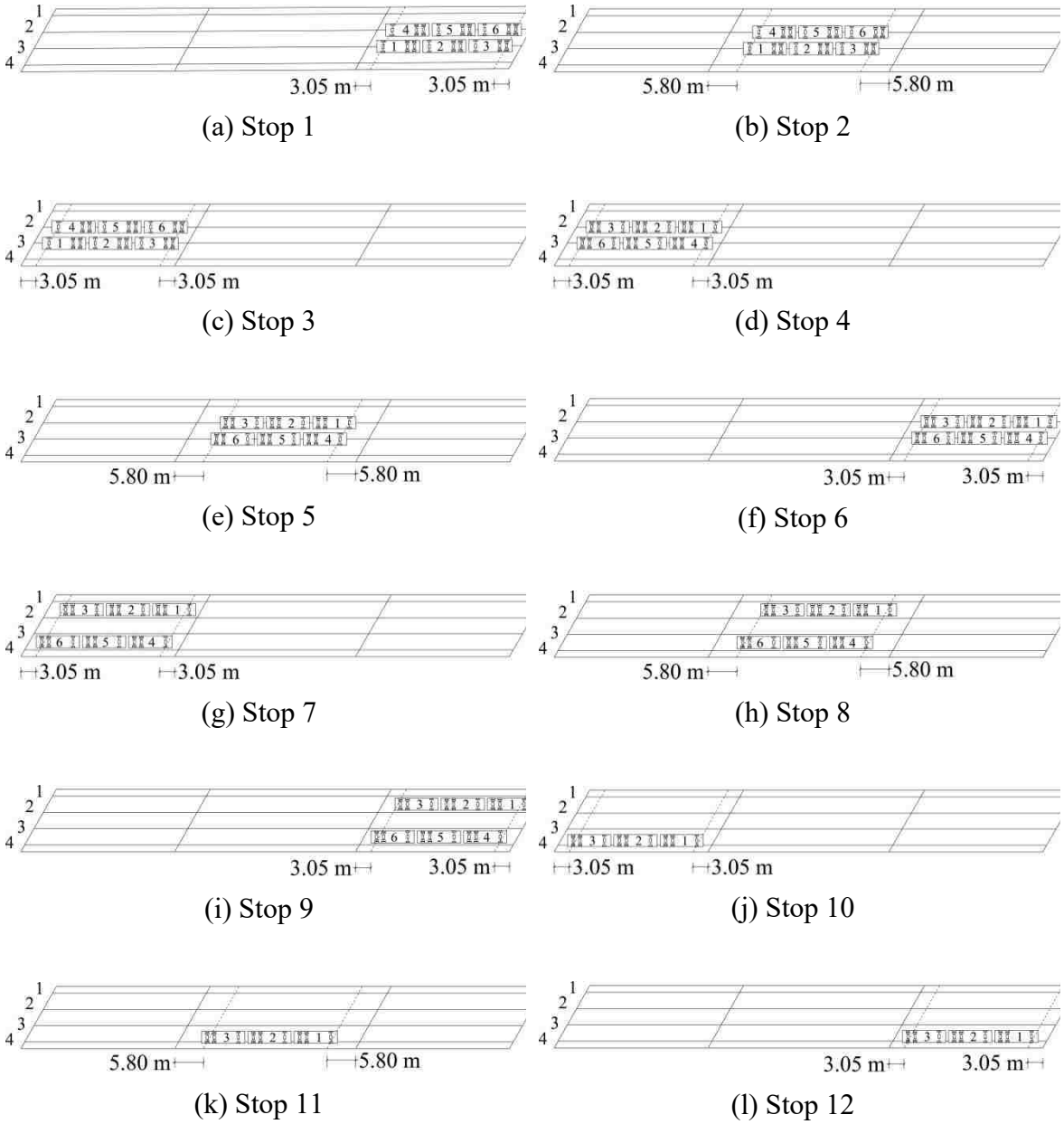

Figure 5. Static load test configurations.
Conversion factor: 1 m = 3.28 ft.

The trucks' exterior axles were separated 0.60 m (2 ft) from the barrier's edge [Figure 6(b)]. These first nine stops simulated two-lane load cases. For stops 10–12 [Figure 5(j)–5(l)], a lane of three trucks was driven from west to east along the south side of the bridge, and the trucks were separated 0.60 m (2 ft) from the barrier's edge [Figure 6(c)]. The trucks' weights (as reported by MoDOT personnel) are listed in Table 1.

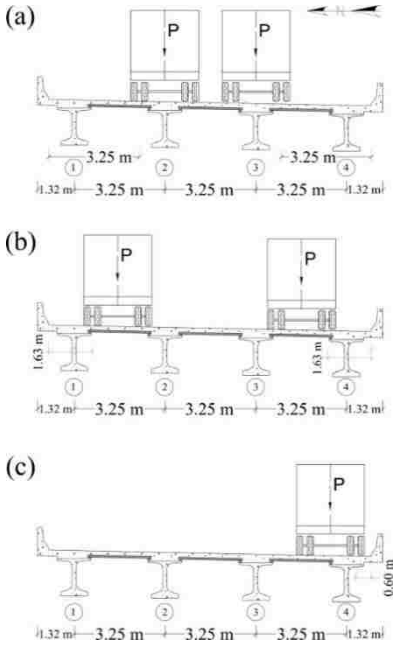

Figure 6. Distance from trucks' exterior axle to barrier's edge.
(a) Stops 1–6; (b) stops 7–9; (c) stops 10–12. Conversion factor: 1 m = 3.28 ft.

Table 1. Truck weights.

Test Day	Truck	Rear (kN)	Front (kN)	Total (kN)
1, 2*	1	158.2	74.0	232.2
1, 2*	2	161.6	57.2	218.8
1, 2*	3	150.3	56.0	206.3
1, 2*	4	178.0	75.3	253.3
1, 2*	5	170.2	77.9	248.1
1, 2*	6	166.4	71.6	238.0
3	1	164.6	61.1	225.7
3	2	180.3	70.8	251.1
3	3	169.1	70.4	239.5

Note: * Trucks remained loaded with the same weight on both days. Conversion factor: 1 kN = 0.2248 kip.

5.2. DYNAMIC LOAD TESTS

A truck was driven at speeds ranging from 16 km/h (10 mi/h) to 97 km/h (60 mi/h) during different dynamic load tests (Figure 4). During each test, the speed was kept constant starting with 16 km/h (10 mi/h). Then, the speed was increased at a rate of 16km/h (10mi/h) until the maximum speed of 96 km/h (60 mi/h) was attained for the last test. The maximum dynamic and static responses were compared to estimate the experimental dynamic load allowance. Experimental data was recorded with the RSV-150 at a sampling rate of 120 Hz. The truck was driven over the south side of the bridge (along the west–east and east–west directions), separated 0.60 m (2 ft) from the safety barrier's edge [Figure 6 (c)].

6. TEST RESULTS

6.1. STATIC LOAD TESTS

The vertical deflections resulting from the load stops described above are given in Figures 7–11. A preliminary examination of the data indicates the accuracy of the vertical deflection values estimated with the data recorded by the ATS. It is observed that the bridge's spans showed a continuous response to the load applied during the tests.

Figures 7–9 present the vertical deflections obtained along girder 3 for the stops 1–9 described above. The largest vertical deflection was obtained for span 2 (during stop 5) corresponding to a value of 10.1 mm (0.40 in.). This value was less than the maximum allowable live-load deflection of $L/800$ = 45.7 mm (1.8 in.), recommended by current US bridge design codes (AASHTO 1992, 2012).

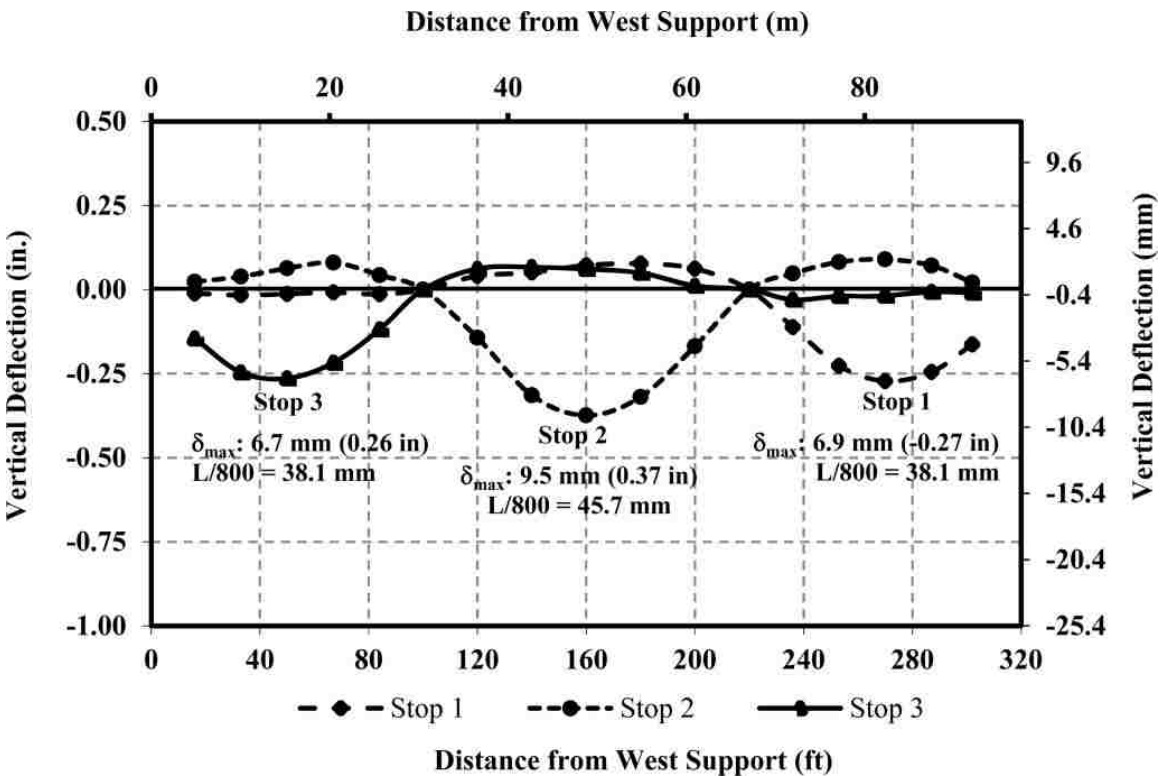

Figure 7. Girder 3's vertical deflection (stops 1–3).

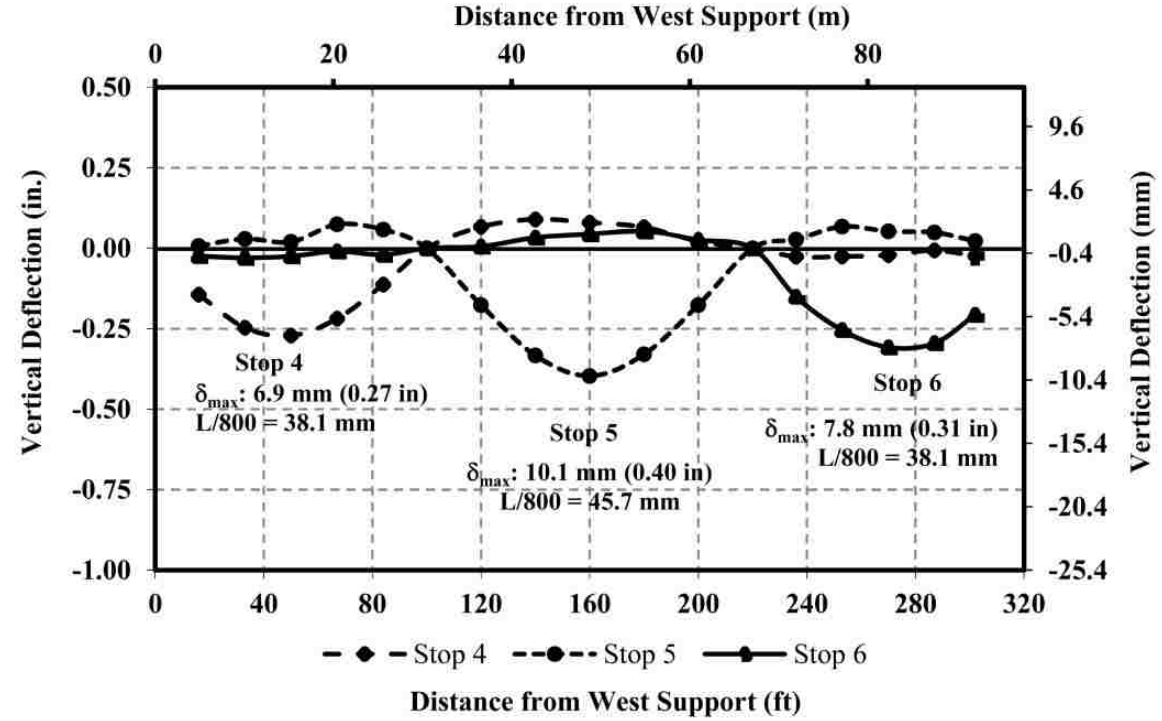

Figure 8. Girder 3's vertical deflection (stops 4–6).

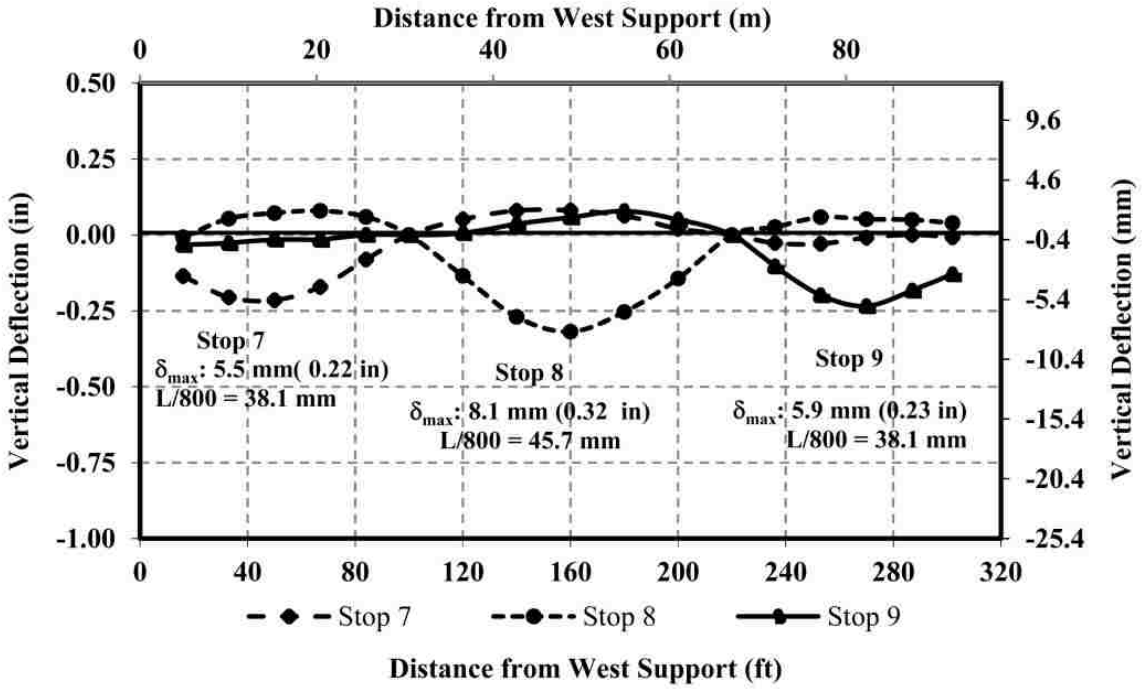

Figure 9. Girder 3's vertical deflection (stops 7–9).

For load stops 10–12, vertical deflections were not recorded along girder 3. For these load stops, the vertical deflections were collected at the girders' midspan (across the bridge's transverse direction), and their values are shown in Figs. 10–11.

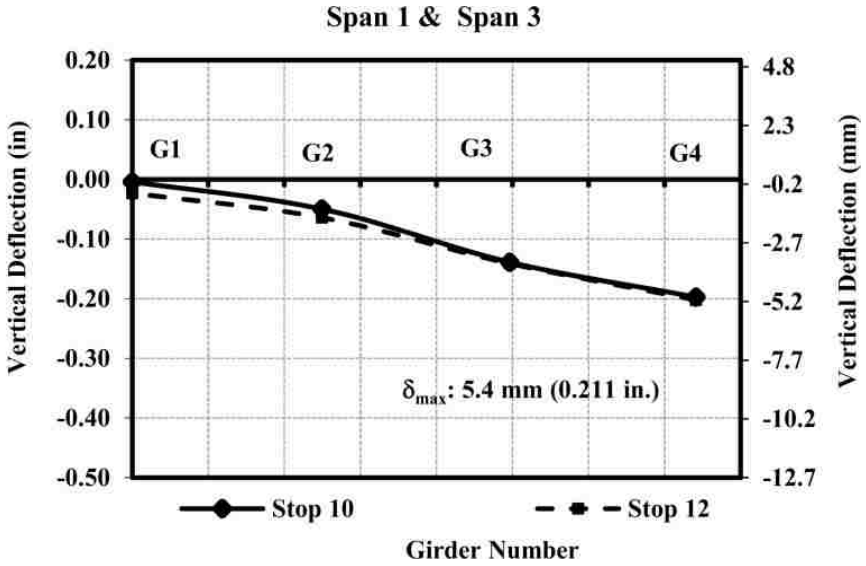

Figure 10. Vertical deflections at midspans 1 and 3 (stops 10 and 12).

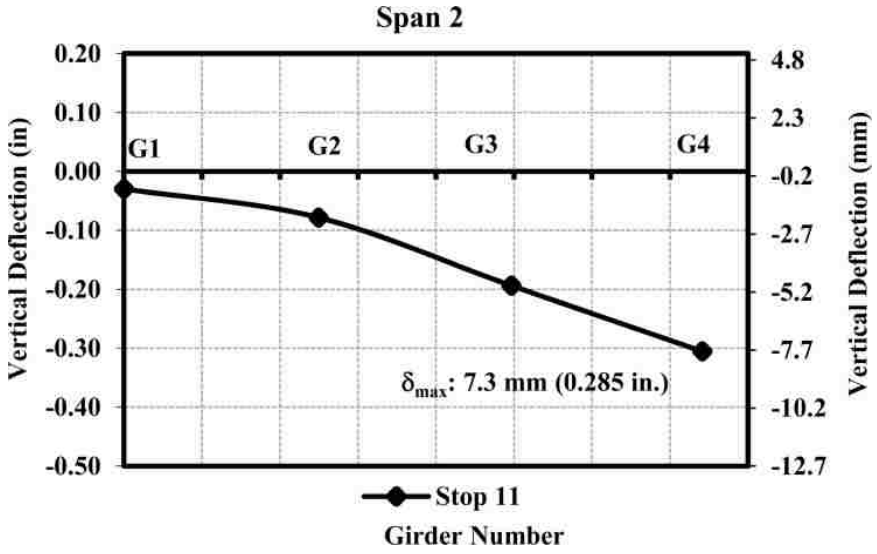

Figure 11. Vertical deflections at midspan 2 (stop 11).

The experimental vertical deflections at the girders' midspan (along the transverse direction) obtained during load stops 1–12 are listed in Table 2. The error committed by the ATS when it collected data is listed within parentheses. In the case of two lanes loaded, comparable values were obtained corresponding to stops 1 and 3 (used to compare span 3 and 1's responses when the trucks were facing west), stops 4 and 6 (loading spans 1 and 3 when trucks were facing east, far from safety barriers), and stops 7 and 9 (loading spans 1 and 3, trucks facing east, closer to safety barriers). Larger deflections were obtained for the girders near the truck loads in the case of one lane loaded. For stops 10 and 12 (span 1 and 3's response), a larger difference ratio was observed when girders 1 and 2 of both end spans (1 and 3) were compared. This difference may be related to the accuracy of the ATS [±0.1 mm (0.004 in.) in vertical deflection measurements] that is close to the measured deflection values. When one lane was loaded (stops 10–12), the error committed by the ATS when recording girders 1 and 2's vertical deflection varied between 5% and 100% (Table 2, columns 3 and 4). This

suggests that the magnitude of the loads applied during a diagnostic test should be large enough so that the span loaded directly undergoes vertical deflections larger than 2 mm. This level of load will ensure that the measurement error is kept below 5% when the ATS is employed to record data. In general, the girders' response in spans 1 and 3 (two lanes loaded) was within the same order of magnitude, implying that the spans' response during the first series of diagnostic tests was independent of the type of material used to fabricate the PC girders (i.e., conventional concrete and normal strength self-consolidating concrete). For load stops 1–9 (two-lane loads), the maximum error was below 2%.

Table 2. Vertical deflection at midspan (mm).

Stop	Span	δ_{G1} (mm)	δ_{G2} (mm)	δ_{G3} (mm)	δ_{G4} (mm)
Two Lanes Loaded					
1	3	4.2 (2%)	7.1 (1%)	6.9 (1%)	4.6 (2%)
2	2	6.3 (2%)	9.7 (1%)	9.5 (1%)	6.2 (2%)
3	1	5.1 (2%)	6.9 (1%)	6.7 (1%)	4.9 (2%)
4	1	4.2 (2%)	6.7 (1%)	6.9(1%)	4.4 (2%)
5	2	6.4 (2%)	9.8 (1%)	10.1 (1%)	6.4 (2%)
6	3	4.9 (2%)	8.4 (1%)	7.8 (1%)	5.2 (2%)
7	1	4.9 (2%)	5.1 (2%)	5.5 (2%)	5.7 (2%)
8	2	7.3 (1%)	7.8 (1%)	8.1 (1%)	7.6 (1%)
9	3	4.4 (2%)	5.5 (2%)	5.9 (2%)	5.9 (2%)
One Lane Loaded					
10	1	0.1 (100%)	1.3 (8%)	3.5 (3%)	5.0 (2%)
11	2	0.8 (13%)	2.0 (5%)	4.9 (2%)	7.7 (1%)
12	3	1.2 (8%)	2.1 (5%)	3.5 (3%)	5.4 (2%)

Note: Conversion factor:1 in = 25.4 mm.

6.2. DYNAMIC LOAD TESTS

The dynamic load allowance (DLA) has been commonly defined as the ratio of the maximum dynamic and static responses regardless of whether the two maximum responses occur simultaneously (Bakht and Pinjarkar 1989, Deng et al. 2015). Equation

(1) was employed to estimate the experimental DLA of Bridge A7957 as reported in (Hernandez and Myers 2017):

$$DLA^{exp} = \frac{D_{dyn}{}^{max} - D_{sta}{}^{max}}{D_{sta}{}^{max}} \quad (1)$$

where DLA^{exp} = experimental dynamic load allowance; $D_{dyn}{}^{max}$ = maximum dynamic (measured) vertical deflection (mm); and $D_{sta}{}^{max}$ = maximum static deflection (mm). Some researchers (Paultre et al. 1992, Deng et al. 2015) have stated that the maximum static response of a bridge can be obtained by (1) conducting a quasi-static test where vehicles move across the bridge at a low speed between 5–16 km/h (3–10 mi/h); (2) filtering the measured dynamic response with a low-pass filter to eliminate the dynamic components of signal; or (3) using finite element models (FEM) to calculate the static response when the vehicle weight and loading position are known.

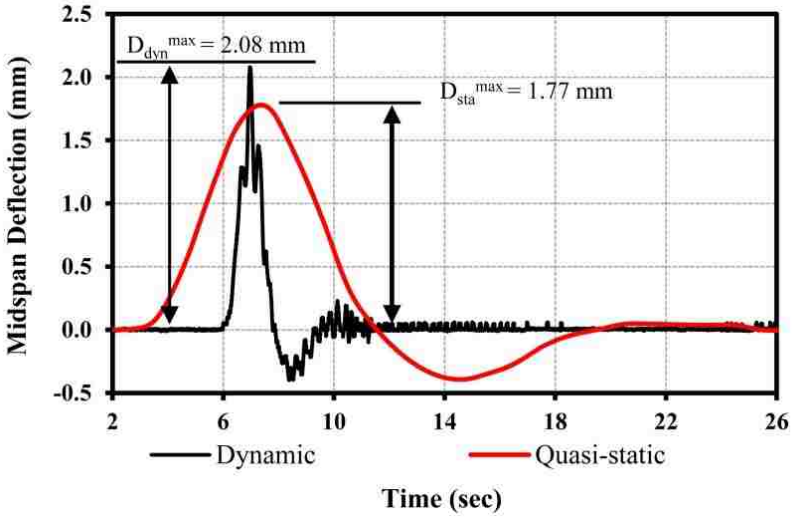

Figure 12. Maximum static and dynamic vertical deflection.
Conversion factor:1 in = 25.4 mm.

In this study, the first option was used to obtain Bridge A7957's DLA (i.e., the values of the D_{dyn}^{max} and D_{sta}^{max} were recorded with the RSV-150 and used to estimate the DLA^{exp}). Dynamic and quasi-static deflection values reported in (Hernandez and Myers 2017) were used to obtain the DLA of Bridge A7957. Figure 12 shows the maximum static and dynamic vertical deflection recorded with the RSV-150 when the truck passed over the bridge at speed of 96 km/h (60 mi/h). The bridge's static and dynamic maximum deflections recorded for the different speeds are listed in Table 3 (rows 3 and 4). Equation (2) was employed to estimate the experimental dynamic amplification factor, DAF^{exp}, listed in row 4 of Table 3:

$$DAF^{exp} = (1 + DLA^{exp}) \tag{2}$$

When the maximum experimental dynamic load allowance value ($DLA^{exp} = 0.175$) listed in Table 3 was compared to the AASHTO LRFD design value presented in (AASHTO 2012), it was observed that the value proposed by AASHTO LRFD ($DLA = 0.33$) was conservative at this initial stage of Bridge A7957's service life. Differences between the experimental and analytical DLA values have repercussions in the assessment and load rating of a bridge structure. For instances, the remaining capacity of a bridge component obtained by means of an analytical load rating might be underestimated when the theoretical value is larger than the experimental DLA. These differences might be attributed to several in-situ factors that are not considered by the approach proposed in current design and evaluation codes (AASHTO 2010). The focus of bridge design specifications is to estimate the value of the dynamic load allowance based on several assumptions that cover a large spectrum of bridges fabricated with different materials, span lengths, and specific in-situ conditions. In this study, the experimentally

obtained DLA values consider in-situ parameters that may improve the bridge's static and dynamic response such as unintended support constraints and continuity, skew angle, contribution of secondary bridge components, and soil-structure interaction. Other parameters such as the surface roughness of a bridge slab, have been recognized as one of the main causes of excitation in vehicle-induced bridge vibrations (Wang and Huang 1992). A poor road surface condition is a key factor in the underestimation of the DLA by current design and evaluation codes. However, the dynamic impact of moving traffic can be reduced if maintenance of the road surface is scheduled regularly. For this study, as the bridge road surface condition was smooth at the time of the load test, its influence was assumed to be unimportant. Moreover, the static and dynamic response of Bridge A7957's spans will vary in the long term as their PC girders (fabricated with conventional concrete and SCC) age or are subjected to overloads. The experimental protocol followed in this study is a useful tool that can be employed to update the DLA of the bridge at different stages of its service life and can provide an in-service, as-built characterization of the bridge's performance. Further research is necessary to isolate the influence of beneficial or detrimental in-situ parameters to the dynamic response of prestressed bridge structures.

Table 3. Dynamic load allowance.

	Truck Speed (km/h)					
	16	32	48	64	80	96
D_{sta}^{max} (mm)	1.77	1.77	1.77	1.77	1.77	1.77
D_{dyn}^{max} (mm)	1.77	1.79	1.79	1.77	2.03	2.08
DLA^{exp}	0.000	0.010	0.010	0.000	0.150	0.175
DAF^{exp}	1.000	1.010	1.010	1.000	1.150	1.175

Note: Conversion factor:1 in = 25.4 mm. 10 mi/h = 16 km/h.

7. FINITE ELEMENT MODELING (FEM)

The commercial finite element (FE) software ABAQUS(Simulia 2012) was used to develop 3D, linear, FE models of Bridge A7957 simulating each of the load stops depicted in Figs. 5–6. The bridge's geometry was created from construction documents and modeled with 20-node, three-dimensional solid elements (Figure 13). The FE models simulated the bridge's geometry considering the primary members (CIP RC deck and PC girders) and secondary members (RC safety barriers and diaphragms). Each bridge component material was assumed to be linear elastic for the level of load applied during the tests. The modulus of elasticity (MOE) of the different bridge components were obtained by averaging the results of MOE tests conducted on companion specimens the same day of the tests. The MOE values of the different bridge component's materials employed to define the geometry of the bridge in ABAQUS are listed in Table 4 as reported in (Hernandez and Myers 2015b, 2016b). Two different sets of MOE values were the model input, depending on whether the static load stop was conducted on days 1 and 2, or day 3 (Table 1). The boundary conditions (supports) were simulated as pin supports by (1) restraining the translation along the global axis *X* (i.e., $u_1 = 0$) of all the nodes located on a middle line (perpendicular to the global *X* axis) on the contact interface between the girders' bottom flange and supports (east and west ends); (2) restraining the translation along the global axis *Y* (i.e., $u_2 = 0$) of a node located at the center of the contact interface between the girders' bottom flange and supports; and (3) restraining the translation along the global axis *Z* (i.e., $u_3 = 0$) of all the nodes located on the contact interface between the girder's bottom flange and supports. The vertical deflection values presented elsewhere (Hernandez and Myers 2016a) were compared to

FEM deflection results to calibrate the FEMs and to reproduce the bridge's initial in-service response with reasonable accuracy. The parameters used to calibrate the FE models included (1) real MOE values of the different bridge components employed to simulate the bridge's geometry; (2) adjusted support conditions to match FEM and experimental vertical deflections; and (3) secondary members (RC safety barriers and diaphragms) included in the FE models. The locations of the trucks over the slab deck and distances between the axles of the trucks were simulated as recorded for each load stop configuration. The truck axles' weight was simulated as concentrated forces applied at the locations where the trucks' wheels loaded the deck. Their values, as reported by MoDOT personnel, were previously presented (Table 1).

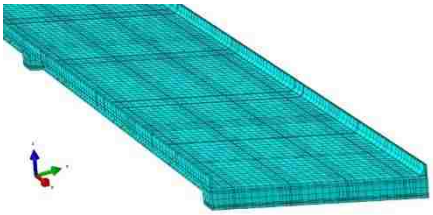

Figure 13. Bridge A7957' FEM geometry.

Table 4. Modulus of elasticity of bridge's components (GPa).

Bridge Component	Test Days (1–2)	Test Day 3
Girders (span 1)	38.80	41.20
Girders (span 2)	39.30	42.25
Girders (span 3)	38.70	39.99
Safety Barrier	35.51	33.78
Deck and Diaphragm	31.03	31.03

Notes: Conversion factor:1 GPa = 145.04 ksi.

8. FEM RESULTS

Figures 14–17 present the vertical deflections obtained with the FEM simulations superimposed to the experimental results. The largest difference between the experimental and FEM deflections was close to 10% for all the interior girders. The

difference might be attributed to two possible sources: first, a slight variation on the application of the truck load on each span; second, the accuracy of the ATS might have affected the measured deflections due to the level of load applied during the test. This difference will be monitored and corrected in future tests by taking caution regarding the location of the truck loads and level of load applied. In general, the FEM simulations represent the bridge's response for the different load configurations with a reasonable accuracy. These calibrated FEMs will be used to predict the response of the bridge in future diagnostic tests and to conduct "virtual" tests simulating the bridge's response of load stops that were not conducted in the field.

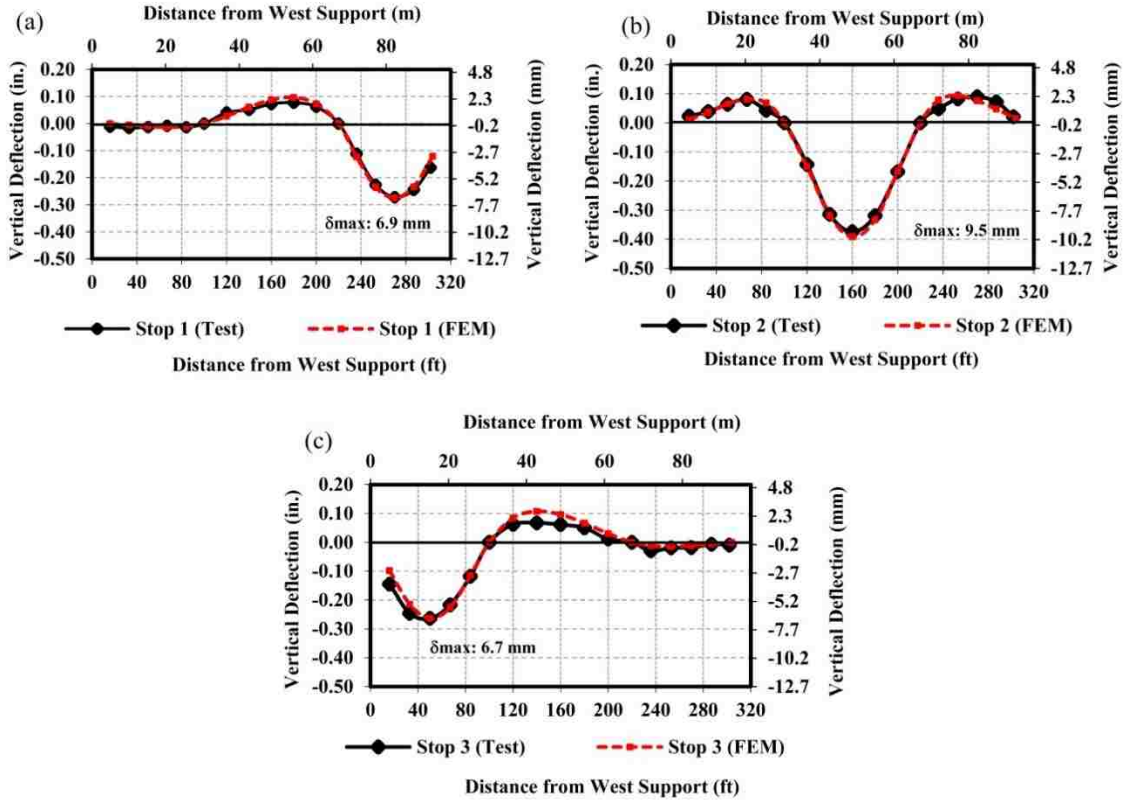

Figure 14. Test vs. FEM results (stops 1–3).

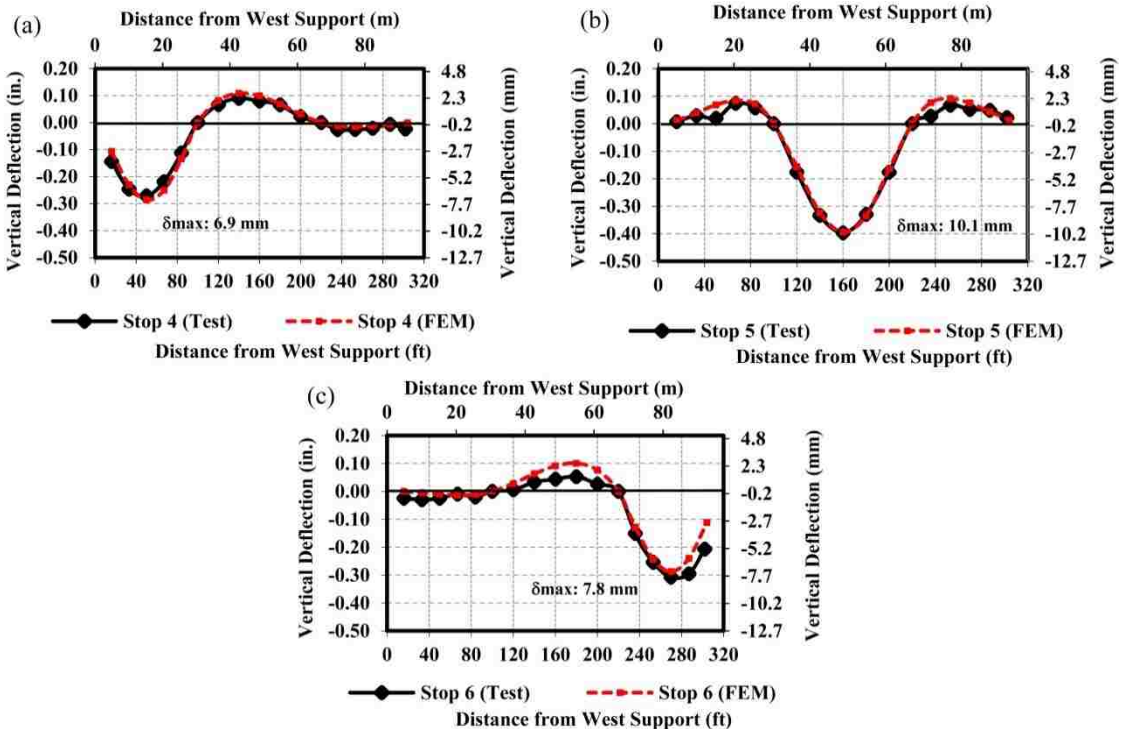

Figure 15. Test vs. FEM results (stops 4–6).

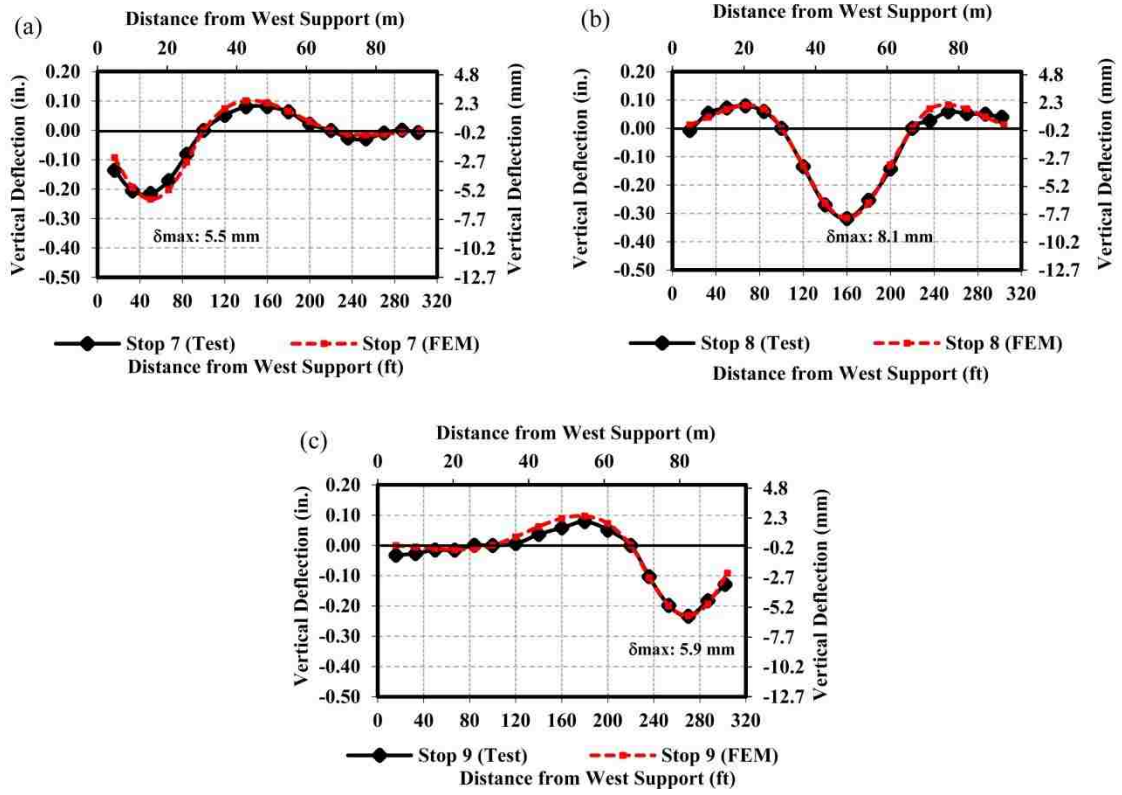

Figure 16. Test vs. FEM results (stops 7–9).

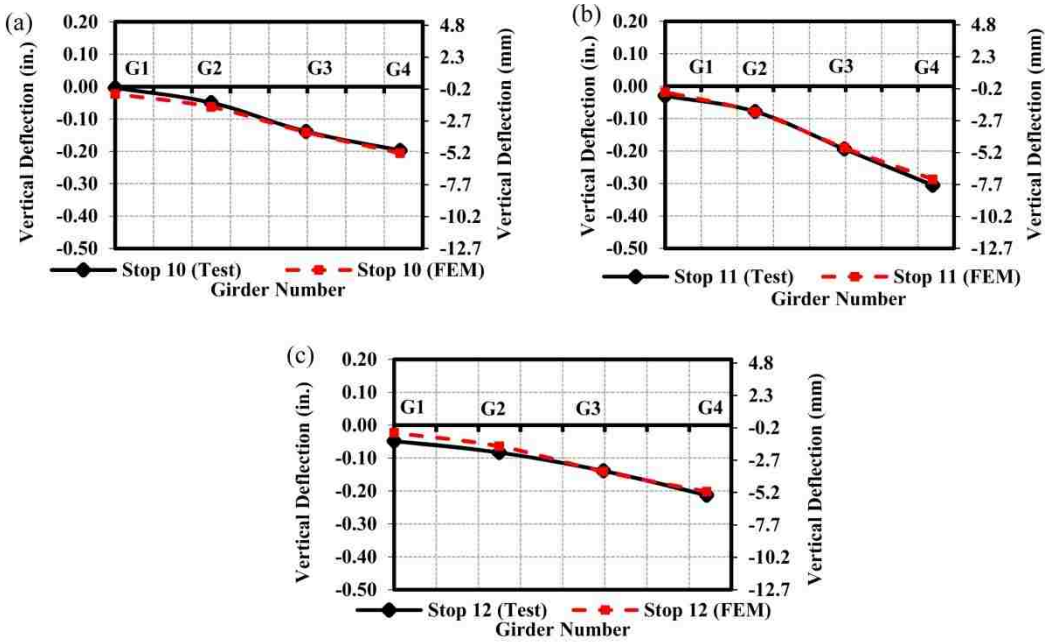

Figure 17. Test vs. FEM results (stops 10–12).

9. SUMMARY AND CONCLUDING REMARKS

The Missouri Department of Transportation executed the first full-scale structure implementation of high-strength self-consolidating concrete (HS-SCC) on Bridge A7957. The first series of diagnostic tests was successfully conducted on Bridge A7957. Static tests were performed to compare the end spans' in-service response and to establish a benchmark of the different spans. These results will be employed to obtain an experimental load rating baseline of Bridge A7957. The structural performance of conventional concrete (span 1) and normal-strength self-consolidating concrete (span 3) PC girders was comparable, suggesting that the short-term structural performance of NS-SCC and HS-SCC PC girders should not prevent its implementation in infrastructure projects. The first series of dynamic load tests were conducted on Bridge A7957 to experimentally establish its baseline dynamic response. The dynamic load allowance (DLA) of Bridge A7957 was obtained from field measurements, which was less

conservative than the current value proposed by the AASHTO LRFD Bridge Design Specifications. The difference might be attributed to the presence of in-situ parameters that improve the bridge's response and are not considered by modern design and evaluation codes. Further research is necessary to isolate the influence of the beneficial or detrimental in-situ parameters to the dynamic response of prestressed bridge structures. In the long term, the static and dynamic response of Bridge A7957's spans will vary as the PC girders, fabricated with conventional concrete and SCC, age or are subjected to overloads. Therefore, it is recommended to continuously monitor and compare the spans' in-service performance to detect any change due to variations in the mechanical properties of the materials (i.e., modulus of elasticity and prestress losses). The experimental protocol followed in this study is a useful tool that can be employed to update the DLA of the bridge at different ages of its service life and can provide an in-service, as-built characterization of the bridge's static and dynamic performance. Finite element models of Bridge A7957 were developed and calibrated using experimental data collected during the different static load stops. The finite element models could represent the bridge's static response with an acceptable level of accuracy. These refined models will be used to predict the bridge's behavior in future diagnostic tests.

AUTHOR CONTRIBUTIONS

ACI member Eli S. Hernandez is a Ph.D. Candidate at Missouri University of Science and Technology, Rolla, Missouri. He received both his BS and his MS from Universidad de los Andes, Merida, Venezuela. He is an associate member of ACI Committee 435, Deflection of Concrete Building Structures and ACI Committee 342,

Evaluation of Concrete Bridges and Bridge Elements. His research interests include fiber-reinforced polymers for strengthening applications and evaluation of bridges.

John J. Myers, Ph.D., P.E., F.ACI, F.ASCE, F.TMS, is a Professor and Associate Dean at Missouri University of Science and Technology, Rolla, MO. He received his BAE from Pennsylvania State University, University Park, PA. He earned both his MS and his PhD from the University of Texas at Austin, Austin, TX. He is the current Chair of ACI Subcommittee 440-L, FRP-Durability. His research interests include advanced concrete materials and fiber-reinforced polymers in strengthening applications.

ACKNOWLEDGEMENTS

The authors gratefully acknowledge the financial support provided by the Missouri Department of Transportation and the National University Transportation Center (NUTC) at Missouri University of Science and Technology.

REFERENCES

American Association of State Highway and Transportation Officials. (AASHTO). (1992). Standard Specifications for Highway Bridges, Washington, DC.

American Association of State Highway and Transportation Officials. (AASHTO). (2010). The Manual for Bridge Evaluation (2nd Edition) with 2011, 2013, 2014 and 2015 Interim Revisions, Washington, DC.

American Association of State Highway and Transportation Officials. (AASHTO). (2012). LRFD Bridge Design Specifications (6th Edition), Washington, DC.

Bakht, B., and Pinjarkar, S. G. (1989). "Dynamic testing of highway bridges. A review." Transportation Research Record 1223, TRB, Washington, D.C., 93-100.

Cai, C. S., and Shahawy, M. (2003). "Understanding capacity rating of bridges from load tests." Pract Period Struct Des Constr, 10.1061/(ASCE)1084-0680(2003)8:4(209), 209-216.

Corp, D. S. S. (2012). "Abaqus Analysis User's Manual." Dassault Systèmes Simulia Corp, Providence, RI. USA.

Deng, L., Yu, Y., Zou, Q., and Cai, C. S. (2015). "State-of-the-art review of dynamic impact factors of highway bridges." J Bridge Eng, 10.1061/(ASCE)BE.1943-5592.0000672, 20 (5), 04014080.

Hernandez, E. S., Griffin, A., and Myers, J. J. (2014). "Balancing extended service life and sustainable concrete material usage in Missouri Bridge A7957." Proc., Struct. Faults & Repair: European Bridge Conference (SF&R), London, England, UK.

Hernandez, E. S., and Myers, J. J. (2015). "Use of self-consolidating concrete and high volume fly ash concrete in Missouri Bridge A7957." ACI SP 304–6, 85-100.

Hernandez, E. S., and Myers, J. J. (2016a). "Field load test and girder distribution factors of Missouri Bridge A7957." 2016 PCI Convention and National Bridge Conference. Nashville, TN.

Hernandez, E. S., and Myers, J. J. (2016b). "Initial in-service response and lateral load distribution of a prestressed self-consolidating concrete bridge using field load tests." Proc., The Fifth International Symposium on Life-Cycle Civil Engineering (IALCCE 2016), CRC Press, Delf, The Netherlands. 1072-1079.

Hernandez, E. S., and Myers, J. J. (2016c). "Monitoring the initial structural performance of a prestressed self-consolidating concrete bridge." Proc., 8th International RILEM Symposium on Self-Compacting Concrete (SCC2016), RILEM Publications SARL, Washington, DC. 401-411.

Hernandez, E. S., and Myers, J. J. (2017). "Dynamic load allowance of a prestressed concrete bridge through field load tests." SMAR 2017 Fourth Conference on Smart Monitoring, Assessment and Rehabilitation of Civil Structures. Zurich, Switzerland.

Keske, S. D., Miller, D. E., Barnes, R. W., and Schindler, A. K. (2014). "Live-load response of in-service bridge constructed with precast, prestressed self-consolidating concrete girders." PCI Journal, 59 (4), 63-76.

Khayat, K. H., and Mitchell, D. (2009). "Self-consolidating concrete for precast, prestressed concrete bridge elements." National Cooperative Highway Research Program Report 628, NCHRP 628, Transportation Research Board, Washington, DC, 2009, pp. 99.

McSaveney, L., Papworth, F., and Khrapko, M. (2011). "Self compacting concrete for superior marine durability and sustainability." Concrete in Australia, 37 (2), 59-64.

Merkle, W. J., and Myers, J. J. (2004). "Use of the total station for load testing of retrofitted bridges with limited access." Proc., Smart Structures and Materials 2004 - Sensors and Smart Structures Technologies for Civil, Mechanical, and Aerospace Systems, San Diego, CA. 687-694.

Myers, J. J., Hernandez, E. S., Alghazali, H., Griffin, A., and Smith, K. (2016). "Self-consolidating concrete (SCC) and high-volume fly ash concrete (HVFAC) for infrastructure elements: implementation." cmr 16-011, Missouri University of Science and Technology, Rolla, Missouri, Jun. 2016, pp. 725.

Myers, J. J., Volz, J., Sells, E., Porterfield, K., Looney, T., Tucker, B., and Holman, K. (2012). "Self-consolidating concrete (SCC) for infrastructure elements." cmr 13-003_A, Missouri University of Science and Technology, Rolla, Missouri, Aug. 2012, pp. 219.

Ouchi, M., Sada-aki, N., Thomas, O., Hallberg, S.-E., and Myint, L. (2003). "Applications of self-compacting concrete in Japan, Europe and the United States." ISHPC, ISHPC, US Federal Highway Administration. Office of Bridge Technology.

Paultre, P., Chaallal, O., and Proulx, J. (1992). "Bridge dynamics and dynamic amplification factors: a review of analytical and experimental findings." Can J Civ Eng, 19 (2), 260-278.

Wang, T. L., and Huang, D. (1992). "Cable stayed bridge vibration due to road surface roughness." Journal of Structural Engineering, doi:10.1061/(ASCE)0733-9445(1992)118:5(1354), 118 (5), 1354-1374.

III. LOAD DISTRIBUTION OF A PRESTRESSED SELF-CONSOLIDATING CONCRETE BRIDGE

E.S. Hernandez[1] and J.J. Myers[2]

[1]Ph.D. Candidate of the Civil, Architectural & Environmental Engineering Department, Missouri University of Science and Technology, 205 Pine Building, 1304 N Pine St, Rolla, MO 65409; email: ehd36@mst.edu

[2]Associate Dean, Professor of the Civil, Architectural & Environmental Engineering Department; Missouri University of Science and Technology; 325 Butler-Carlton Hall, 1401 N Pine St., Missouri University of Science and Technology, Rolla, MO 65409; email: jmyers@mst.edu

ABSTRACT

Bridge A7957 is the first Missouri Department of Transportation (MoDOT) infrastructure in which self-consolidating concrete (SCC) and high-strength self-consolidating concrete (HS-SCC) were implemented. The objective of this research was to monitor the initial in-service behavior of the precast-prestressed concrete primary elements of Bridge A7957 and to experimentally obtain the load distribution factors of the bridge. An initial series of diagnostic load tests was conducted on the bridge's superstructure. Embedded sensors recorded strain variations at instrumented girder sections during different load configurations. An automated total station (ATS) measured the girders' vertical deflection at several sections for different load configurations. Lateral distribution factors were estimated from experimental data (displacements and

strains), finite element models (displacements and strains), and by using the AASHTO LRFD Bridge Design Specifications. Distribution factors estimated with the AASHTO LRFD equations resulted in conservative values compared to experimental and numerical results. No significant difference was observed between the SCC and conventional concrete members' response during this first series of field load tests.

Keywords: Diagnostic load tests, girder distribution factors, load distribution factors, service response, SCC.

1. INTRODUCTION

During the last two decades, self-consolidating concrete (SCC) and high-strength self-consolidating consolidating concrete (HS-SCC) have been successfully implemented in infrastructure projects due to its potential features (Ouchi et al. 2003, McSaveney et al. 2011, Keske et al. 2014, Hernandez and Myers 2015b). The flowable characteristic of SCC results in a better consolidation and placement resulting in fewer voids and honeycombing. A more condensed microstructure increases the concrete's durability properties, leading to a longer service life of the structure. This, combined with reductions in labor and equipment costs as well as decreased maintenance expenses, lessens the project's overall initial costs. In addition, HS-SCC brings to SCC's main attributes an enhanced flexural performance achieved because of increasing the SCC's compressive strength. This stronger flexural feature brings the possibility to reduce the number of main carrying members and interior supports of bridge structures. Despite these and other advantages that come with using SCC and HS-SCC, there are some concerns related to its structural behavior due to its constituent materials and proportions.

The effect of the larger paste content and the smaller coarse aggregate size utilized in the mixture is of particular interest (Myers et al. 2012). Consequently, it is essential to monitor the in-service response of full scale highway infrastructure utilizing self-consolidating and high-strength self-consolidating PC/PS concrete members.

The AASHTO LRFD Bridge Design Specifications (AASHTO 2012) presented a methodology for estimating the lateral load distribution factors that quantify the percentage of the live load applied to a bridge that is carried by a primary supporting member. This approach permits to simplify a three-dimensional (3D) structural analysis into a one-dimensional (1D) problem, which is easier for design engineers to handle (Barker and Pucket 2013). Live load effects, such as bending moments and shear forces, are multiplied by these factors to obtain a design effect that is applied to the 1D member instead of the whole 3D system. The AASHTO LRFD does not propose a method that evaluates how live loads are distributed among the girders for in-service assessments of bridge structures. Instead, this approach proposes a methodology that can be applied to bridges with a wide range of span lengths, girders' spacing and stiffness to conservatively estimate distribution factors for bridge design (Harris 2010).

An alternative for effectively evaluating the in-service performance of a bridge structure and its live load-carrying capacity is provided by field load tests. In general, the AASHTO Manual for Bridge Evaluation (MBE) defines two different types of test options: proof load tests and diagnostic load tests (AASHTO 2010). Proof load tests are employed to obtain the maximum safe live load a bridge can withstand without undergoing inelastic deformations, while diagnostic load tests are used to better understand a bridge's in-service behavior. Diagnostic tests are used to validate design

assumptions and to verify the performance of a structure, most times improved, by implicitly considering in-situ field parameters deemed as beneficial for the bridge's response (Cai and Shahawy 2003). The aim of this research was to oversee the initial in-service response of the precast-prestressed (PC/PS) concrete primary elements of Bridge A7957. A diagnostic test strategy was designed and executed on Bridge A7957 to achieve this goal. In the following sections, the instrumentation, field test program and a comparison between the PC/PS conventional concrete (CC) and SCC members' initial in-service response is presented. In addition, comparisons between the lateral load distribution factors obtained from field measurements, FEM, and the AASHTO LRFD approach are presented in order to estimate the differences that arise when these three alternative approaches are employed to conduct an evaluation of the in-service response of a prestressed concrete bridge.

2. BRIDGE A7957 DESCRIPTION

Bridge A7957, located along Highway 50 in Osage County, Missouri, is a three-span, continuous, PC/PS concrete bridge with a skew angle of 30 degrees (Figure 1). Each span has PC/PS concrete Nebraska University (NU) 53 girders fabricated with different concrete mixtures. Girders in the first span are 30.48 m long and made of conventional concrete (MoDOT's Class A mixture) with a target strength of 55.2 MPa. The second span's girders measure 36.58 m and were fabricated with an HS-SCC mixture of 68.9 MPa. Girders in the third span are 30.48 m long and employ SCC with a nominal compressive strength of 55.2 MPa.

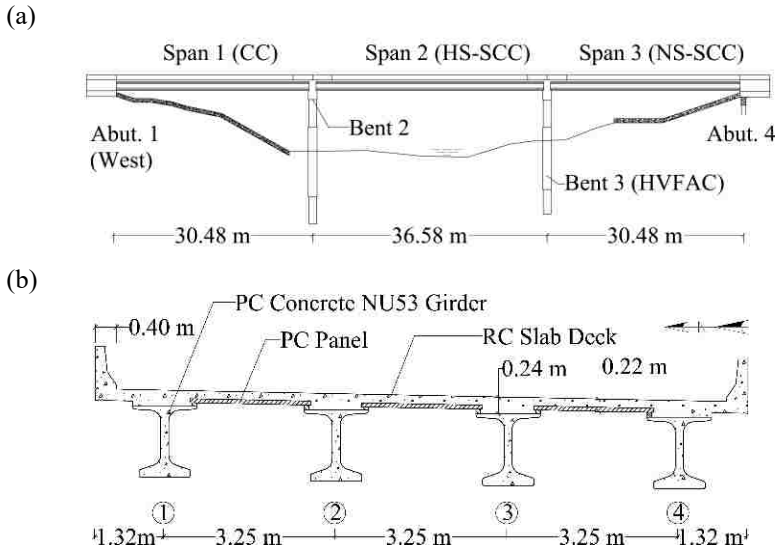

Figure 1. Bridge A7957: (a) elevation; (b) cross-section.

PC/PS concrete panels, with a target compressive strength of 55.2 MPa, span between the girders' top flange underneath the cast-in-place (CIP) reinforced concrete (RC) slab deck in the transverse direction [Figure 1(b)]. The CIP deck was cast with a 25% fly ash replacement of a portland cement mixture with design strength of 27.6 MPa. The bridge superstructure is supported by two abutments and two intermediate bents [Figure 1(a)]. The second intermediate bent and abutments were cast with a concrete mixture that had a 20% fly ash replacement of portland cement and a nominal compressive strength of 20.7 MPa. The third intermediate bent was built using high-volume fly ash concrete (HVFAC) with a 50% fly ash replacement of portland cement and a specified compressive strength of 20.7 MPa.

3. FIELD DATA ACQUISITION

Bridge A7957's structural elements were instrumented during its preconstruction stage. The instrumented elements included: two PC/PS girders per span and two PC/PS

panels (Figure 2). The instrumented panels were deployed at the second midspan, between girder lines 2 and 3, and girder lines 3 and 4, respectively. The type of sensors employed and their installation details are described in the following subsections.

3.1. EMBEDDED SENSORS

A total of 86 vibrating wire strain gauges (VWSG) with built-in thermistors (type EM-5) were used to monitor strain variations from fabrication through service life (Hernandez and Myers 2015b) .

3.1.1. Prestressed Concrete Girders. A total of 62 VWSGs were installed in all spans within the PC/PS girders of lines 3 and 4 before casting. The PC/PS girders' cluster locations at which VWSGs were installed are illustrated in Figure 2. Within girders of spans 1 and 3, the instrumentation clusters were located at two critical sections: the first at the midspan and the second approximately 0.61 m from the support centerline of bents 2 and 3. The clusters in span 2 were arranged at three different cross-sections: one at the midspan and the other sections approximately 0.61 m from each support centerline. Details on the VWSGs installed at the girders' near-support and midspan sections before the concrete was cast are illustrated in Figure 3.

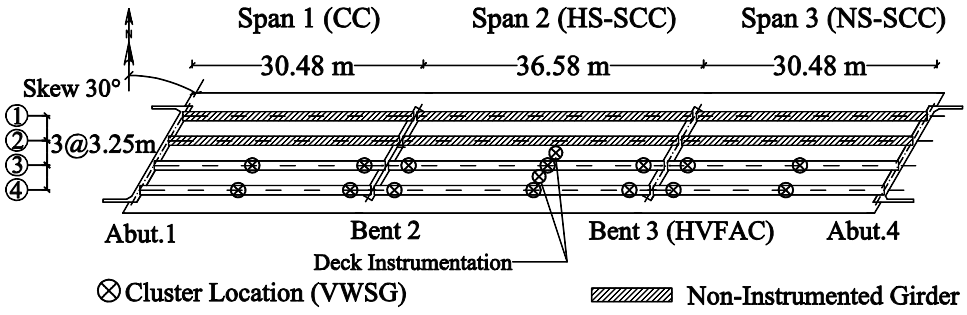

Figure 2. Embedded bridge instrumentation.

The following notation was used to define the location of the VWSGs within the PC/PS girders:

TD: 150 mm (6 in.) from the deck's bottom fiber

BD: 50 mm (2 in.) from the deck's bottom fiber (midspan only)

TF: 50 mm (2 in.) below the girder's top fiber

CGC: center of gravity of composite section

CGU/CGI: center of gravity of non-composite section (midspan only)

CGS: center of gravity of prestressed strands

BF: 50 mm (2 in.) from girder's bottom fiber

3.1.2. Cast-In-Place Deck and Prestressed Concrete Panels. Twenty VWSGs were installed within the CIP RC deck (Figures 2-3) in the longitudinal direction (sensors TD and BD). A VWSG was transversely deployed at the mid-height of two selected PC/PS panels [Figure 3(a)]. Finally, two VWSGs were located in the bridge's transverse direction, between girder lines 2 and 3 and girder lines 3 and 4. These two sensors were placed directly above the panels' sensors, separated 114 mm from the panels' top fiber [Figure 3(a)].

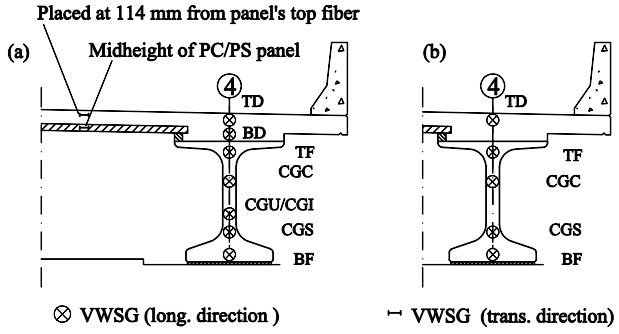

Figure 3. VWSG installation.
(a) Midspan cluster; (b) near-end clusters.

3.2. REMOTE NON-CONTACT EQUIPMENT

An automated total station (ATS), Leica TCA2003 with an accuracy of 1 mm + 1 ppm (distance measurements) and 0.5 arc-seconds (angular measurements), was employed to record the girders' vertical deflection during the live load tests. Twenty-four critical locations were selected to monitor the superstructure response. During the field test, the ATS continuously read the bar codes on the horizontal and vertical planes by projecting a laser ray to the targets (prisms) mounted on the structure (Hernandez and Myers 2018a). The accuracy of the ATS has been reported to be ±0.1 mm (0.004 in.) in vertical deflection measurements (Merkle and Myers 2004). Fifteen ATS prisms were deployed along the third girder at 1/6L, 1/3L, 1/2L, 2/3L, and 5/6L of each span. In addition, three prisms were placed at the girders' midspan (1/2L) for each span (Figure 4). MoDOT H20 dump trucks loaded the bridge superstructure during the tests (Hernandez and Myers 2016a).

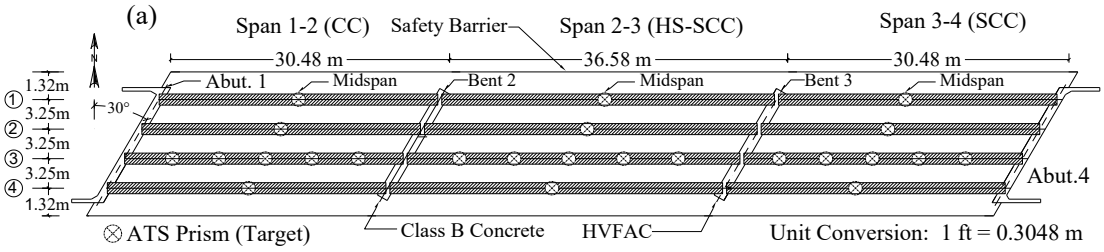

Figure 4. Prisms' location layout.

4. FIELD TEST PROGRAM

A monitoring test program, consisting of the performance of a series of field load tests, was developed to oversee Bridge A7957's service response. The first series of diagnostic load tests was performed in April and August of 2014. A total of thirteen test

configurations are reported herein. The following subsections describe the test procedures and load stop configurations planned to obtain the maximum girders' response in each span. Six H20 dump trucks were employed during the first part of the first series of load tests (April 2014), and three trucks were used in the second part of the tests (August 2014). The trucks were fully loaded with gravel and sand before the tests were started. Figure 5 illustrates the average dimensions of the trucks.

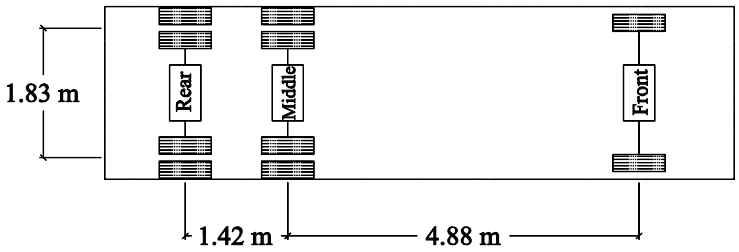

Figure 5. H20 dump truck (average dimensions).

Table 1 lists each truck's weight as reported by MoDOT personnel during the tests. The weight of each truck was assumed to be uniformly distributed between the truck's rear and middle axles. The rear axle weight corresponds to the total weight carried by a truck's rear and middle axles (Figure 5).

Table 1. Trucks' weight.

Test Day	Truck	Rear (kN)	Front (kN)	Total (kN)
1, 2*	1	158.2	74.0	232.2
1, 2*	2	161.6	57.2	218.8
1, 2*	3	150.3	56.0	206.3
1, 2*	4	178.0	75.3	253.3
1, 2*	5	170.2	77.9	248.1
1, 2*	6	166.4	71.6	238.0
3	1	164.6	61.1	225.7
3	2	180.3	70.8	251.1
3	3	169.1	70.4	239.5

Note: * Trucks remained loaded with the same weight on both days. Conversion factor: 1 kN = 0.2248 kip

Figures 6-7 show the load stop configurations used to obtain the maximum bridge's response when a single lane or two lanes were loaded. For the first six load stops, the center of each truck's exterior wheels was placed 3.25 m from the safety barrier's interior edge, as shown in Figure 6(a). In the case of load stops 1-3, two lanes of trucks were driven from east to west and were parked at the center of spans 3, 2, and 1, respectively, as illustrated in Figures 7(a)-7(c).

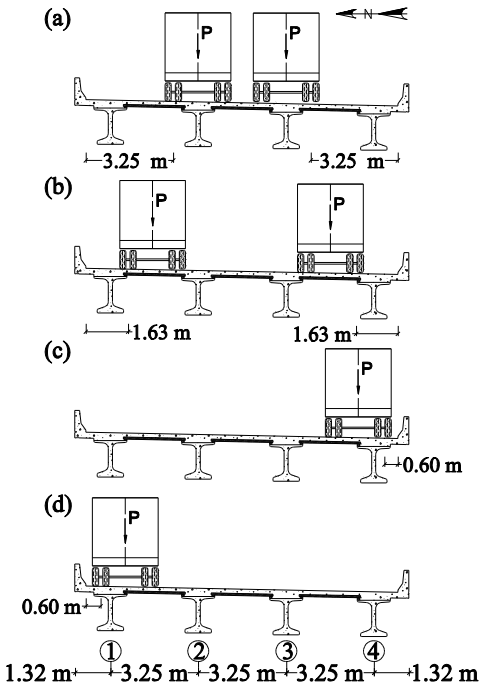

Figure 6. Trucks' distance to safety barrier.

For load stops 4-6, the trucks were driven from west to east and placed at the center of spans 1, 2, and 3, respectively [Figures 7(d)-7(f)]. In stop configurations 7-9 [Figures 7(g)-7(i)], the trucks were driven from west to east, and their exterior axles were located 1.63 m from the barrier's edge [Figure 6(b)]. Load stops 1-9 represented two-lane loads acting on the Bridge A7957's superstructure.

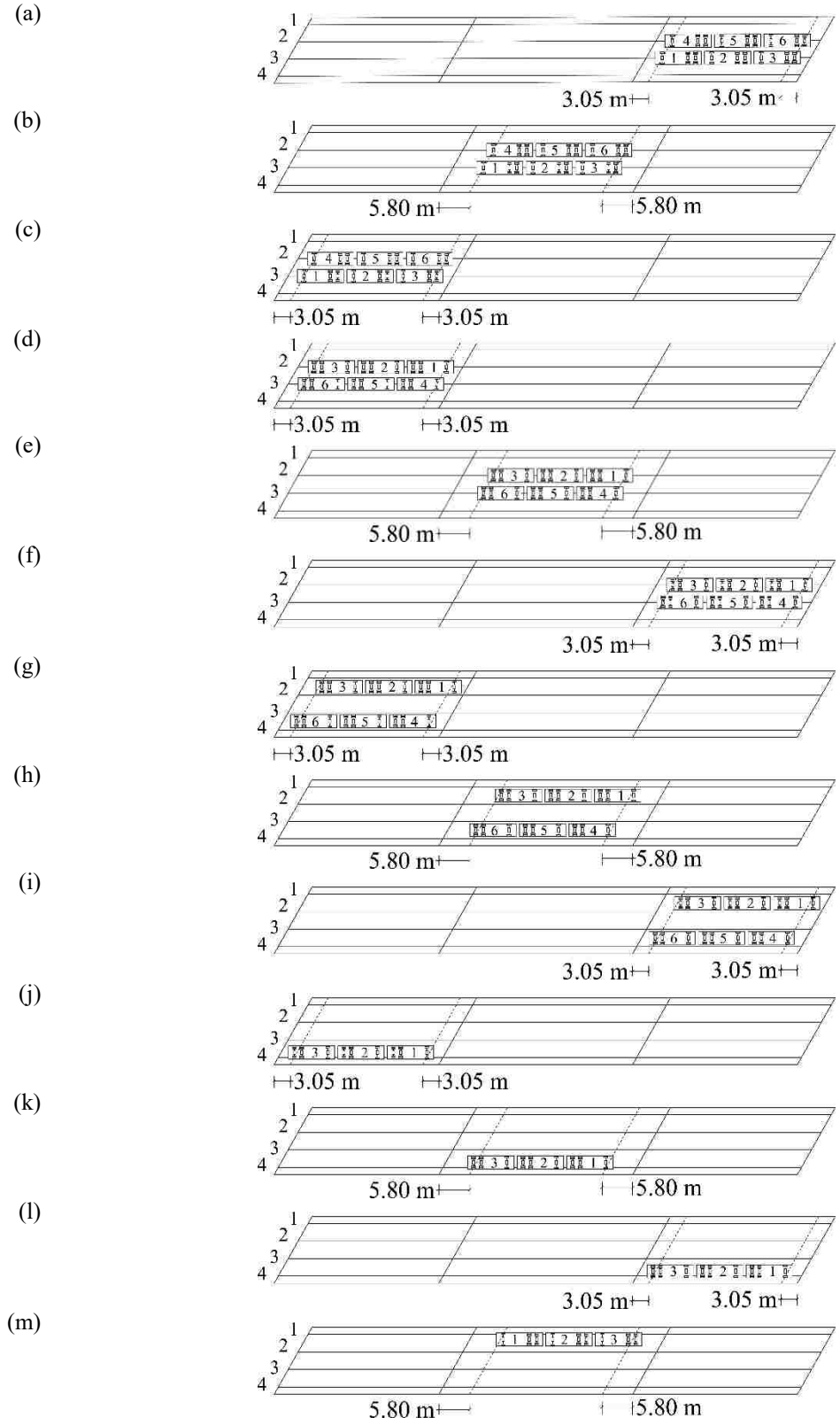

Figure 7. Static load test configurations.

For load stops 10-12 [Figures 7(a)-7(c)], one lane of trucks was moved from west to east, and the trucks were parked on the south side of the bridge, 0.60 m from the barrier's edge [Figure 6(c)]. For load stop 13 [Figure 7(m)], the lane of trucks was driven from east to west, and was placed on the north side of the bridge, 0.60 m from the safety barrier's edge as depicted in Figure 6(d).

5. TEST RESULTS

In the next subsections the static test results obtained during the first series of load tests are presented.

5.1. LONGITUDINAL STRAINS

The girders' bottom flange strain, estimated from experimental data recorded at midspan sections, are reported in Table 2. These values correspond to the two-lane and one-lane load configurations described in the previous section.

Table 2. Experimental longitudinal strains (με).

Stop	Span	ε_{G1}	ε_{G2}	ε_{G3}	ε_{G4}
Two lanes loaded					
1	3	45	83	89	48
2	2	55	95	92	54
3	1	46	84	87	49
4	1	49	87	84	46
5	2	54	92	95	55
6	3	48	89	83	45
7	1	-	-	73	65
8	2	-	-	80	75
9	3	-	-	67	58
One lane loaded					
10	1	-	-	44	64
11	2	4	17	51	78
12	3	-	-	43	65
13	2	78	51	17	4

Larger strains were collected at the exterior and interior girders' mid-span near the area loads were applied. The measured strain values, obtained from two-lane load stop configurations acting on spans 1 and 3 (i.e. stops 1 versus 3, stops 4 versus 6, and stops 7 versus 9), were compared. No significant difference was noted in the in-service exterior and interior girders' response of spans 1 and 3. In load stops 7 and 9 (two-lane load cases), the difference in the reported strain values for the interior and exterior girders was closed to 10 percent. This difference may be attributed to two possible causes. First, the trucks' axle loading the bridge during these load stops might have been placed at locations that differed from the sites (span central regions) shown in Figures 7(g) and 7(i). Second, the test stops might not have lasted enough time to allow the bridge to undergo the total expected flexural response. Both possible sources shall be investigated in future series of load tests. However, the data collected for the two-lane load configurations in spans 1 (CC girders) and span 3 (SCC girders) were very close. These values suggest that the flexural response of these spans was independent of the materials employed to fabricate the PC/PS girders.

5.2. VERTICAL DEFLECTIONS

Table 3 presents the vertical deflections obtained at midspan for the load stops described in the previous section. As in the case of the experimental strains, larger deflections were recorded for the girders close to the region of application of the test loads. Comparable values, corresponding to stops 1 and 3, stops 4 and 6, and stops 7 and 9 (two lanes loaded) were obtained in spans 1 and 3. For one-lane loaded cases (stops 10 and 12), a larger difference ratio was observed when girders 1 and 2 of spans 1 and 3

were compared. This difference can be attributed to the accuracy of the ATS that is close to the measured deflection values. In future load tests, the magnitude of the loads should be planned so that the bridge undergoes vertical deflections larger than the ATS accuracy.

Table 3. Experimental vertical deflections (mm).

Stop	Span	Δ_{G1}	Δ_{G2}	Δ_{G3}	Δ_{G4}
Two lanes loaded					
1	3	4.2	7.1	6.9	4.6
2	2	6.3	9.7	9.5	6.2
3	1	5.1	6.9	6.7	4.9
4	1	4.2	6.7	6.9	4.4
5	2	6.4	9.8	10.1	6.4
6	3	4.9	8.4	7.8	5.2
7	1	4.9	5.1	5.5	5.7
8	2	7.3	7.8	8.1	7.6
9	3	4.4	5.5	5.9	5.9
One lane loaded					
10	1	0.1	1.3	3.5	5.0
11	2	0.8	2.0	4.9	7.7
12	3	1.2	2.1	3.5	5.4
13	2	8.6	5.4	2.6	1.0

Note: Experimental measurements were truncated to the accuracy of the ATS (Hernandez and Myers 2015a, 2018a). Conversion factor: 1 in. = 25.4 mm

In general, the response of the girders in spans 1 and 3 was within the same order of magnitude indicating that the spans' response during the first load tests was independent of the type of material used to fabricate the PC/PS concrete girders.

6. FINITE ELEMENT MODELS

The commercial finite element analysis (FEA) software ABAQUS (Simulia 2012) was used to develop 3D, linear, finite-element models (FEMs) of the bridge superstructure for each of the load stop configurations presented in Figures 6-7. The bridge's geometry was created from construction documents and was modeled with solid elements (Figure 8). The bridge's geometry was modeled considering (1) the primary

members (CIP RC deck and PC/PS concrete girders); (2) the secondary members (RC safety barriers and diaphragms). Each bridge component material was assumed to be linear elastic for the level of load applied during the tests. The modulus of elasticity (MOE) of the different parts was obtained by averaging the results of MOE tests conducted on companion specimens the same day of the tests. Table 4 lists the different bridge components' MOE values used to create the finite element simulations as reported by (Hernandez and Myers 2015b). Two different sets of MOE values were used as input of the FEMs, depending whether the load stop was conducted on day 1 (April 2014) or day 2 (August 2014).

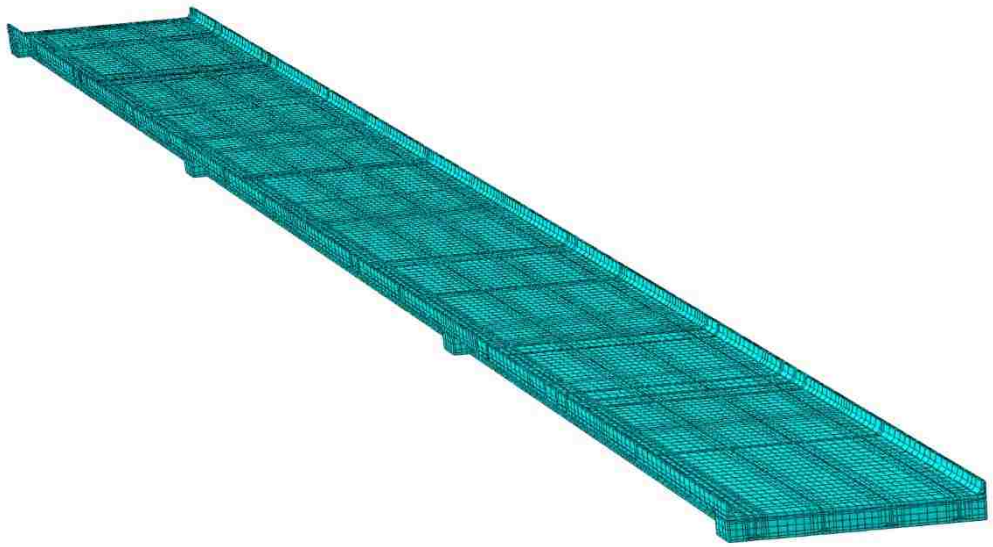

Figure 8. Bridge geometry modeled with FEM.

Experimental deflection values reported by Hernandez and Myers (2016c) were utilized to calibrate and reproduce a FEM geometry that could predict the bridge's response with a reasonable level of accuracy. The calibrated FEM may be used to perform "virtual load tests" simulating load configurations that were not used in the field.

The trucks' positions over the slab deck and distances between the trucks' axles were simulated as recorded for each load configuration.

Table 4. Bridge components' MOE (GPa).

Bridge Component	Day 1	Day 2
Girders (Span 1)	38.80	41.20
Girders (Span 1)	39.30	42.25
Girders (Span 1)	38.70	39.99
Safety Barrier	35.51	33.78
CIP Deck, Diaphragms	31.03	31.03

Note: Conversion factor: 1 GPa. = 145 ksi

Concentrated forces were applied at the location of the trucks' wheels to simulate the axle's weight values reported by MoDOT personnel during the test as presented in Table 1 . Table 5 reports the girders' bottom longitudinal strains at mid-span obtained from the FEM simulations. In general, the finite element models predicted the bridge's response for the different load configurations with a reasonable level of accuracy.

Table 5. FEM longitudinal strains (με).

Stop	Span	ε_{G1}	ε_{G2}	ε_{G3}	ε_{G4}
Two lanes loaded					
1	3	46	86	89	42
2	2	55	101	102	50
3	1	44	86	84	41
4	1	42	87	89	47
5	2	50	101	100	54
6	3	44	87	89	46
7	1	56	70	69	67
8	2	67	80	79	74
9	3	58	69	69	63
One lane loaded					
10	1	4	16	41	66
11	2	2	18	47	76
12	3	4	16	41	65
13	2	76	46	18	2

The largest difference between the obtained experimental and FEM strains was close to 10% for all the interior and exterior girders during most of the load stops. The exception was observed for the exterior girder's strain collected during stop 13 which showed a 50% difference. This higher difference may be attributed to the proximity of the measured strain value to the accuracy of the VWSG sensor. Table 6 presents the experimental deflections recorded for the load stops described in the previous section. Larger deflections were observed for the girders in the near the truck loads. Comparable values, corresponding to stops 1 and 3, stops 4 and 6, and stops 7 and 9 (two lanes loaded) were obtained in spans 1 and 3. For one-lane loaded cases (stops 10 and 12), a larger difference ratio was observed when girders 1 and 2 of spans 1 and 3 were compared.

Table 6. FEM vertical deflections (mm).

Stop	Span	Δ_{G1}	Δ_{G2}	Δ_{G3}	Δ_{G4}
Two lanes loaded					
1	3	4.4	7.1	6.9	4.1
2	2	5.9	10.1	9.9	5.5
3	1	4.1	6.8	6.7	3.9
4	1	4.1	7.0	7.2	4.5
5	2	5.5	9.8	10.0	5.8
6	3	4.3.	7.1	7.3	4.4
7	1	5.0	5.7	6.0	5.6
8	2	6.8	7.7	8.0	7.5
9	3	5.1	5.7	5.9	5.5
One lane loaded					
10	1	0.6	1.6	3.6	5.2
11	2	0.5	2.0	4.8	7.3
12	3	0.6	1.6	3.6	5.1
13	2	7.3	4.8	2.0	0.5

This difference can be attributed to the accuracy of the ATS that is close to the measured deflection values. In future load tests, the magnitude of the loads shall be

planned so that the bridge undergoes vertical deflections larger than the precision of the ATS. In general, the response of the girders in spans 1 and 3 was within the same order of magnitude indicating that the spans' response during the first load tests was independent of the type of material used to fabricate the PC/PS concrete girders.

7. LATERAL LOAD DISTRIBUTION

Lateral distribution factors obtained from field measurements and FEM simulations are defined herein as load distribution factors (LDF). In addition, lateral distribution factors obtained using the AASHTO LRFD approach (AASHTO 2012) are referred to as girder distribution factors (GDF) following the nomenclature used by Cai and Shahawy (2003).

7.1. EXPERIMENTAL LOAD DISTRIBUTION FACTORS

The LDFs for the exterior and interior girders were computed using strain and deflection experimental values.

7.1.1. Field Longitudinal Strains. The LDFs were estimated using experimental strain measurements as follows:

$$LDF_{\varepsilon i}^{E} = n\frac{\varepsilon_i^E}{\sum_i^k \varepsilon_i^E} \quad (1)$$

where $LDF^{E}_{\varepsilon i}$ = experimental load distribution factor of the *i*th girder obtained with longitudinal strains; ε^{E}_{i} = experimental longitudinal strain of the bottom flange (of the *i*th girder at midspan; *n* = number of lanes loaded; and *k* = number of girders.

The bottom-flange strains of PC/PS girders 1 and 2 were required to compute the LDF. As mentioned above, VWSGs were installed at cluster locations along girder lines 3 and 4 (Figures 2-3), which allowed direct recording of the strains for girder's 3 and 4 for each load stop configuration. The girders 1 and 2's strains were indirectly obtained by using the bridge's symmetry and assuming that mirrored image load configurations could produce a symmetrical response of the interior and exterior girders (lines 3 and 4) during the load test. For two-lane load cases, stops 3 and 4 (span 1), stops 2 and 5 (span 2), and stops 1 and 6 (span 3) were considered as symmetrical (Figure 7). Stops 11 and 13 (span 2) were also considered symmetrical load stops for the case of one lane loaded (Figure 7). For instance, during stop 2, girder 3 and 4's strains were directly measured from the installed sensors (Table 5, columns 5-6).

Table 7. Experimental LDFs (estimated with strain measurements).

Stop	Span	$LDF^{E}_{\varepsilon 1}$	$LDF^{E}_{\varepsilon 2}$	$LDF^{E}_{\varepsilon 3}$	$LDF^{E}_{\varepsilon 4}$
Two lanes loaded					
1	3	0.340	0.626	0.672	0.362
2	2	0.372	0.642	0.622	0.365
3	1	0.346	0.632	0.654	0.368
4	1	0.368	0.654	0.632	0.346
5	2	0.365	0.622	0.642	0.372
6	3	0.362	0.672	0.626	0.340
One lane loaded					
11	2	0.027	0.113	0.340	0.520
13	2	0.520	0.340	0.113	0.027

The strains for girders 1 and 2, as reported for stop 2 (Table 5, columns 3-4), were interpreted from the measurements for stop 5 (collected by sensors installed within girders 3 and 4). The same approach was employed to obtain the strains for girders 1 and 2 for the rest of the load stop configurations. The strain values for girders 1 and 2 were not obtained for those load stops without a mirrored load stop image, as was the case of

stops 7-10 and 12. Table 7 presents the LDF values computed using the experimental strains reported in Table 2. No significant difference was observed when the interior and exterior girders' LDFs of spans 1 and 3 were compared.

7.1.2. Field Deflections. The experimental LDFs were estimated using deflection measurements in the following manner:

$$LDF^{E}_{\delta i} = n\frac{\delta^{E}_{i}}{\sum_{i}^{k}\delta^{E}_{i}} \tag{2}$$

where $LDF^{E}_{\delta i}$ = experimental load distribution factor of ith girder estimated with deflection measurements; and δ^{E}_{i} = experimental deflection of the ith girder at midspan. Table 8 lists the LDF values computed using the experimental strains reported in Table 3.

Table 8. Experimental LDFs (estimated with deflection measurements).

Stop	Span	$LDF^{E}_{\delta 1}$	$LDF^{E}_{\delta 2}$	$LDF^{E}_{\delta 3}$	$LDF^{E}_{\delta 4}$
Two lanes loaded					
1	3	0.368	0.623	0.605	0.404
2	2	0.397	0.612	0.599	0.391
3	1	0.432	0.585	0.568	0.415
4	1	0.378	0.604	0.622	0.396
5	2	0.391	0.599	0.618	0.391
6	3	0.373	0.639	0.593	0.395
7	1	0.462	0.481	0.519	0.538
8	2	0.474	0.506	0.526	0.494
9	3	0.406	0.507	0.544	0.544
One lane loaded					
10	1	0.010	0.131	0.354	0.505
11	2	0.052	0.130	0.318	0.500
12	3	0.098	0.172	0.287	0.443
13	2	0.489	0.307	0.148	0.057

The LDF values reported in Table 8 are comparable to the LDF listed in Table 7 suggesting that both variables can be used to estimate the lateral load distribution experimentally.

7.2. NUMERICAL LOAD DISTRIBUTION

7.2.1. FEM Longitudinal Strains. The LDFs were estimated using the numerical strain valuess obtained with FEM simulations as follows:

$$LDF_{\varepsilon i}^{FEM} = n\frac{\varepsilon_i^{FEM}}{\sum_i^k \varepsilon_i^{FEM}} \tag{3}$$

where $LDF^{FEM}{}_{\varepsilon i}$ = numerical (FEM) load distribution factor of the *i*th girder estimated using longitudinal strains; and $\varepsilon^{FEM}{}_i$ = numerical (FEM) longitudinal strain of the bottom flange (of the *ith* girder at midspan.

7.2.2. FEM Deflection. The experimental LDFs were estimated using the numerical deflection values determinded with the FEM simulations in the following manner:

$$LDF_{\delta i}^{FEM} = n\frac{\delta_i^{FEM}}{\sum_i^k \delta_i^{FEM}} \tag{4}$$

where $LDF^{FEM}{}_{\delta i}$ = numerical (FEM) load distribution factor of ith girder estimated using deflection measurements; n = number of lanes loaded; $\delta^{FEM}{}_i$ = numerical (FEM) deflection of the ith girder at midspan; and k = number of girders. The FEM LDF values, reported in Table 9, were determined using Equation (3) and the FEM longitudinal strains reported in Table 5. It was noted that the FEM and experimental LDFs were comparable

and within the same order of magnitude. The FEM LDF values, reported in Table 10, were determined using Equation (4) and the FEM vertical deflections reported in Table 6.

Table 9. FEM LDFs (estimated with strain values).

Stop	Span	$LDF^{FEM}{}_{\delta 1}$	$LDF^{FEM}{}_{\delta 2}$	$LDF^{FEM}{}_{\delta 3}$	$LDF^{FEM}{}_{\delta 4}$
Two lanes loaded					
1	3	0.350	0.654	0.677	0.319
2	2	0.357	0.656	0.662	0.325
3	1	0.345	0.675	0.659	0.322
4	1	0.317	0.657	0.672	0.355
5	2	0.328	0.662	0.656	0.354
6	3	0.331	0.654	0.669	0.346
7	1	0.427	0.534	0.527	0.511
8	2	0.447	0.533	0.527	0.493
9	3	0.448	0.533	0.533	0.486
One lane loaded					
10	1	0.031	0.126	0.323	0.520
11	2	0.014	0.126	0.329	0.531
12	3	0.032	0.127	0.325	0.516
13	2	0.535	0.324	0.127	0.014

Table 10. FEM LDFs (estimated with deflection values).

Stop	Span	$LDF^{E}{}_{\varepsilon 1}$	$LDF^{E}{}_{\varepsilon 2}$	$LDF^{E}{}_{\varepsilon 3}$	$LDF^{E}{}_{\varepsilon 4}$
Two lanes loaded					
1	3	0.391	0.631	0.613	0.364
2	2	0.376	0.643	0.631	0.350
3	1	0.381	0.633	0.623	0.363
4	1	0.360	0.614	0.632	0.395
5	2	0.354	0.630	0.643	0.373
6	3	0.372	0.615	0.632	0.381
7	1	0.448	0.511	0.538	0.502
8	2	0.453	0.513	0.533	0.500
9	3	0.459	0.514	0.532	0.495
One lane loaded					
10	1	0.055	0.145	0.327	0.473
11	2	0.034	0.137	0.329	0.500
12	3	0.055	0.147	0.330	0.468
13	2	0.500	0.329	0.137	0.034

As in the case of the LDFs estimated with experimental and numerical strain values, It was noted that the experimental and numerical LDFs determined with deflection results were comparable and within the same order of magnitude suggesting that the accuracy of the FEM simulations is reasonable. The calibrated FEM models can be used to conduct virtual load test of the bridge superstructure considering load test configurations that were not performed in the field due to time restrictions.

7.3. AASHTO GIRDER DISTRIBUTION FACTORS

The AASHTO LRFD methodology (AASHTO 2012) was used to compute the interior and exterior girder distribution factors (GDFs) for single and multiple loaded lanes. The GDF for an interior girder with two or more (multiple) design lanes loaded was estimated using the following expression:

$$GDF_i^m = 0.075 + \left(\frac{S}{2900}\right)^{0.4}\left(\frac{S}{L}\right)^{0.2}\left(\frac{K_g}{Lt_s{}^3}\right)^{0.1} \quad (5)$$

where S = girder spacing (mm); L = span length (mm); t_s = deck thickness; K_g = stiffness parameter (mm^4); $K_g = n(I_g+e_g{}^2A_g)$; e_g = girder eccentricity (vertical distance from the girder's centroid to the slab's centroid); n = modular ratio (E_{girder}/E_{slab}); E = modulus of elasticity of the concrete computed as $57000(f'_c)^{0.5}$; f'_c = nominal compressive strength of concrete; I_g = girder's moment of inertia (mm^4); and A_g = area of the girder's cross section (mm^2). The interior girder's GDF with a single lane loaded was computed as follows:

$$GDF_i^s = 0.06 + \left(\frac{S}{4300}\right)^{0.4}\left(\frac{S}{L}\right)^{0.3}\left(\frac{K_g}{Lt_s{}^3}\right)^{0.1} \quad (6)$$

The exterior girder's GDF for two or more design lanes loaded was computed with the following expressions

$$GDF_e^m = e(GDF_i^m) \tag{7}$$

$$e = 0.77 + \frac{d_e}{2800} \geq 1 \tag{8}$$

where d_e = horizontal distance from exterior girder's centroid to barrier's edge (mm). The simple static distribution approach, also known as the lever rule, was employed to estimate the exterior GDF for a single lane loaded. Equation (9) was written by assuming a hinge at an interior support (girder 2 or 3) and by summing moments, produced by the forces and reactions, about girder 2 or 3 (depending on which support was selected to obtain the GDF). For example, the forces acting to the left side of girder 2 (when a hinge is assumed at this support) are the reaction and load *P* for girder 1 [Figure 6(d)]. Thus:

$$GDF_e^s = m_p\left(\frac{S + d_e - 1524}{S}\right) \tag{9}$$

where m_p = multiple presence factor (equal to 1.2 for a single lane loaded). A skew factor was estimated with Equations 7-8 to modify the AASHTO GDF values.

$$SF = 1 - C_1(\tan\theta)^{1.5} \tag{10}$$

$$C_1 = 0.25\left(\frac{K_g}{Lt_s{}^3}\right)^{0.25}\left(\frac{S}{L}\right)^{0.5} \tag{11}$$

where *SF* = skew correction factor (if $30^o \leq \theta \leq 60^o$); and θ = skew angle. Table 11 summarizes the bridge's parameters employed to determine the exterior and interior girders' GDF.

Table 11. Bridge design parameters.

Variable	Spans 1 and 3	Span 2
Ag (mm2)	479.9x103	479.9x103
Ig (mm4)	1.2383x1011	1.2383x1011
Kg (mm4)	702.207x109	785.936x109
de (mm)	914	914

Table 12 lists the GDF values obtained according to AASHTO LRFD approach.

Table 12. AASHTO LRFD GDFs.

Span	Case (lanes loaded)	*GDFi*	*GDFi* (corrected)	*GDFe*	*GDFe* (corrected)
1, 3	≥ 2	0.819	0.783	0.901	0.861
1, 3	1	0.558	0.533	0.975	0.932
2	≥ 2	0.788	0.756	0.866	0.832
2	1	0.528	0.507	0.975	0.936

Note: Skew factors were used to modify the GDFs.

8. RESULTS AND DISCUSSION

The interior and exterior lateral distribution factors are designated as the maximum estimated LDF or GDF when single-lane or multiple-lane load cases are evaluated. Several critical load scenarios were assessed to obtain the maximum effect acting within the bridge's primary members. The interior load distribution, LDF_{int}, which was calculated from experimental data and FEM results, corresponded to 0.672 and 0.677, respectively. Furthermore, the exterior load distribution factor, LDF_{ext}, attained from test and FEM data was 0.520 and 0.535, respectively. The maximum difference observed was close to 3%, suggesting that the calibrated FEM were capable of reproducing the bridge's behavior with an acceptable level of accuracy for the level of load applied during the diagnostic load tests.

The computed AASHTO LRFD interior and exterior girder distribution factors, GDF_{int} and GDF_{ext}, were 0.783, and 0.936, respectively. These values represent approximately a 17% and 80% difference for the interior and exterior girder lateral load distribution factors. These results imply that the AASHTO LRFD GDF values are more conservative than the LDF values obtained from experimental data and FEM simulations.

It should be noted that the AASHTO LRFD methodology is suitable for bridge design. Consequently, this methodology is not intended to assess the load distribution response of existing bridges for which diagnostic load tests have demonstrated to be more appropriate.

9. CONCLUSIONS

The first series of diagnostic load tests was conducted on Bridge A7957 to evaluate the initial in-service response and the lateral load distribution of its PC/PS members. The structural behavior of the SCC and CC PC/PS girders was comparable, suggesting that the structural performance of SCC and HS-SCC PC/PS girders should not prevent its implementation in future infrastructure projects. Finite element models of the bridge were developed to predict the bridge's behavior for the different load configurations. The FEM were capable of predicting the bridge's response with an acceptable level of accuracy. These calibrated models will be used to predict the bridge's response of future in-service live load tests. LDF were estimated from field measurements and FEM simulations, and GDFs were obtained using the AASHTO LRFD approach. The AASHTO LRFD GDFs resulted in larger values compared to experimental LDF. These differences may be attributed to several causes. The AASHTO

LRFD equations were developed to be applied to different types of bridges with a wide range of span lengths, girders spacing, and stiffness. LDF, obtained from field tests, implicitly consider field conditions such and unintended support restraints, skew angle, contribution of secondary members, and multiple presence factors, which may contribute to improve the bridge's in-service structural performance. More research should be conducted to evaluate such differences and the range of applicability of each approach.

ACKNOWLEDGEMENTS

The authors gratefully acknowledge the financial support provided by the Missouri Department of Transportation (MoDOT) and the National University Transportation Center (NUTC) at the Missouri University of Science and Technology (Missouri S&T). A special thank you is addressed to the Civil, Architectural, and Environmental Engineering Department and the Center for Infrastructure Studies at Missouri S&T for the support received during the realizations of this study.

REFERENCES

American Association of State Highway and Transportation Officials. (AASHTO). (2010). The Manual for Bridge Evaluation (2nd Edition) with 2011, 2013, 2014 and 2015 Interim Revisions, Washington, DC.

American Association of State Highway and Transportation Officials. (AASHTO). (2012). LRFD Bridge Design Specifications (6th Edition), Washington, DC.

Barker, R. M., and Pucket, J. A. (2013). Design of Highway Bridges: An LRFD Approach, John Wiley & Sons, 3rd Edition, Hoboken, N.J. USA.

Cai, C. S., and Shahawy, M. (2003). "Understanding capacity rating of bridges from load tests." Pract Period Struct Des Constr, 10.1061/(ASCE)1084-0680(2003)8:4(209), 209-216.

Harris, D. K. (2010). "Assessment of flexural lateral load distribution methodologies for stringer bridges." Eng Struct, 10.1016/j.engstruct.2010.06.008, 32 3443-3451.

Hernandez, E. S., and Myers, J. J. (2015a). "In-situ field test and service response of Missouri Bridge A7957." 16th European Bridge Conference (EBC16), Edinburgh, Scotland, UK.

Hernandez, E. S., and Myers, J. J. (2015b). "Use of self-consolidating concrete and high volume fly ash concrete in Missouri Bridge A7957." Sustainable Performance of Concrete Bridges and Elements Subjected to Aggressive Environments: Monitoring, Evaluation and Rehabilitation, ACI SP 304 (6). 85-100.

Hernandez, E. S., and Myers, J. J. (2016a). "Field load test and girder distribution factors of Missouri Bridge A7957." Proc., 2016 PCI Convention and National Bridge Conference, Nashville, TN.

Hernandez, E. S., and Myers, J. J. (2016b). "Field Load Test and Girder Distribution Factors of Missouri Bridge A7957." 2016 PCI Convention and National Bridge Conference, Nashville, TN, USA.

Hernandez, E. S., and Myers, J. J. (2016c). "Monitoring the initial structural performance of a prestressed self-consolidating concrete bridge." Proc., 8th International RILEM Symposium on Self-Compacting Concrete (SCC2016), RILEM Publications SARL, Washington, DC. 401-411.

Hernandez, E. S., and Myers, J. J. (2018). "Diagnostic test for load rating of a prestressed SCC bridge." Evaluation of Concrete Bridge Behavior Through Load Testing - International Perspective, ACI SP 323 (13).

Keske, S. D., Miller, D. E., Barnes, R. W., and Schindler, A. K. (2014). "Live-load response of in-service bridge constructed with precast, prestressed self-consolidating concrete girders." PCI Journal, 59 (4). 63-76.

McSaveney, L., Papworth, F., and Khrapko, M. (2011). "Self compacting concrete for superior marine durability and sustainability." Concrete in Australia, 37 (2). 59-64.

Merkle, W. J., and Myers, J. J. (2004). "Use of the total station for load testing of retrofitted bridges with limited access." Proc., Smart Structures and Materials 2004 - Sensors and Smart Structures Technologies for Civil, Mechanical, and Aerospace Systems, San Diego, CA. 687-694.

Myers, J. J., Volz, J., Sells, E., Porterfield, K., Looney, T., Tucker, B., and Holman, K. (2012). "Self-consolidating concrete (SCC) for infrastructure elements." cmr 13-003_A, Missouri University of Science and Technology, Rolla, Missouri, Aug. 2012, pp. 219.

Ouchi, M., Sada-aki, N., Thomas, O., Hallberg, S.-E., and Myint, L. (2003). "Applications of self-compacting concrete in Japan, Europe and the United States." ISHPC, ISHPC, US Federal Highway Administration. Office of Bridge Technology.

Simulia (2012) Abaqus Analysis User's Manual. Version 6.12. Providence, RI. USA, Dassault Systèmes Simulia Corp.

IV. STRENGTH EVALUATION OF PRESTRESSED CONCRETE BRIDGES BY DYNAMIC LOAD TESTING

E.S. Hernandez[1] and J.J. Myers[2]

[1]Ph.D. Candidate of the Civil, Architectural & Environmental Engineering Department, Missouri University of Science and Technology, 205 Pine Building, 1304 N Pine St, Rolla, MO 65409; email: ehd36@mst.edu

[2]Associate Dean, Professor of the Civil, Architectural & Environmental Engineering Department; Missouri University of Science and Technology; 325 Butler-Carlton Hall, 1401 N Pine St., Missouri University of Science and Technology, Rolla, MO 65409; email: jmyers@mst.edu

ABSTRACT

The load rating of a bridge can be obtained by means of field load testing. The dynamic load allowance or impact factor is one of the parameters used to establish a bridge's flexural capacity during the rating evaluation process. The focus of this study centered on comparing Bridge A7957's dynamic load allowance obtained by experimental and analytical methods proposed in three different design and evaluation codes. To attain this goal, Bridge A7957 was instrumented with accelerometers at different locations. For different dynamic tests, the spans' response was measured with the accelerometers and a laser vibrometer. The dynamic load allowance was obtained experimentally and analytically using current design and evaluation codes. The impact factors obtained analytically resulted in larger values compared to the experimental

results. This difference might have repercussions in the strength evaluation results of bridge structures.

Keywords: Dynamic load allowance, impact factor, prestressed concrete bridges, strength evaluation.

1. INTRODUCTION

Field testing has largely confirmed reserves of strength capacity in existing bridges despite their age and existing condition. The sources that explain these differences might be diverse and may be attributed to field parameters that are not considered during the design or strength evaluation process of a bridge structure. The impact factor (IM) or dynamic load allowance (DLA) is a parameter that can be verified by means of a dynamic load test (Cai and Shahawy 2003, AASHTO 2010). Most design codes consider the dynamic load effects, by increasing the magnitude of the static live load applied to a bridge structure in some fraction. An accurate estimation of the DLA yields safe and rational load ratings of existing bridge structures. However, the complex nature of the factors affecting the DLA makes it difficult to estimate its value during the design and strength evaluation of a bridge (Barker and Pucket 2013).

The main objective of this study was to obtain the dynamic load allowance of Bridge A7957 by analytical and experimental methods to compare differences that may arise when both approaches are employed in bridge design and evaluation. To achieve this goal, the dynamic response of Bridge A7957's exterior spans was recorded with accelerometers and a laser vibrometer. The dynamic load allowance (or impact factor) was estimated using the analytical provisions proposed by the Ontario Highway Bridge

Design Code (OHBDC) (OMTC 1983), the American Association of State Highway and Transportation Officials (AASHTO) Standard Specifications (AASHTO 1992), and the AASHTO LRFD Bridge Design Specifications (AASHTO 2012). The experimental DLA was estimated by comparing the measured dynamic and static responses of the bridge structure. The following sections detail the instrumentation plan and the static and dynamic tests conducted on Bridge A7957 to estimate its experimental dynamic load allowance before the structure was open in service.

2. ANALYTICAL AND EXPERIMENTAL DYNAMIC LOAD ALLOWANCE

Design codes have traditionally proposed analytical expressions to estimate the dynamic load allowance of a bridge structure as a function of the span length or the fundamental frequency of a bridge. In 1983, the Ontario Highway Bridge Design Code (OHBDC) presented an approach that allows to estimate the DLA in terms of the fundamental frequency of the bridge structure as Figure 1 illustrates.

The AASHTO Standard Specifications (AASHTO 1992) recommend an expression to estimate the impact factor in terms of the span length, L, as presented in Equation (1):

$$IM = \frac{15.24}{L + 38} \leq 0.30 \tag{1}$$

In 1994, the AASHTO LRFD Bridge Design Specifications (AASHTO 2012) replaced the term *impact factor* used in the AASHTO Standard Specifications (AASHTO 1992) with the term *dynamic load allowance*. A DLA value independent of the span

length was adopted as equal to 0.33 (33% of the static live load) for bridge components other than the deck.

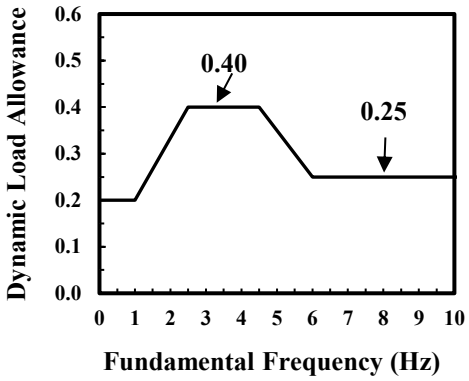

Figure 1. Dynamic load allowance vs. fundamental frequency.
(OMTC 1983, Paultre et al. 1992).

Several experimental definitions of the DLA have been reported in literature (Bakht and Pinjarkar 1989). As presented by Deng et al. (2015), the DLA is commonly defined as the ratio of the maximum dynamic and static responses regardless of whether the two maximum responses occur simultaneously. Equation (2) allows to calculate the DLA according to this definition.

$$DLA = \frac{R_{dyn} - R_{sta}}{R_{sta}} \tag{2}$$

where DLA = dynamic load allowance; R_{dyn} = maximum dynamic response; and R_{sta} = maximum static response. The estimation of the static response can be obtained by: (1) conducting a quasi-static test where vehicles move across the bridge at a low speed between 5–16 km/h; (2) filtering the measured dynamic response with a low-pass filter to eliminate the dynamic components of the signal; and (3) using finite element models

(FEM) to calculate the static response when the vehicle weight and loading position are known (Paultre et al. 1992, Deng et al. 2015). In this study, the first and third options were selected and compared to estimate Bridge A7957's DLA.

3. BRIDGE DESCRIPTION

Bridge A7957, built along Highway 50 in Osage County, Missouri, is a three-span, continuous, precast-prestressed (PC/PS) concrete bridge with a 30-degree skew angle (Figures 2 and 3), and excellent road surface condition. Each span has PC/PS concrete Nebraska University 53 (NU53) girders (Hernandez and Myers 2015b, Hernandez and Myers 2016a). The first span's girders are 30.48 m long and fabricated with conventional concrete (CC), defined by the Missouri Department of Transportation (MoDOT) as a Class A mixture, with a compressive strength of 55.2 MPa.

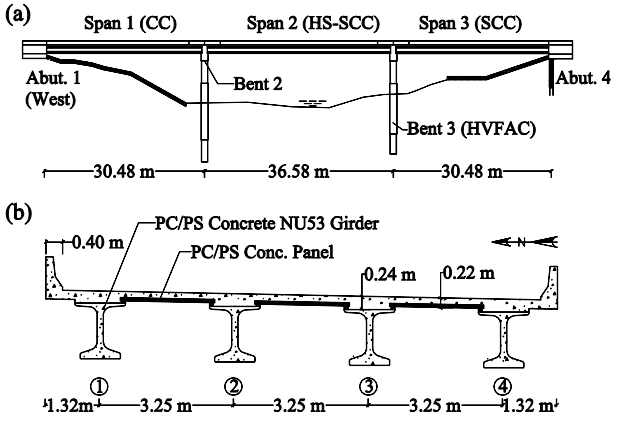

Figure 2. Bridge A7957. (a) elevation; (b) cross-section.

The second span's girders are 36.58 m long and cast with high-strength self-consolidating concrete (HS-SCC) of 68.9 MPa. Girders in the third span are 30.48 m long and employed normal-strength self-consolidating concrete (NS-SCC) with a nominal

compressive strength of 55.2 MPa. The cast-in-place (CIP) deck was built with a 25% fly ash replacement of a portland cement mixture with design compressive strength of 27.6 MPa. The PC/PS concrete panels, with a target compressive strength of 55.2 MPa, span between the girders' top flange underneath the CIP deck in the transverse direction [Figure 2(b)]. The superstructure is supported by two abutments and two intermediate bents [Figure 2(a)] with target compressive strength of 20.7 MPa. The second intermediate bent and abutments were cast with a concrete mixture that used a 20% fly ash replacement of portland cement and a nominal compressive strength of 20.7 MPa. The third intermediate bent was built using high-volume fly ash concrete (HVFAC) with a 50% fly ash replacement of portland cement and a specified compressive strength of 20.7 MPa.

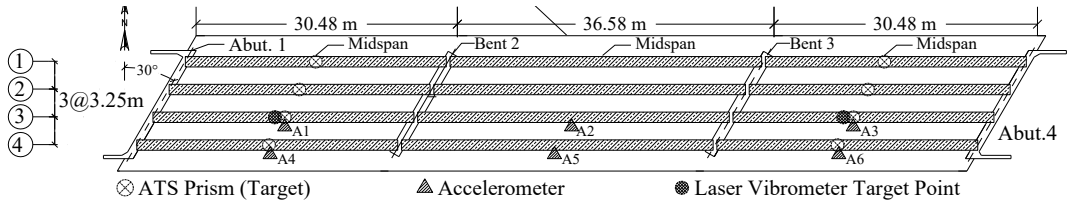

Figure 3. Bridge A7957 plan view and instrumentation layout.

4. FIELD TEST EQUIPMENT

The instrumentation was designed to collect: (1) the static vertical deflection at midspan of girders 1–4 (spans 1 and 3); (2) the dynamic deflection at midspan of girder 3 (spans 1 and 3); and (3) girder 3 and 4's vertical acceleration at midspan locations (Fig. 3). The details about the sensors employed and their installation are described next.

4.1. ACCELEROMETERS

Six accelerometers were deployed on the bridge superstructure to record the vertical acceleration at midspan sections of PC/PS concrete girders 3 and 4 (Figure 3). Figures 3 and 4(a) show details of the measurement instruments mounted to the girders' bottom flange (only at midspan sections).

4.2. AUTOMATED TOTAL STATION (ATS)

An automated total station (ATS), Leica TCA 2003, was used to estimate the girders' deflection during the static test conducted on the first and third spans. The ATS recorded the coordinates of targets (prisms) placed at the exterior-span girders' bottom flange (at midspan sections), as illustrated in Figures 3-4. The ATS has an accuracy of 1 mm ± 1 ppm (distance measurements) and 0.5 arc-seconds (angular measurements). The accuracy of the ATS has been reported as 0.1 mm in vertical deflection measurements (Merkle and Myers 2004).

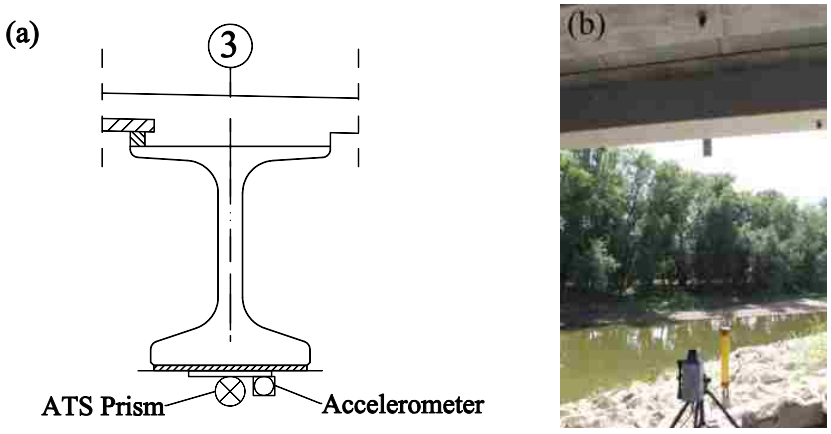

Figure 4. Girder 3's instrumentation.
(a) ATS prism and accelerometer. (b) Remote sensing vibrometer (RSV-150).

4.3. REMOTE SENSING VIBROMETER

The remote sensor vibrometer (RSV-150), shown in Figure 4(b), was employed to record the dynamic bridge response (vertical deflection) of the exterior spans' girder 3 (at midspan). The RSV-150 has a bandwidth up to 2 MHz for nondestructive test (NDT) measurements and can detect the vibration and displacement of distant structures. The accuracy of the RSV-150 to record the dynamic response of a point is ± 0.025mm.

5. FIELD TEST PROCEDURE

Static and dynamic tests were conducted on Bridge A7957. The following subsections depict the test procedure and load configurations planned to obtain the maximum static and dynamic responses of the bridge superstructure.

5.1. STATIC TEST

Static load tests were performed on the exterior spans of the bridge. A MoDOT H20 dump truck was utilized to obtain the maximum static response of the bridge superstructure. Quasi-static tests were conducted by passing the truck at a crawl speed of 16 km/h. Figure 5 shows the average truck's dimensions and weight. Figure 6 illustrates the load configuration applied to spans 1 and 3 during the static tests 1and 2

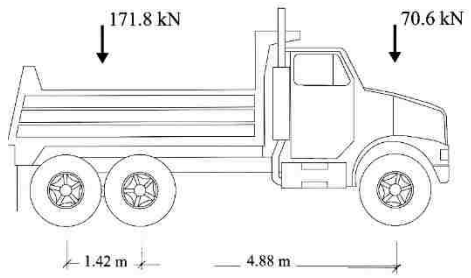

Figure 5. MoDOT H20 dump truck (average dimensions).

5.2. DYNAMIC TEST

Speeds varying from 16 km/h to 96.6 km/h were used during the dynamic load tests. For each test, the truck speed was increased at a rate of 16 km/h until the maximum speed of 96 km/h was attained. The maximum dynamic and static responses were compared to estimate the experimental dynamic load allowance. Experimental data was recorded with the RSV-150 at a sampling rate of 120 Hz. The truck was driven over the south side of the bridge (along the west–east and east–west directions), separated 0.60 m from the safety barrier's edge.

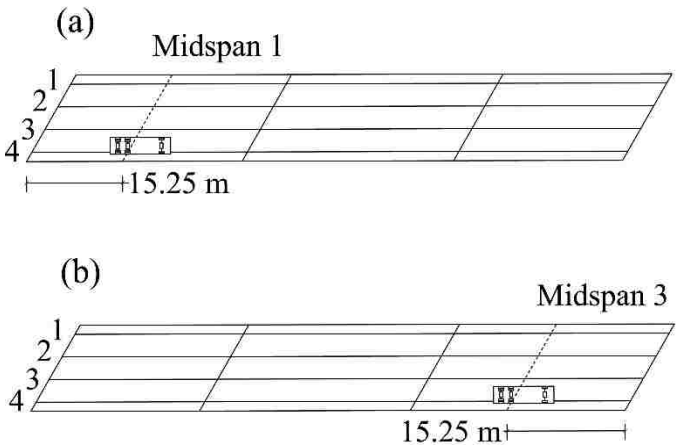

Figure 6. Static test configurations.
(a) Static test 1 (span 1). (b) Static test 2 (span 3).

6. FINITE ELEMENT MODELING

The commercial finite element software ABAQUS (Simulia 2012) was employed to create 3D, linear, finite-element simulations of Bridge A7957 for each of the load stops described in Figure 6. The bridge's geometry was created from construction documents and was modeled with solid elements (Figure 7). The finite element models simulated the bridge's geometry considering the primary members (CIP RC deck and PC/PS concrete

girders) and secondary members (RC safety barriers and diaphragms). Each bridge component material was assumed to be linear elastic for the level of load applied during the tests. The modulus of elasticity (MOE) of the different bridge components was obtained by averaging the results of MOE tests conducted on companion specimens the same day of the tests. Table 1 lists the modulus of elasticity of the different bridge component that were used to create the finite element simulations as reported by and (Hernandez and Myers 2015a, 2016b). Two different sets of MOE values were used as the FEM input, depending on whether the load stop was conducted in April or August of 2014. Experimental deflection values reported by Hernandez and Myers (2016c) were utilized to calibrate the finite element models and to reproduce a geometry that could predict the bridge's response with a reasonable level of accuracy. The trucks' positions over the slab deck and distances between the trucks' axles were simulated as recorded for each load configuration. Concentrated forces were applied at the location of the trucks' wheels to simulate the axle's weight values reported by MoDOT personnel.

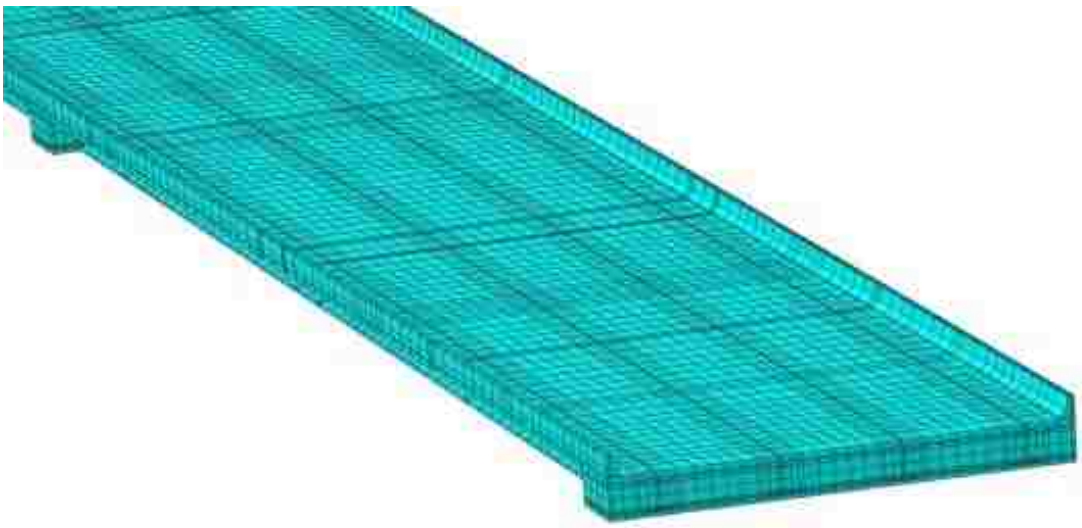

Figure 7. Bridge A7957's finite element model geometry.

Table 1. Bridge components' MOE.

Bridge Component	April Test (GPa)	August Test (GPa)
Span 1's Girders	38.80	41.20
Span 2's Girders	39.30	42.25
Span 3's Girders	38.70	39.99
Safety Barriers	35.51	33.78
CIP Deck, Diaphragms	31.03	31.03

7. LOAD TEST RESULTS

The vertical static deflection measured at midspan locations of the end spans 1 and 3's girders are shown in Figure 8. Although both exterior spans have the same geometry (Figure 2) and were subjected to the same truck load, a 5% difference was observed between the deflection responses recorded at midspan 1 and 3. The difference might be attributed to: first, a slight variation on the application of the truck load on each span; second, the accuracy of the ATS might have affected the experimental values due to the low level of load applied during the test. This difference may be corrected in future tests by taking caution regarding the location of truck loads and the level of load used during the test. The level of load applied needs to be relatively high so that the error of ATS measurements is kept low during data recording. In addition, Girder 3's static deflection at midspan (Figure 8) was compared to the quasi-static (filtered) response recorded with the RSV-150 when the truck passed over the bridge at a crawl speed of 16 km/h and the static deflection value obtained with the FEM simulations. These comparisons were conducted to verify if the quasi-static deflection recorded with the RSV-150 was representative of the bridge's static response and could be used to estimate the dynamic load allowance.

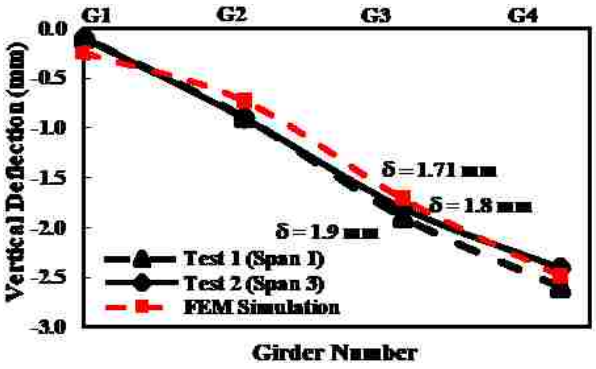

Figure 8. Vertical static deflection (girders' midspan).

Figure 9(a) presents the acceleration response collected with sensor A1 (Figure 3) deployed at girder 3's midspan.

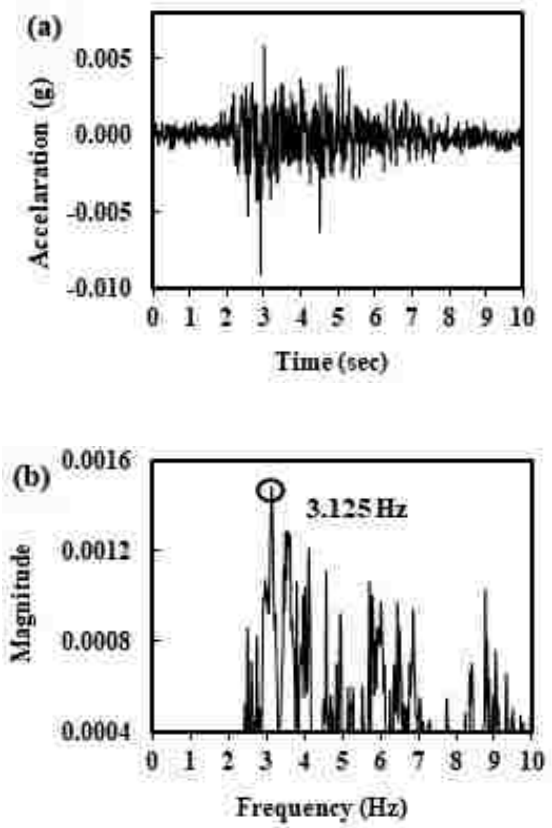

Figure 9. Dynamic response.
(a) Measured acceleration. (b) Natural frequency extracted through FFT.

This acceleration data was recorded when the truck was driven from west to east at 96 km/h. Figure 9(b) presents the fundamental frequency estimated from Fast Fourier Transformation (FFT) applied to the recorded acceleration data shown in Figure 9(a). The fundamental frequency of the bridge corresponded to a value of 3.125 Hz. Using the approach proposed by the OMTC (1983), this fundamental frequency yields a dynamic load allowance value of 0.40 according to Figure 1. Figure 10 shows that the quasi-static deflection recorded with RSV-150 was very close to the static deflection collected with the ATS (1.77 mm vs. 1.80 mm) and the value obtained from FEM simulations (1.77 mm vs. 1.71 mm) shown in Figure 8. Consequently, the filtered quasi-static response of the spans was assumed to be the maximum static deflection of girder 3's midspan and was employed to estimate the exterior spans' DLA for the different truck speeds employed during the dynamic test.

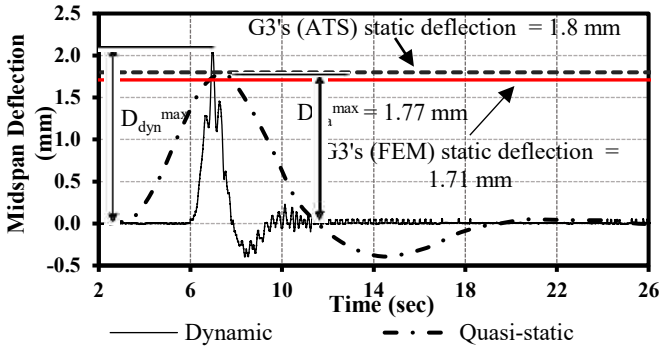

Figure 10. Maximum static and dynamic vertical deflection.

In addition, Figure 10 presents the maximum dynamic deflection (2.08 mm) measured with the RSV-150 when the truck speed was 96 km/h. The experimental DLA was estimated with Equation (3).

$$DLA^{exp} = \frac{DLA_{dyn}^{max} - DLA_{sta}^{max}}{DLA_{sta}^{max}} \quad (3)$$

where DLA^{exp} = experimental dynamic load allowance; $D_{dyn}{}^{max}$ = maximum dynamic (measured) vertical deflection (mm); and $D_{sta}{}^{max}$ = maximum static deflection obtained from passing the test truck at a crawl speed (mm). Table 2 lists shows in row 1 the trucks used to pass the truck over the bridge during the test. The bridge's maximum dynamic and static deflection recorded for the different speeds during the dynamic tests are presented in rows 2 and 3, respectively. In addition, the experimental values of the DLA corresponding to different truck speeds are presented in row 4. The maximum experimental DLA value was 0.175 corresponding to a truck speed of 96 km/h. The values of the experimental dynamic amplification factor, DAF^{exp}, are presented in row 5 and were estimated using Equation (4):

$$DLA^{exp} = \left(1 + DLA^{exp}\right) \quad (4)$$

Table 2. Experimental and analytical dynamic load allowance.

Speed (km/h)	16	32	48	64	80	96
$D_{dyn}{}^{max}$ (mm)	1.77	1.79	1.79	1.77	2.03	2.08
$D_{sta}{}^{max}$ (mm)	1.77	1.77	1.77	1.77	1.77	1.77
DLA^{exp}	0.000	0.010	0.010	0.000	0.150	0.175
DFA^{exp}	1.000	1.010	1.010	1.000	1.150	1.175
DLA*	0.40	0.40	0.40	0.40	0.40	0.40
IM** (Spans 1 & 3)	0.222	0.222	0.222	0.222	0.222	0.222
IM (Span 2)	0.204	0.204	0.204	0.204	0.204	0.204
DLA***	0.33	0.33	0.33	0.33	0.33	0.33

Values were estimated according to: * Ontario Highway Bridge Design Specification (OMTC 1983); ** AASHTO Standard Specifications (AASHTO 1992); and *** AASHTO LRFD Bridge Design Specifications (AASHTO 2012). Conversion factor: 16 km / h = 10 mi /h.

The DLA estimated as a function of the bridge's fundamental frequency proposed by the OHBDC (OMTC 1983) is presented in row 6. The impact factor obtained with the AASHTO Standard Specifications (AASHTO 1992) and the DLA obtained using the AASHTO LRFD Bridge Design Specifications (AASHTO 2012) are listed in rows 7 through 9. By comparing the maximum experimental DLA to the values obtained using these design specifications (OMTC 1983, AASHTO 1992, 2012), it was determined that the analytical methods provided more conservative values compared to the experimental approach. This variation may have different sources and may directly affect the strength evaluation result or load rating of an existing bridge obtained by the analytical methods proposed in current evaluation codes.

8. CONCLUSIONS

The dynamic load allowance of Bridge A7957 was successfully obtained from field measurements and by using three design specifications (OMTC 1983, AASHTO 1992, 2012). The DLA obtained with the design specifications resulted in larger values compared to the values obtained experimentally. This disparity might be attributed to the presence of in-situ factors not considered by the theoretical methods proposed in current design and evaluation codes. More importantly, the variation between the experimental and analytical DLA values may have repercussions in the rating factor of existing bridge structures. Further research is needed to understand the source of these variations.

ACKNOWLEDGEMENTS

The authors gratefully acknowledge the financial support provided by the Missouri Department of Transportation (MoDOT) and the National University Transportation Center (NUTC) at Missouri University of Science and Technology (Missouri S&T). The authors would like to thank the System and Process Assessment Research Lab (SPAR) at Missouri University of Science and Technology for allowing the use of the Remote Sensor Vibrometer (RSV-150) during the load tests.

REFERENCES

American Association of State Highway and Transportation Officials. (AASHTO). (1992). Standard Specifications for Highway Bridges, Washington, DC.

American Association of State Highway and Transportation Officials. (AASHTO). (2010). The Manual for Bridge Evaluation (2nd Edition) with 2011, 2013, 2014 and 2015 Interim Revisions, Washington, DC.

American Association of State Highway and Transportation Officials. (AASHTO). (2012). LRFD Bridge Design Specifications (6th Edition), Washington, DC.

Bakht, B., and Pinjarkar, S. G. (1989). "Dynamic testing of highway bridges. A review." Transportation Research Record 1223, TRB, Washington, D.C., 93-100.

Barker, R. M., and Pucket, J. A. (2013). Design of Highway Bridges: An LRFD Approach, John Wiley & Sons, 3rd Edition, Hoboken, N.J. USA.

Cai, C. S., and Shahawy, M. (2003). "Understanding capacity rating of bridges from load tests." Pract Period Struct Des Constr, 10.1061/(ASCE)1084-0680(2003)8:4(209), 209-216.

Deng, L., Yu, Y., Zou, Q., and Cai, C. S. (2015). "State-of-the-art review of dynamic impact factors of highway bridges." J Bridge Eng, 10.1061/(ASCE)BE.1943-5592.0000672, 20 (5). 04014080.

Hernandez, E. S., and Myers, J. J. (2015a). "In-situ field test and service response of Missouri Bridge A7957." 16th European Bridge Conference (EBC16), Edinburgh, Scotland, UK.

Hernandez, E. S., and Myers, J. J. (2015b). "Use of self-consolidating concrete and high volume fly ash concrete in Missouri Bridge A7957." Sustainable Performance of Concrete Bridges and Elements Subjected to Aggressive Environments: Monitoring, Evaluation and Rehabilitation, ACI SP 304 (6). 85-100.

Hernandez, E. S., and Myers, J. J. (2016a). "Field load test and girder distribution factors of Missouri Bridge A7957." Proc., 2016 PCI Convention and National Bridge Conference, Nashville, TN.

Hernandez, E. S., and Myers, J. J. (2016b). "Initial in-service response and lateral load distribution of a prestressed self-consolidating concrete bridge using field load tests." Proc., The Fifth International Symposium on Life-Cycle Civil Engineering (IALCCE 2016), CRC Press, Delf, The Netherlands. 1072-1079.

Hernandez, E. S., and Myers, J. J. (2016c). "Monitoring the initial structural performance of a prestressed self-consolidating concrete bridge." Proc., 8th International RILEM Symposium on Self-Compacting Concrete (SCC2016), RILEM Publications SARL, Washington, DC. 401-411.

Merkle, W. J., and Myers, J. J. (2004). "Use of the total station for load testing of retrofitted bridges with limited access." Proc., Smart Structures and Materials 2004 - Sensors and Smart Structures Technologies for Civil, Mechanical, and Aerospace Systems, San Diego, CA. 687-694.

Ontario Ministry of Transportation and Communications (OMTC). (OMTC). (1983). Ontario Highway Bridge Design Code (2nd Edition), Downsview, ON, Canada.

Paultre, P., Chaallal, O., and Proulx, J. (1992). "Bridge dynamics and dynamic amplification factors: a review of analytical and experimental findings." Can J Civ Eng, 19 (2). 260-278.

Simulia (2012) Abaqus Analysis User's Manual. Version 6.12. Providence, RI. USA, Dassault Systèmes Simulia Corp.

V. EXPERIMENTAL LOAD RATING OF BRIDGES IN LRFR FORMAT. I: APPROACH

E.S. Hernandez[1] and J.J. Myers[2]

[1]Ph.D. Candidate of the Civil, Architectural & Environmental Engineering Department, Missouri University of Science and Technology, 205 Pine Building, 1304 N Pine St, Rolla, MO 65409; email: ehd36@mst.edu

[2]Associate Dean, Professor of the Civil, Architectural & Environmental Engineering Department; Missouri University of Science and Technology; 325 Butler-Carlton Hall, 1401 N Pine St., Missouri University of Science and Technology, Rolla, MO 65409; email: jmyers@mst.edu

ABSTRACT

Field tests have largely confirmed reserves of strength capacity in existing bridges, particularly in the case of prestressed concrete bridges, despite their visual condition and age. Sources that explain the difference in the strength capacity are diverse and may be attributed to the presence of several in-situ parameters that are not considered during the design or load rating (strength evaluation) of a bridge structure. This study aimed at presenting a strength evaluation protocol using experimental data collected with reliable measurement devices to perform the load rating of prestressed concrete (PC) bridges in Load and Resistance Factor Rating (LRFR) format. This methodology will enable bridge owners to consider in-situ parameters that contribute to improve a bridge's response by using field load tests. In addition, this experimental approach permits

removing the contribution from unreliable parameters and keeping the reliable site-specific benefits. Bridge A7957's experimental data and proposed experimental evaluation methodology are expected to encourage more discussion among bridge designers and evaluators to better understand and improve current bridge analysis, design, and evaluation practices of prestressed concrete bridges.

Keywords: Field load testing; load rating; prestressed concrete, strength evaluation.

1. INTRODUCTION

Infrastructure facilities constitute a major part of the national asset. According to the National Bridge Inventory (NBI) database reported by the Federal Highway Administration (FHWA) at the end of 2017, there are nearly 614,400 bridges in the United States. Approximately 9.1% of them (56,007) are structurally deficient and 13.6% (83,557) are functionally obsolete (FHWA 2017). After conducting an inspection, a bridge is classified as "structurally deficient" if one or more of their components, such as the deck, superstructure, or substructure, result in a condition rating of "poor" or "worse" (Bhide 2004). Similarly, a bridge may be classified as "functionally obsolete" if it does not meet current design standards. In Missouri, there are approximately 24,487 bridges; 13% of them are considered structurally deficient, and 12.5% of them have been classified as functionally obsolete. Major decisions must be made to allocate dwindling funds for repairing, rehabilitating, and replacing this deficient or obsolete infrastructure.

Load rating is the strength evaluation procedure employed to estimate the allowable in-service load that a bridge structure can withstand without suffering damage and the maximum load that the structure can carry without undergoing collapse or failure.

This evaluation is a major basis in prioritizing maintenance operations, allocating economic resources, and making decisions concerning load posting and permit load decisions. Traditionally, bridge evaluation standards (AASHTO 2010) prescribe two approaches to load rating: analytical calculations and field testing. Analytical ratings are based on simplifying assumptions and may not closely reflect a realistic response of a bridge due to its current physical condition.

Conversely, field testing presents a more realistic visualization of the live-load capacity of a bridge because it provides an in-service, as-built characterization of its performance. Field testing permits the verification of design and analysis assumptions such as actual lateral load distribution, dynamic load allowance (impact factor), influence line position, degree of composite action, and unintended support restraint. Although field testing applications may sometimes be hindered by costs, time, test truck requirements, traffic interruptions, safety, difficulty to access a bridge structure, and difficulty to install sensors, it is the most accurate approach. Load testing permits (1) better understanding of the response of bridges fabricated with innovative designs and new construction technologies, (2) evaluating the response of posted and deteriorated bridges, and (3) evaluating a bridge's response to permit and nonstandard vehicles (ACI 2016). In general, the American Association of State Highway and Transportation Officials (AASHTO) Manual for Bridge Evaluation (MBE) defines two different options for load testing: diagnostic load tests and proof load tests (AASHTO 2010). Independent of the method employed to conduct a strength evaluation (analytical or experimental), load rating a bridge structure involves good "engineering judgment" to guarantee that the

rating results minimize the economic impacts on the community served by the bridge without sacrificing the public's safety at the same time.

The focus of this study was centered on monitoring and conducting a flexural strength evaluation of the prestressed Bridge A7957's main supporting members which were newly built. To achieve this goal, a systematic methodology proposed by Barker (1999, 2001) was employed to isolate the contribution of field factors that improve a bridge's performance and thus its load rating. The advantage of Barker's approach is that field contributing factors that are not reliable after a certain level of service load can be removed from the experimental rating calculations yielding to a more reliable prediction of a bridge's behavior. Barker's methodology was developed from load tests conducted on a posted steel girder bridge and was presented in allowable stress design (ASD) format. For this study, Baker's approach was modified to be implemented in PC bridges according to the current AASHTO LRFD/LRFR evaluation guidelines (AASHTO 2010). This paper is the first part of two companion articles that summarize the technical aspects of the application of the Barker's modified approach to prestressed concrete bridges. This first part summarizes the proposed experimental load rating procedures and presents the modified equations that should be employed to experimentally evaluate prestressed concrete bridges in LRFR format.

2. RESEARCH SIGNIFICANCE

The experimental load rating and evaluation methodology presented herein will enable monitoring changes in the performance of prestressed concrete bridges. The load rating of a bridge may be updated using site-specific data to estimate a more realistic live

load capacity of its superstructure during different stages of its service life. The main contributions of the proposed monitoring and experimental strength evaluation approach are twofold: (1) present an instrumentation and load test program that may be used to monitor a bridge's response during service life, and (2) provide an experimental strength evaluation protocol in the current LRFD/LRFR format that will enable bridge owners to make rational decisions related to maintenance, load posting, rehabilitation, and demolition of existing prestressed and reinforced concrete bridges.

3. AASHTO GUIDELINES FOR BRIDGE EVALUATION

Throughout the years, design and evaluation techniques have been proposed by engineers to dispense satisfactory safety margins. The first approaches were based on the engineers' judgment and confidence in the analysis of the load effects and the strength of the materials employed. As the analysis and evaluation methods advanced and the quality control for materials was refined, the design procedures were improved. To better understand the differences between current load rating practices, the following discussion presents a summary of AASHTO analytical and experimental guidelines for bridge design and evaluation.

3.1. ANALYTICAL LOAD RATING

The AASHTO MBE (AASHTO 2010) is currently consistent with three AASHTO design philosophies, namely allowable stress design (ASD), load factor design (LFD), and load and resistance factor design (LRFD). In the next subsections, the three theoretical load rating methods are presented in chronological order as adopted by AASHTO.

3.1.1. Allowable Stress Rating (ASR). The first national highway design specification, adopted by AASHTO in 1931, was based on the ASD until the beginning of the 1970s. In the AASHTO ASD method, an allowable or admissible stress is defined as a fraction of the strength capacity of a structural component. The structural effect resulting from the applied loads may not exceed this allowable limit to ensure the structural member safety. Procedures to conduct load ratings of existing bridges based on the ASD approach were presented in the AASHTO Manual for Maintenance Inspection of Bridges (AASHTO 1970). The resulting strength evaluation procedure is referred to as the allowable stress rating (ASR) method.

3.1.2. Load Factor Rating (LFR). At the beginning of the 1970s, as the design of reinforced concrete and steel structures were presented in terms of "ultimate strength" and "plastic design," respectively, the load analysis employed in the AASHTO ASD design specifications was improved. Adjustments were made by adding load factors as an attempt to represent the relative uncertainty in predicting actions such as vehicle loads and earthquake effects. These specifications also introduced a "capacity reduction" factor to downgrade the theoretical strength of an element to account for uncertainties in the predictability of its capacity. The resulting design and strength evaluation methodologies are referred to as the load factor design (LFD) and load factor rating (LFR), respectively.

In 1994, the LFR approach was included in the Manual for Condition Evaluation of Bridges (AASHTO 1994), which allows strength evaluations to be determined by either ASR or LFR. Both approaches rate bridge components at two levels: operating and inventory. The operating rating level reflects the maximum permissible live load to which

a structure may be subjected during a period in time. Conversely, load ratings based on the inventory rating level compare the estimated capacity of an existing bridge with that of a new bridge. The rating factor of a bridge component in ASR and LFR (AASHTO 1994) is computed by

$$RF = \frac{C - A_1 D}{A_2 L(1 + I)} \quad (1)$$

where RF = rating factor (expressed as a ratio of the design live load effect); C = member capacity; D = dead load effects; $L(1+I)$ = live load and impact factor; and A_1 and A_2 = factors for dead and live load, respectively. In Equation (1), $A_1 = A_2 = 1$ (ASR's operating and inventory levels); $A_1 = 1.3$ (LFR's operating and inventory levels); $A_2 = 1.3$ (LFR's operating level); and $A_2 = 2.16$ (LFR's inventory level).

3.1.3. Load and Resistance Factor Rating (LRFR). In 1998, the AASHTO LRFD bridge design specifications were proposed as the primary design method for highway bridges. These specifications represented the first AASTHO effort to integrate modern principles of structural reliability and probabilistic models of loads and resistance into the design of highway bridges. In addition, these specifications introduced reliability-based limit state concepts into the design philosophy by using calibrated load and resistance factors that satisfy uniform safety levels corresponding to each limit state. The approach was extended to the evaluation of bridges with the completion of the Manual for Condition Evaluation and Load and Resistance Factor Rating (LRFR) of Highway Bridges (MCE) published in 2003 (AASHTO 2003). The MCE is the first bridge strength evaluation approach in the United States presenting a structural reliability format (LRFR). A more recent update of the LRFR procedure is found in the AASHTO

Manual for Bridge Evaluation (MBE) updated in 2010 (AASHTO 2010). The rating factor of a bridge component in the LRFR approach is obtained (Minervino et al. 2004, AASHTO 2010) by

$$RF = \frac{C - \gamma_{DC}DC - \gamma_{DW}DW \pm \gamma_P P}{\gamma_L LL(1 + IM)} \quad (2)$$

where RF = rating factor; C = capacity = $\varphi\varphi_c\varphi_s R_n \geq 0.85\varphi R_n$ (strength limit states); C = f_R (service limit states); f_R = allowable stress specified in LRFD specifications (Minervino et al. 2004, AASHTO 2012); φ = LRFD resistance factor; φ_c = condition factor; φ_s = system factor; R_n = nominal member resistance; DC = dead load effect due to structural components and attachments; DW = dead load effect due to wearing surface and utilities; P = permanent loads other than dead loads (e.g., post-tensioning); LL = live load effect; IM = dynamic load allowance (impact factor); γ_{DC} = LRFD load factor for structural component and attachments; γ_{DW} = LRFD load factor for wearing surfaces and utilities; γ_P = LRFD load factor for permanent loads other than dead loads; and γ_L = evaluation live load factor.

3.2. EXPERIMENTAL LOAD RATING (LOAD RATING THROUGH LOAD TESTING)

The essential purpose of load testing is to provide a better understanding about a bridge's service response by considering site-specific parameters (i.e., boundary conditions, unintended composite action, unintended continuity, additional stiffness provided by non-structural members, effect of deterioration and damage, skew angle, and soil-structure interaction) (Stallings and Yoo 1993, Chajes et al. 2000, AASHTO 2010).

Load testing provides evaluators with a better understanding of a bridge's in-service performance, and most of the time the bridge's analytical load capacity is improved after performing a field load test.

Load rating of bridges through load testing includes the observation of a bridge's response measurement when it is subjected to predetermined loadings that do not alter the elastic response of the structure. The principle of load rating through load testing is the comparison of the field response of the bridge under test loads with its theoretical performance as predicted by the analysis (TRB 1998). In general, there are two types of nondestructive tests: diagnostic and proof load tests.

3.2.1. Diagnostic Load Test. Diagnostic load tests use service loads and are performed to determine certain response characteristics of the bridge (e.g., lateral load distribution, dynamic load allowance, and longitudinal load distribution). After conducting a diagnostic load test, the experimental data is used to modify the bridge's analytical load rating, which reflects a more realistic response of the structure. This is achieved through a simple rating adjustment factor applied to the calculated ratings (TRB 1998, AASHTO 2010) by

$$RF_T = RF_C K \tag{3}$$

where RF_T = load rating factor for the live-load capacity based on the load test results; RF_C = rating factor based on calculations prior to incorporating test results; K = adjustment factor resulting from the comparison of measured test behavior with the analytical model (represents the benefits of the field load test, if there are any). The adjustment factor is estimated by

$$K = 1 + K_a K_b \tag{4}$$

where K_a = factor that accounts for both the benefit derived from the load test, if any, and consideration of the section factor (area, section modulus, etc.); $K_a = (\varepsilon_C / \varepsilon_T)$-1; ε_T = maximum member strain measured during the load test; ε_C = corresponding calculated strain due to the test vehicle at its position on the bridge which produced ε_T; and K_b = factor that accounts for the understanding of the load test results when compared with those predicted by theory.

3.2.2. Proof Load Tests. In proof load tests, higher loads are applied to the

proof load tests, higher loads are applied to the bridge structure than in diagnostic load tests. This type of test allows verifying the maximum safe load capacity of a bridge and provides confidence of a bridge's capacity to carry the full rating load and some extra (factored) live load capacity. If a target load is attained within the test, it is concluded that the bridge has a margin of safety to withstand the rating load in the event of an overload during regular operation. The MBE (AASHTO 2010) presents a procedure for determining the target proof load (L_T) suitable for a specific bridge. This live load factor is multiplied by the rating vehicle weight (RVW) to determine the test load that must be applied for a valid proof test. The target proof load is given by

$$L_T = X_{PA} L_R (1 + IM) \tag{5}$$

where L_R = comparable unfactored live load due to the rating vehicle for the lanes loaded; IM = dynamic load allowance; and X_{PA} = target adjusted live-load factor that accounts for the live load uncertainties that are not evaluated by the test. This factor is estimated by

$$X_{PA} = X_P\left(1 + \frac{\sum \%}{100}\right) \quad (6)$$

where X_P = target live-load factor that is applied to the test load and is needed to bring the bridge's rating factor to 1.0. The factor X_P should have a base value of 1.40 to ensure the same reliability level employed in the load factors used in analytical rating computations. Similarly, the factor X_{PA} should not be larger than 2.2 or less than 1.3.

Currently, this analytical strength evaluation procedure proposed in the AASHTO MBE (AASHTO 2010) tends to be overly conservative due to simplified assumptions made to represent a bridge's response. Analytical load ratings underestimate the real bridge response, particularly in the case of PC bridges. Field testing has proven that bridges possess additional strength compared to what analytical methods predict because analytical load rating approaches are intended for general situations (Ghosn et al. 1986). The most predominant parameters that explain the increment in capacity have been largely investigated (Stallings and Yoo 1993, TRB 1998, Barker 1999, 2001, Cai and Shahawy 2003) and identified as: (1) actual lateral live load distribution, (2) actual dynamic load allowance (i.e., impact factor), (3) unaccounted section stiffness, such as in curbs and railings, (4) actual longitudinal live load distribution, (5) actual section dimensions, (6) bearing restrain effects, and (7) unintended or additional composite action. A bridge structure response obtained by means of load testing contains a combination of these factors. Contributing factors such as the lateral load distribution or the dynamic load allowance are considered welcome benefits that improve a bridge's load rating and may be relied on during the service life of a bridge. Conversely, factors such as unintended composite action and bearing restraining forces are unreliable because

their contribution may not be present when service loads exceed certain levels (TRB 1998, Barker 1999, 2001, Cai and Shahawy 2003). Accordingly, it is critical to provide bridge evaluators with an experimental bridge evaluation methodology that allows to isolate and estimate the contribution from these site-specific parameters and permits removing the unreliable contributing factors from a strength evaluation conducted by means of load testing.

4. EXPERIMENTAL RATING OF BRIDGES BY QUANTIFYING FIELD TEST PARAMETERS (BAKER'S APPROACH)

Barker (1999) proposed a systematic procedure to estimate the contribution of the aforementioned parameters and to remove the contribution of unreliable factors such as bearing restraint effects and unintended composite action from an experimental load rating. Baker's approach directly relates the analytical and experimental ratings, enables bridge evaluators and authorities to confirm the origin of the factors that tend to increase a bridge load rating, and allows for the removal of unreliable contributing factors from the load rating results. Baker quantified in-situ test parameters from a test program performed on a posted steel girder bridge and presented this methodology in ASR format. In this study, Baker's approach is adapted to perform experimental strength evaluations of PC bridges. In addition, this strength evaluation methodology for prestressed concrete bridges will be presented in LRFR format to be consistent with current evaluation practices recommended by the AASHTO MBE (AASHTO 2010).

5. EVALUATION OF PRESTRESSED CONCRETE BRIDGES USING FIELD LOAD TESTS

The AASHTO LRFD (AASHTO 2012) design load rating corresponding to the Strength I limit state will be utilized to establish the analytical and experimental load ratings of PC bridges. The flexural analytical load rating is performed based on the AASHTO LRFD HL-93 loading as a measure of the performance of an existing bridge to current LRFD bridge design specifications (AASHTO 2010). Other limit states and rating vehicles can be employed in a similar fashion. The analytical rating is given as follows

$$RT_A = \frac{(C_A - \gamma_{DC}M_{DC} - \gamma_{DW}M_{DW} \pm \gamma_P M_P)}{\gamma_{LL}DF_A M_{LL}(1 + IM_A)} RVW \quad (7)$$

where RT_A = analytical rating = $RF_A(RVW)$; RF_A = analytical rating factor; C_A = analytical capacity = $\varphi\varphi_C\varphi_S Mn_A \geq 0.85\varphi Mn_A$ (strength limit states); Mn_A =analytical (nominal) flexural resistance; M_{DC} = analytical dead load moment; M_{DW} = dead load moment due to wearing surface and utilities; M_P = analytical permanent load moment due to loads other than dead loads (e.g., post-tensioning); DF_A = analytical girder distribution factor; M_{LL} = analytical live moment for RVW; and IM_A = analytical dynamic load allowance (impact factor).

Diagnostic load tests can be employed to obtain the elastic response of a prestressed concrete bridge. If experimental data is used to determine a bridge load rating. Then, Equation (7) will be modified in the following manner:

$$RT_E = \frac{(C_E - \gamma_{DC}M_{DC} - \gamma_{DW}M_{DW} \pm \gamma_P M_P)}{\gamma_{LL}\frac{M_{RVW}}{M_{TRK}}M_T(1 + IM_E)} RVW \quad (8)$$

where RT_E = experimental bridge rating = $RF_E(RVW)$; RF_E = experimental rating factor; RVW = rating vehicle weight; C_E = experimental capacity = $\varphi\varphi_C\varphi_S Mn_E \geq 0.85\varphi Mn_E$ (strength limit states); Mn_E = experimental flexural resistance; M_{RVW} = analytical rating vehicle moment (used to evaluate the bridge's response for different analytical rating vehicles); M_{TRK} = analytical test truck moment; M_T = experimental total moment; and IM_E = experimental dynamic load allowance. No experimental distribution factor (DF) is present in Equation (8) since the measurement of M_T directly includes the portion of the exterior load supported by each girder. The term M_{RVW} / M_{TRK} normalizes the actual test truck to an equivalent rating response.

Field tests have largely confirmed reserves of strength capacity in existing bridges, particularly in the case of PC concrete bridges despite their visual condition and age. Field tests yield higher experimental ratings compared to analytical ratings because these provide a bridge response that considers beneficial in-situ parameters that improve a bridge's in-service behavior. The experimental load rating obtained with Equation (8) is composed of the sum of these site-specific parameters (Barker 1999, 2001). Bridge evaluators may want to remove the contribution from those parameters that are not reliable at a certain level of service load. Equation (8) will be somewhat modified to identify and isolate the sources of the additional capacity obtained with an experimental strength evaluation compared to the analytical approach. Equation (9) presents the modified version of Equation (8):

$$RT_E = \frac{(C_E - \gamma_{DC}M_{DC} - \gamma_{DW}M_{DW} \pm \gamma_P M_P)}{\gamma_{LL}\frac{M_{RVW}}{M_{TRK}}(1 + IM_E)\left(\frac{M_E}{M_{LE}}\frac{M_{LE}}{DF_E}\frac{M_T}{M_E}\right)DF_E} RVW \qquad (9)$$

where M_E = experimental elastic moment with bearing restraint effect removed; M_{LE} = experimental elastic moment adjusted for longitudinal distribution; DF_E = experimental load distribution factor. The variables incorporated into Equation (9) cancel each other so that the experimental load rating obtained with Equation (9) yields the same experimental load rating obtained with Equation (8). Equation (9) is divided by Equation (7) to reveal the source of the apparent additional capacity obtained with an experimental load rating:

$$\frac{RT_E}{RT_A} = \left[\left(\frac{C_E - \gamma_{DC} M_{DC} - \gamma_{DW} M_{DW} \pm \gamma_P M_P}{C_A - \gamma_{DC} M_{DC} - \gamma_{DW} M_{DW} \pm \gamma_P M_P} \right) \left(\frac{DF_A}{DF_E} \right) \left(\frac{1 + IM_A}{1 + IM_E} \right) \left(\frac{M_{LL}}{\frac{M_{LE}}{DF_E} \frac{M_{RVW}}{M_{TRK}}} \right) \right] \left(\frac{M_{LE}}{M_E} \right) \left(\frac{M_E}{M_T} \right) \quad (10)$$

The relation between the experimental and analytical load ratings can be rewritten in the following manner:

$$RT_E = \left[\rho_c \rho_g \rho_i \rho_k \rho_l \rho_b \right] RT_A \quad (11)$$

where ρ_c = contribution to experimental load rating from capacity (differences between experimental and nominal material strength properties) = $(C_E - \gamma_{DC} M_{DC} - \gamma_{DW} M_{DW} \pm \gamma_P M_P) / (C_A - \gamma_{DC} M_{DC} - \gamma_{DW} M_{DW} \pm \gamma_P M_P)$; ρ_g = contribution factor due to lateral distribution = DF_A/DF_E; ρ_i = contribution from dynamic load allowance (impact factor) = $(1+IM_A)/(1+IM_E)$; ρ_k = contribution from additional stiffness = $M_{LL}/[(M_{LE}/DF_E)(M_{RVW}/M_{TRK})]$; ρ_l = contribution factor from longitudinal distribution moment = M_{LE}/M_E;; and ρ_b= bearing restraint force effects = M_E/M_T.

Equation (11) permits isolating and estimating the contribution from those site-specific parameters that improve an experimental load rating and permits removing the

unreliable contributing factors from a strength evaluation conducted by means of load testing.

6. QUANTIFICATION OF SITE-SPECIFIC PARAMETERS USING FIELD TEST DATA

The quantification of the site-specific parameters necessary to apply Equation (11) in an experimental strength evaluation of a PC bridge can be summarized as follows (Barker 1999, 2001):

1. Inspect the bridge to determine the actual dimensions, properties, and dead load.
2. Use NDT technology to collect the mechanical properties of the different bridge's components. This step includes obtaining compressive strength of concrete (f'c), modulus of elasticity of concrete (Ec), and modulus of rupture of concrete (fr) data from the field.
3. Estimate the experimental girder distribution factor (DF_E).
4. Estimate the experimental dynamic load allowance (IM_E).
5. Determine the bearing restraint forces and moment (M_{BR}).
6. Remove axial stress from critical section stress profile.
7. Calculate the experimental total moment (M_T).
8. Calculate the elastic moment (M_E) at the critical section.

   Calculate the elastic longitudinal adjustment moment at the critical section (M_{LE}).

6.1. EXPERIMENTAL LOAD DISTRIBUTION FACTOR

The girder distribution factor is the fraction of the total applied moment resisted by an individual load-carrying member. The girder distribution factor can be computed

using the measured strains recorded at the girders' bottom flange across the transverse bridge's section (Ghosn et al. 1986, Stallings and Yoo 1993, Kim and Nowak 1997, Cai and Shahawy 2003, Harris et al. 2010, Hernandez and Myers 2016b):

$$DF_E = n\frac{\varepsilon_{Gi}}{\sum_{i=1}^{k}\varepsilon_{Gi}} \tag{12}$$

where DF_E = experimental load distribution factor of *ith* girder obtained from strain values; ε_{Gi} = bottom flange strain of the *ith* girder at mid-span; n = number of lanes loaded; and k = number of girders. Alternatively, the experimental girder distribution factor can be estimated using the measured deflections recorded at the girders' midspan using the following expression:

$$DF_E = n\frac{\delta_{Gi}}{\sum_{i=1}^{k}\delta_{Gi}} \tag{13}$$

where δ_{Gi} = vertical deflection of the *ith* girder at mid-span.

6.2. EXPERIMENTAL DYNAMIC LOAD ALLOWANCE

Several experimental definitions of the dynamic load allowance have been reported in literature (Bakht and Pinjarkar 1989, Paultre et al. 1992). In this study, the experimental DLA is defined as the ratio of the maximum dynamic and static responses of a girder (Deng et al. 2015, Hernandez and Myers 2017) and is estimated according to:

$$IM_E = \frac{R_{dyn} - R_{sta}}{R_{sta}} \tag{14}$$

where R_{dyn} = maximum (measured) dynamic response; and R_{sta} = maximum static response. The estimation of the static response can be obtained conducting a quasi-static

test where vehicles move across the bridge at a crawl speed of less than 16 km/h (10 mi/h) (Paultre et al. 1992, Deng et al. 2015). Control speeds ranging from 16 km/h (10 mi/h) to 96.6 km/h (60 mi/h) were used during the dynamic load tests to obtain the maximum dynamic response (Hernandez and Myers 2018b).

6.3. BEARING RESTRAINT EFFECTS

The bearing restraint effect is provided by a bearing force causing a moment about the center of gravity of the girders' cross section. Figure 1 presents the sign convention used to consider the effect of the bearing restrain forces and moments.

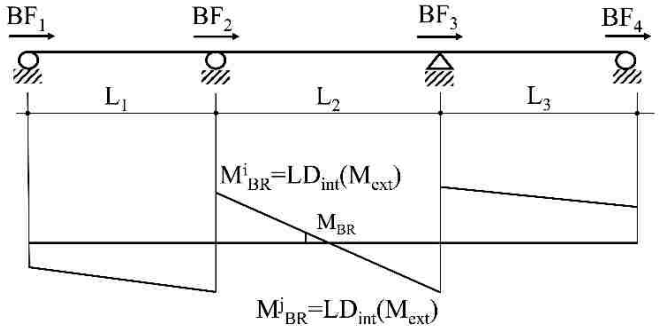

Figure 1. Bearing restraint forces and moment.

The bearing force at an abutment can be estimated with the force in the bottom flange at the support by (Barker 1999)

$$BF = A_{bf}\sigma_{bf}, \tag{15}$$

where BF = bearing force; A_{bf} = area of the bottom flange at the bearing; and σ_{bf} = measured stress on the bottom flange of the bearing. The bearing force at the interior supports (piers) is obtained by placing strain gauges at both sides of the bearing and is estimated by

$$BF = \frac{(\sigma_{bfj} - \sigma_{bfi})A_{bf}}{2} \tag{16}$$

where σ_{bfj} = stress at the right face of the support; and σ_{bfi} = stress at the left face of the support. The equivalent external applied moment (M_{ext}) caused by the bearing restraint effect at a support is estimated by

$$M_{ext} = BF * y_b \tag{17}$$

where y_b = distance from the neutral axis to bottom flange layer. The moment distribution method can be employed to distribute the external moment to each face of a support (Figure 1).

If the main load-carrying member stiffness can be assumed to be constant throughout the span, the distribution can be obtained by (Barker 1999)

$$LD_{int} = \frac{\left(\frac{1}{L_i}\right)}{\sum\left(\frac{1}{L_i}\right)} \tag{18}$$

where LD_{int} = longitudinal moment distribution factor at pier i; and Li = span length of the ith span on each face of the support.

For a critical section located at the midspan, the bearing restraint moment effect is computed by

$$M_{BR} = \frac{(M_{BRi} + M_{BRj})}{2} \tag{19}$$

where M_{BR} = bearing restraint moment at a midspan critical section; M^i_{BR} = bearing restraint moment at the first pier location; and M^j_{BR} = bearing restraint moment at the second pier location (Figure 1).

6.4. AXIAL STRESS

Strain gauges should be installed throughout the depth of the member to record the longitudinal strains across the section when the loads applied to the bridge are below the elastic limit. A strain profile can be constructed with the experimental data recorded by the strain gauges as shown in Figure 2.

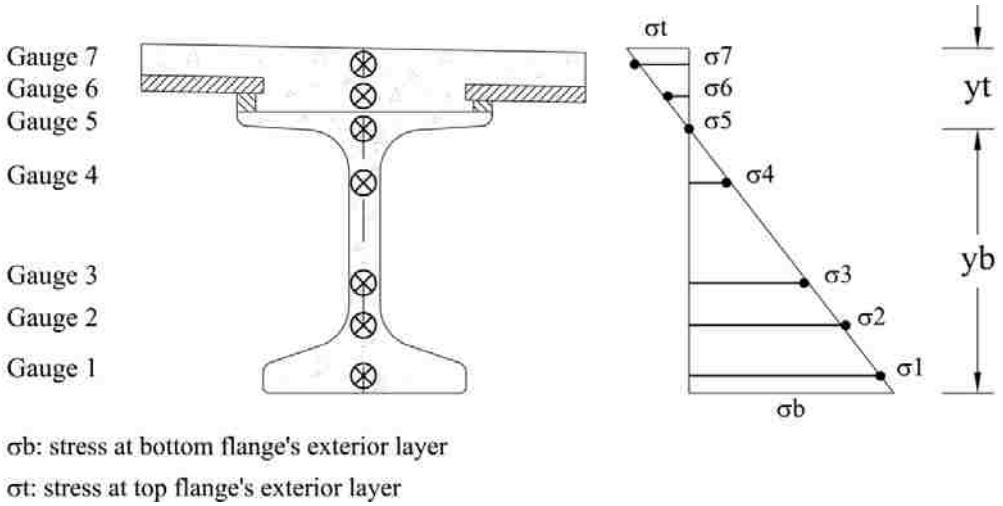

Figure 2. Girder's stress profile at a critical location.

A best fit line is then obtained to estimate the values of the strains at the bottom flange of the girders. From this graph, the following relation can be written as

$$\sigma = \frac{1}{m}(y_b - d_i) \tag{20}$$

where σ = stress within girder section including axial bearing restraint stress; d_i = distance from bottom fiber to the ith layer where the strain gauge is installed; m = slope of the stress profile = y_b / ($\varepsilon_b E_c$); ε_b = strain at the bottom flange; and E_c = Modulus of elasticity of concrete (obtained experimentally the same day a load test is conducted). The overall bearing force (axial force) acting at a section is found by summing the

horizontal forces acting in the free body diagram of the critical section. The additional axial stress due to the bearing force can be computed and removed from the stress profile using the following expression:

$$\sigma_{BF} = \frac{BF}{A_{comp}} \tag{21}$$

where A_{comp} = equivalent concrete composite area = A_{conc} + $n_{slab}(A_{slab})$; A_{conc} = Area of concrete; A_{slab} = Effective slab area; and n_{slab} = modular ratio (E_{slab} / E_c). A section stress profile with the bearing axial force removed can be found as follows:

$$\sigma_m = \frac{1}{m}\left(y_b - \frac{d_i}{2}\right) - \sigma_{BF} \tag{22}$$

6.5. TOTAL EXPERIMENTAL MOMENT

The experimental total moment in a prestressed concrete section (Figure 3) can be estimated by

$$M_T = \frac{2}{3}(y_b + y_t)\frac{\varepsilon_b E_c}{2} A_{tens} \tag{23}$$

where A_{tens} = area of the cross section subjected to tension; and y_t = distance from the neutral axis to the top flange layer.

6.6. EXPERIMENTAL ELASTIC MOMENT

The elastic moment with axial and bearing moment effects removed may be calculated at each critical section as follows (Barker 1999):

$$M_E = M_T - M_{BR} \tag{24}$$

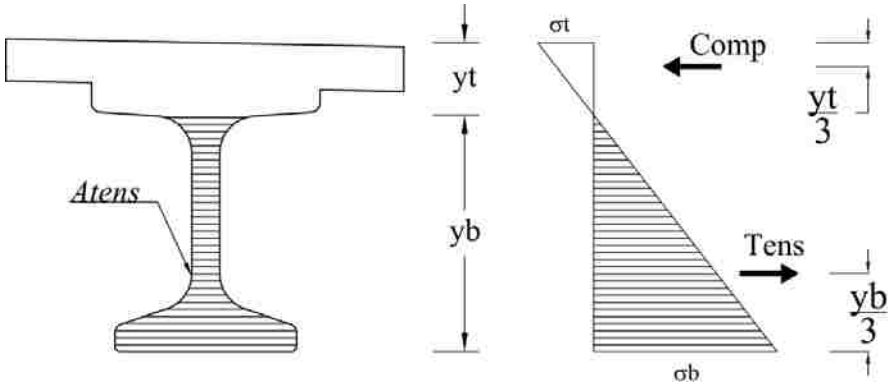

Figure 3. Total experimental moment.

6.7. LONGITUDINAL DISTRIBUTION MOMENT

The contribution factor from the longitudinal distribution moment takes into account the difference between the experimental and analytical elastic moments at the critical section (Figure 4). Barker (1999) proposed an adjustment to the longitudinal distribution moment by forcing equal static moment behavior of the analytical and experimental moments. The adjustment is conducted by selecting three sections within an interior span to construct the span's moment diagram (Figure 4). Then, the analytical moment diagram is constructed for the test load truck. Finally, the static moments are found by using the following set of equations:

$$M_A^{Stat} = M_{A2} - (1-\alpha)M_{A1} - \alpha M_{A3} \tag{25}$$

$$M_E^{Stat} = M_{E2} - (1-\alpha)M_{E1} - \alpha M_{E3} \tag{26}$$

where M_A^{Stat} = static moment for the analytical load truck moment; M_E^{Stat} = static moment for experimental data; M_A = analysis load truck moment at the critical sections (i=1, 2 and 3) within the interior span (1 = left, 2 = maximum, and 3 = right location); M_E = experimental moment at the critical sections (i=1, 2 and 3) within the interior span (1 =

left, 2 = maximum, and 3 = right location); and α = percentage of length to point of maximum moment.

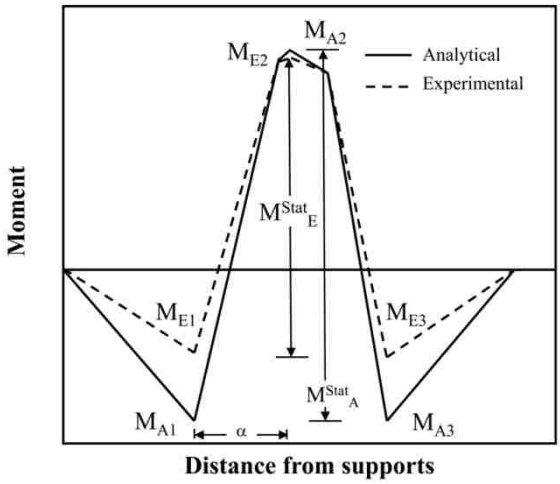

Figure 4. Analytical and experimental moment diagrams.

The experimental elastic moment adjusted for longitudinal distribution is obtained by

$$M_{LE} = \frac{M_E^{Stat}}{M_A^{Stat}} M_{A2} \tag{27}$$

7. CONCLUSIONS

The objective of this study centered on performing an experimental load rating of prestressed concrete bridges. To achieve this goal, a systematic methodology proposed by Barker (1999, 2001) was employed to isolate the contribution of field factors that improve a bridge's in-service performance and thus its load rating capacity. Baker's approach was modified to be implemented in prestressed concrete bridges according to the current AASHTO LRFD/LRFR evaluation guidelines. An experimental load rating of

a bridge reflects an additional bridge capacity compared to what analytical load ratings predict. An experimental load rating provides a combination of in-situ parameters that improve a bridge's behavior, namely (1) actual lateral live load distribution, (2) actual dynamic load allowance (impact factor), (3) unaccounted section stiffness, such as in curbs and railings, (4) actual longitudinal live load distribution, (5) actual section dimensions, (6) and bearing restrain effects. This paper introduces an approach to perform an experimental load rating of prestressed concrete bridges. This experimental methodology allows isolating and estimating the contribution of the aforementioned in-situ beneficial parameters and permits removing the contribution of parameters that might not be present at certain levels of service load yielding a more rational load rating capacity of prestressed concrete bridges.

ACKNOWLEDGEMENTS

The authors would like to acknowledge the Missouri Department of Transportation (MoDOT) and the Tier 1 University Transportation Center RECAST at Missouri S&T for sponsoring this research study. The staff support from the Dept. of Civil, Architectural & Environmental Engineering (CArEE) and Center for Infrastructure Engineering Studies (CIES) at Missouri S&T is also greatly appreciated.

REFERENCES

American Association of State Highway and Transportation Officials. (AASHTO). (1970). Manual for Maintenance Inspection of Bridges, Washington, D.C.

American Association of State Highway and Transportation Officials. (AASHTO). (1994). Manual for Condition Evaluation of Bridges, Washington, DC.

American Association of State Highway and Transportation Officials. (AASHTO). (2003). Manual for Condition Evaluation and Load and Resistance Factor Rating (LRFR) of Highway Bridges, Washington, DC.

American Association of State Highway and Transportation Officials. (AASHTO). (2010). The Manual for Bridge Evaluation (2nd Edition) with 2011, 2013, 2014 and 2015 Interim Revisions, Washington, DC.

American Association of State Highway and Transportation Officials. (AASHTO). (2012). LRFD Bridge Design Specifications (6th Edition), Washington, DC.

American Concrete Institute. (ACI). (2016). "Report on Flexural Live Load Distribution Methods for Evaluating Existing Bridges." ACI 342R-16, Farmington Hills, MI.

Bakht, B., and Pinjarkar, S. G. (1989). "Dynamic testing of highway bridges. A review." Transportation Research Record 1223, TRB, Washington, D.C., 93-100.

Barker, M. G. (1999). "Steel girder bridge field test procedures." Const. Build. Mater., 13 (4). 229-239.

Barker, M. G. (2001). "Quantifying field-test behavior for rating steel girder bridges." J Bridge Eng, doi:10.1061/(ASCE)1084-0702(2001)6:4(254), 6 (4). 254-261.

Bhide, S. (2004). "Material Usage and Condition of Existing Bridges in the U.S." Portland Cement Association (PCA), Skokie, IL, pp.

Cai, C. S., and Shahawy, M. (2003). "Understanding capacity rating of bridges from load tests." Pract Period Struct Des Constr, 10.1061/(ASCE)1084-0680(2003)8:4(209), 209-216.

Chajes, M., Shenton III, H., and O'Shea, D. (2000). "Bridge-Condition Assessment and Load Rating Using Nondestructive Evaluation Methods." Transportation Research Record: Journal of the Transportation Research Board, 10.3141/1696-48, 1696 83-91.

Deng, L., Yu, Y., Zou, Q., and Cai, C. S. (2015). "State-of-the-art review of dynamic impact factors of highway bridges." J Bridge Eng, 10.1061/(ASCE)BE.1943-5592.0000672, 20 (5). 04014080.

FHWA (2017). "National Bridge Inventory (NBI)." <http://www.fhwa.dot.gov/bridge/nbi/no10/defbr15.cfm>. (February 26, 2018, 2016).

Ghosn, M., Moses, F., and Gobieski, J. (1986). "Evaluation of steel bridges using in-service testing." Transportation Research Record 1072, Transportation Research Board, Washington, D.C., 71-78.

Harris, D. K., Cousins, T., Sotelino, E. D., and Murray, T. M. (2010). "Flexural lateral load distribution characteristics of sandwich plate system bridges: parametric investigation." J Bridge Eng, 10.1061/(Asce)Be.1943-5592.0000105, 684-694.

Hernandez, E. S., and Myers, J. J. (2016). "Initial in-service response and lateral load distribution of a prestressed self-consolidating concrete bridge using field load tests." Proc., The Fifth International Symposium on Life-Cycle Civil Engineering (IALCCE 2016), CRC Press, Delf, The Netherlands. 1072-1079.

Hernandez, E. S., and Myers, J. J. (2017). "Dynamic load allowance of a prestressed concrete bridge through field load tests." SMAR 2017 Fourth Conference on Smart Monitoring, Assessment and Rehabilitation of Civil Structures, Zurich, Switzerland.

Kim, S., and Nowak, A. S. (1997). "Load distribution and impact factors for I-girder bridges." J Bridge Eng, doi:10.1061/(ASCE)1084-0702(1997)2:3(97), 97-104.

Minervino, C., Sivakumar, B., Moses, F., Mertz, D., and Edberg, W. (2004). "New AASHTO guide manual for load and resistance factor rating of highway bridges." J Bridge Eng, doi:10.1061/(ASCE)1084-0702(2004)9:1(43), 43-54.

Paultre, P., Chaallal, O., and Proulx, J. (1992). "Bridge dynamics and dynamic amplification factors: a review of analytical and experimental findings." Can J Civ Eng, 19 (2). 260-278.

Stallings, J. M., and Yoo, C. H. (1993). "Tests and ratings of short□span steel bridges." J Struct Eng, doi:10.1061/(ASCE)0733-9445(1993)119:7(2150), 2150-2168.

Transportation Research Board. (TRB). (1998). "Manual for Bridge Rating through Load Testing" Research Results Digest No. 234, Washington, D.C.

VI. EXPERIMENTAL LOAD RATING OF BRIDGES IN LRFR FORMAT. II: CASE STUDY

E.S. Hernandez[1] and J.J. Myers[2]

[1]Ph.D. Candidate of the Civil, Architectural & Environmental Engineering Department, Missouri University of Science and Technology, 205 Pine Building, 1304 N Pine St, Rolla, MO 65409; email: ehd36@mst.edu

[2]Associate Dean, Professor of the Civil, Architectural & Environmental Engineering Department; Missouri University of Science and Technology; 325 Butler-Carlton Hall, 1401 N Pine St., Missouri University of Science and Technology, Rolla, MO 65409; email: jmyers@mst.edu

ABSTRACT

Field tests represent an effective alternative to conduct an evaluation of a bridge's strength capacity. In general, the American Association of State Highway and Transportation Officials (AASHTO) Manual for Bridge Evaluation (MBE) defines two different types of evaluation methodologies: analytical and experimental load ratings. Analytical ratings are based on simplifying assumptions and may result in a conservative load rating values of a bridge. Conversely, experimental load ratings present a more realistic visualization of a bridge's live-load capacity because they provide an as-built characterization of its service response that reflects the bridge's current physical condition. This article is the second part of two companion articles that list the technical details to conduct an experimental evaluation of prestressed concrete bridges quantifying

in-situ parameters that improve their analytical load rating capacity. The primary purpose of this paper is to present a case study application to showcase how this experimental evaluation methodology is applied. It is expected that this systematic approach can be used to update a bridge's load rating capacity at different stages of its service life.

Keywords: Field tests; load rating; prestressed concrete, strength evaluation.

1. INTRODUCTION

As infrastructure facilities continue to age and deteriorate, innovative concrete materials have been developed to increase their service life expectancy. Since the early 1990s, the use of self-consolidating concrete (SCC) has emerged worldwide as an alternative to produce more durable and stronger infrastructure due to its inherent properties (Ouchi et al. 2003, Domone 2006, McSaveney et al. 2011, Keske et al. 2014, Hernandez and Myers 2015b). Some of the SCC's attributes include (1) a highly flowable characteristic that permits better consolidation and ease of concrete placement, resulting in fewer voids and honeycombing; (2) a more condensed microstructure that increases the concrete's durability and mechanical properties; (3) reductions in labor and equipment costs; and (4) decreased maintenance expenses. In addition, high-strength SCC (HS-SCC) added enhanced flexural performance characteristics to NS-SCC's attributes as the result of increasing the normal compressive strength available in SCC mixtures developed in the past two decades. This stronger flexural feature brings the possibility of reducing the number of the main supporting elements (larger girder spacing) and interior supports (longer girder spans) of bridge superstructures with a higher durability compared to conventional concrete of normal strength.

Despite the advantages that come with using SCC, there still is some reluctance to implement this novel material in highway infrastructure on a large scale due to the lack of test bed applications that may help extrapolate SCC's structural and service performance over the long term (WsDOT 2009). The effect of the larger paste content and the smaller coarse aggregate size used in the mixture has been reported as of particular interest (Myers et al. 2012). Researchers have reported a lower expected modulus of elasticity (MOE) and higher prestress losses (e.g., shrinkage and creep) when SCC is used (Khayat and Mitchell 2009, Myers and Bloch 2011). Accordingly, it is critical to monitor the initial and long-term service behavior and strength capacity of full-scale highway infrastructure utilizing SCC in precast-prestressed concrete (PC) members to validate and thus encourage the implementation of this material in highway projects.

Currently, the analytical strength evaluation procedures (referred to as load rating) adopted by the AASHTO MBE (AASHTO 2010) tend to be overly conservative due to simplified assumptions made to represent a bridge's response. Analytical load ratings underestimate the real bridge response, particularly in the case of PC bridges. Field testing has proven that bridges possess additional strength compared to what analytical methods predict due to the presence of some in-situ parameters that improve a bridge's service performance. The most predominant parameters that explain the increment in capacity have been largely investigated (Stallings and Yoo 1993, TRB 1998, Barker 1999, 2001, Cai and Shahawy 2003) and identified as (1) actual lateral live load distribution; (2) actual dynamic load allowance (impact factor); (3) unaccounted section stiffness, such as in curbs and railings; (4) actual longitudinal live load distribution; (5) actual section dimensions; (6) bearing restraint effects; and (7) unintended or additional

composite action. A bridge structure response and load rating obtained by means of load testing contains a combination of these sire-specific factors. Contributing factors such as the lateral load distribution or the dynamic load allowance are considered welcome benefits that improve a bridge's load rating and may be relied on during the service life of a bridge. Conversely, factors such as unintended composite action and bearing restraining forces are unreliable because their contribution may not be present when service loads exceed certain levels (TRB 1998, Barker 1999, 2001, Cai and Shahawy 2003). Accordingly, it is critical to provide bridge authorities with an experimental bridge evaluation methodology that enables removing unreliable contributing factors from a strength evaluation conducted by means of load testing.

This article is the second part of two companion articles that list the technical details to perform the experimental load rating of prestressed concrete bridges quantifying bridge in-situ parameters that improve a bridge's theoretical load rating. The primary purpose of this article is to present a case study application to showcase this experimental evaluation methodology. Bridge A7957, the first implementation project, conducted by the Missouri Department of Transportation (MoDOT), using SCC of normal and high strength in its prestressed concrete members, was selected to demonstrate how these site-specific parameters contribution can be quantified from experimental measurements and considered or removed from the rating capacity evaluation of a PC bridge. The following sections present (1) Bridge A7957 the object of this research study; (2) field instrumentation plan; (3) field test program that included static and dynamic testing; (4) quantification of the site-specific parameters affecting the bridge's load rating; (5) application of the proposed experimental load rating evaluation

approach; and (6) comparisons between the analytical and experimental evaluation results to estimate and present the differences when both methodologies are employed. It is expected that this experimental methodology can be used to update Bridge A7957's load rating capacity and to assess changes in the service performance of its main prestressed concrete members during its service life.

2. RESEARCH SIGNIFICANCE

The experimental load rating protocol showcased herein will enable bridge owners and evaluators to estimate the contribution of in-situ parameters that can be incorporated into a bridge evaluation process to enhance its load rating capacity. By following this systematic approach, the contribution from unreliable parameters can be removed from the bridge capacity evaluation of a prestressed concrete bridge. This evaluation approach represents an opportunity to monitor Bridge A7957's structural performance and available remaining strength as the different component materials age and deteriorate during the service life of the structure. Bridge A7957's data and proposed experimental evaluation methodology are expected to encourage more discussion among bridge evaluators to improve current evaluation practices of prestressed concrete bridges and reduce the possibility of load rating this type of bridges improperly.

3. BRIDGE A7957

To illustrate how the enhancement of a bridge's analytical load rating can be attained, Bridge A7957 in Missouri, was selected to load rate its flexural capacity using the procedures described above. The following subsections provide more details about the bridge, field instrumentation, and field test program.

3.1. BRIDGE DESCRIPTION

Bridge A7957, built along Highway 50 in Osage County, Missouri, is a three-span, continuous, PC bridge (Figure 1) with a skew angle of 30 degrees (Hernandez and Myers 2016b), and excellent road surface condition. Each span has PC/PS concrete Nebraska University (NU) 53 girders fabricated with different concrete mixtures. Girders in the first span are 30.48 m (100 ft) long and made of conventional concrete (MoDOT's Class A mixture) with a target compressive strength of 55.2 MPa (8,000 psi). The second span's girders measure 36.58 m (120 ft) and were fabricated with an HS-SCC mixture of 68.9 MPa (10,000 psi). Girders in the third span are 30.48 m (100 ft) long and employ SCC with a nominal compressive strength of 55.2 MPa (8,000 psi). Precast-prestressed concrete panels, with a target compressive strength of 55.2 MPa (8,000 psi), span between the girders' top flange underneath the cast-in-place (CIP) reinforced concrete (RC) slab deck in the transverse direction [Figure 1(b)].

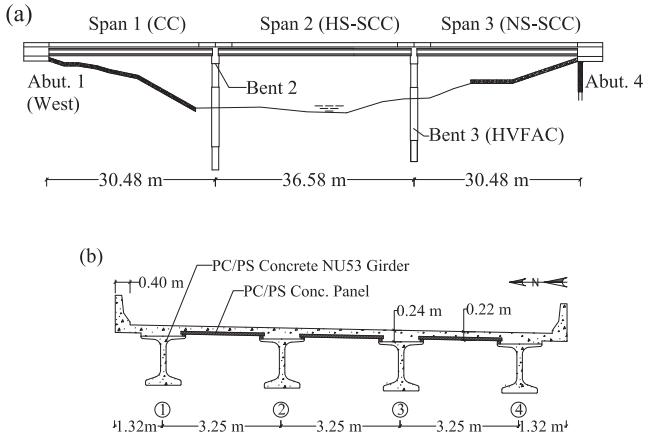

Figure 1. Bridge A7957.
(a) elevation; (b) cross-section. Conversion factor: 1 m = 3.28 ft.

The CIP deck was cast with a 25% fly ash replacement of a portland cement mixture with design strength of 27.6 MPa (4,000 psi). The bridge superstructure is supported by two abutments and two intermediate bents [Figure 1(a)].

3.2. FIELD INSTRUMENTATION

An instrumentation plan was implemented during the preconstruction of Bridge A7957. The data acquisition was designed to be collected by embedded sensors (vibrating wire strain gauges) and non-contact remote data acquisition systems that included an automated total station (ATS) and a remote sensing vibrometer (RSV-150). The type of sensors and equipment employed to collect field data are provided in the following subsections.

3.2.1. Vibrating Wire Strain Gauges. A total of 86 vibrating wire strain gauges (VWSG) with built-in thermistors (type EM-5) were utilized to record the strain and stress variations in the PC girders and RC deck slab from fabrication through service life. Before casting, a total of 62 VWSG were installed in all spans within the PC girders of lines 3 and 4. The PC girder cluster locations at which the VWSG were embedded are illustrated in Figure 2. The instrumentation clusters were selected at two cross-sections within each girder of span 1 and span 3. One section was located at midspan, and the other was placed at approximately 0.60 m (2 ft) from the support centerline of bents 2 and 3. The instrumentation clusters for the center span (span 2) were arranged at three different cross-sections: one at mid-span and two at approximately 0.60 m (2 ft.) from each support centerline. The cluster sections in the second span were arranged at three

different cross-sections: one at the mid-span and the other sections approximately 0.60 m (2 ft) from each support centerline.

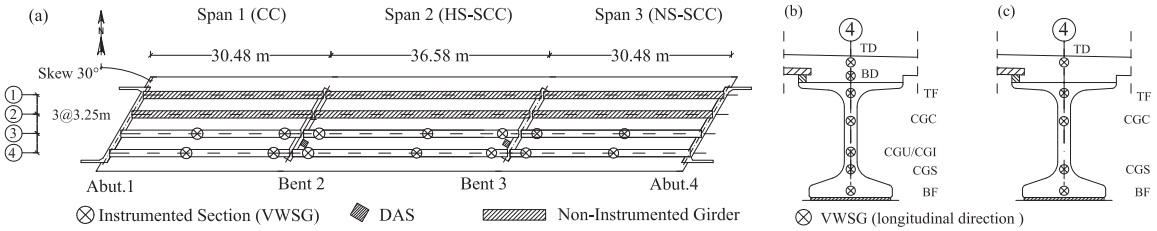

Figure 2. Embedded VWSG installation details.
(a) Cluster locations layout; (b) midspan section; (c) Near-end section.
Conversion factor: 1 m = 3.28 ft.

Details on VWSGs installed at the girders' near-support and mid-span sections before concrete was cast are illustrated in Figures 2(b)–2(c). The following notation was employed to identify the layer where the VWSG sensors were installed across the girders' cross-section:

- TD: 150 mm from the deck's bottom fiber
- BD: 50 mm from the deck's bottom fiber
- TF: 50 mm below the girder's top fiber
- CGC: center of gravity of composite section
- CGU/CGI: center of gravity of non-composite section (only at mid-span clusters)
- CGS: center of gravity of prestressed tendons
- BF: 50 mm from girder's bottom fiber

Twenty VWSGs were placed within the CIP RC slab deck (Figure 2) in the longitudinal direction (sensors TD and BD). A VWSG was transversely deployed at the mid-height of two selected PC/PS panels [Figure 2(b)]. The last two VWSGs were located along the bridge's transverse direction, between girder lines 2 and 3 and girder

lines 3 and 4. These two sensors were placed directly above the panels' sensors, separated 114 mm from the panels' top fiber [Figure 2(c)].

3.2.2. Automated Total Station. An automated total station (ATS), Leica TCA2003 (Figure 3) was employed to record the vertical coordinates of prisms (targets) placed along girder line 3 (Figure 4) during static load tests (Hernandez and Myers 2018a). The accuracy of the vertical deflections estimated using the ATS has been reported to be ±0.1 mm (0.004 in.) by Merkle and Myers (2004). Twenty-four sections were selected to monitor the vertical deflection of the girders.

Figure 3. Non-contact remote data acquisition systems.
(a) Automated total station; (b) remote sensing vibrometer (RSV-150).

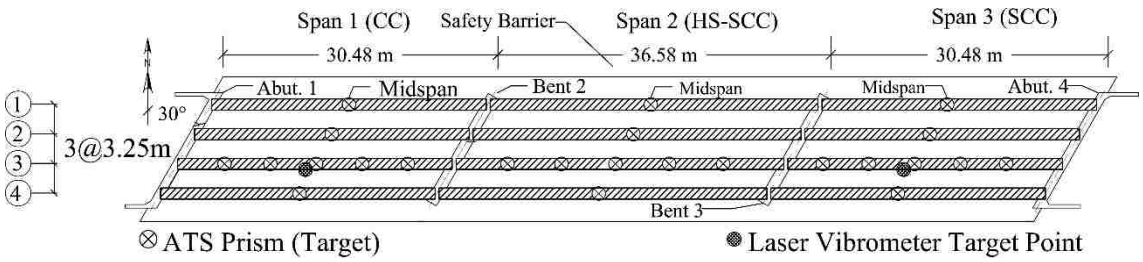

Figure 4. Bridge A7957 load test instrumentation.
Conversion factor: 1 m = 3.28 ft.

Fifteen ATS prisms were deployed along the third girder at 1/6L, 1/3L, 1/2L, 2/3L, and 5/6L of each span. Three additional prisms were mounted at the other girders' midspan (at L/2) in each span (Figure 4).

3.2.3. Remote Sensing Vibrometer. A remote sensing vibrometer (RSV-150) [Figure 3(b)] was used to record the bridge's dynamic vertical deflection of the exterior spans' girder 3 (midspan). The RSV-150 has a bandwidth up to 2 MHz for nondestructive test (NDT) measurements and can detect the vibration and displacement of distant points of structures with limited access. The precision of the RSV-150 is ±0.025 mm (0.001 in.) when it records the dynamic response of a member.

3.3. FIELD TEST PROGRAM

A field test program, which consisted of static and dynamic tests executed on the superstructure of Bridge A7957, was designed to obtain the maximum static and dynamic responses of the bridge superstructure. MoDOT H20 dump trucks (Figure 5) were employed to load the bridge during the tests (Hernandez and Myers 2016b).

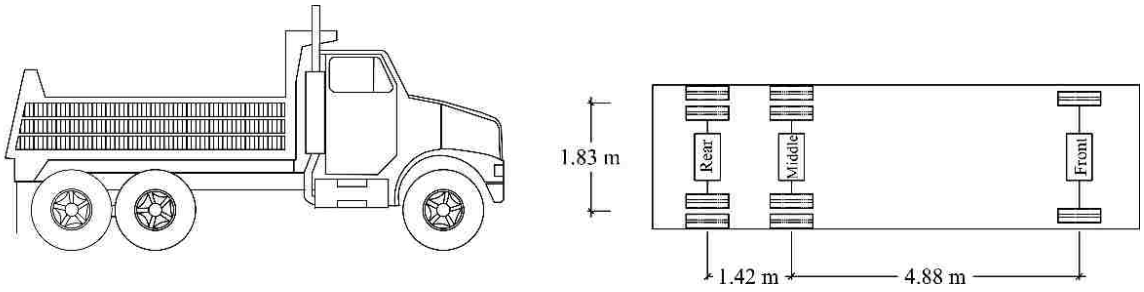

Figure 5. Test truck's average dimensions (MoDOT H20 dump truck).
Conversion factor: 1m = 3.28 ft.

3.3.1. Static Diagnostic Load Tests. Six MoDOT H20 dump trucks were employed during the load tests.

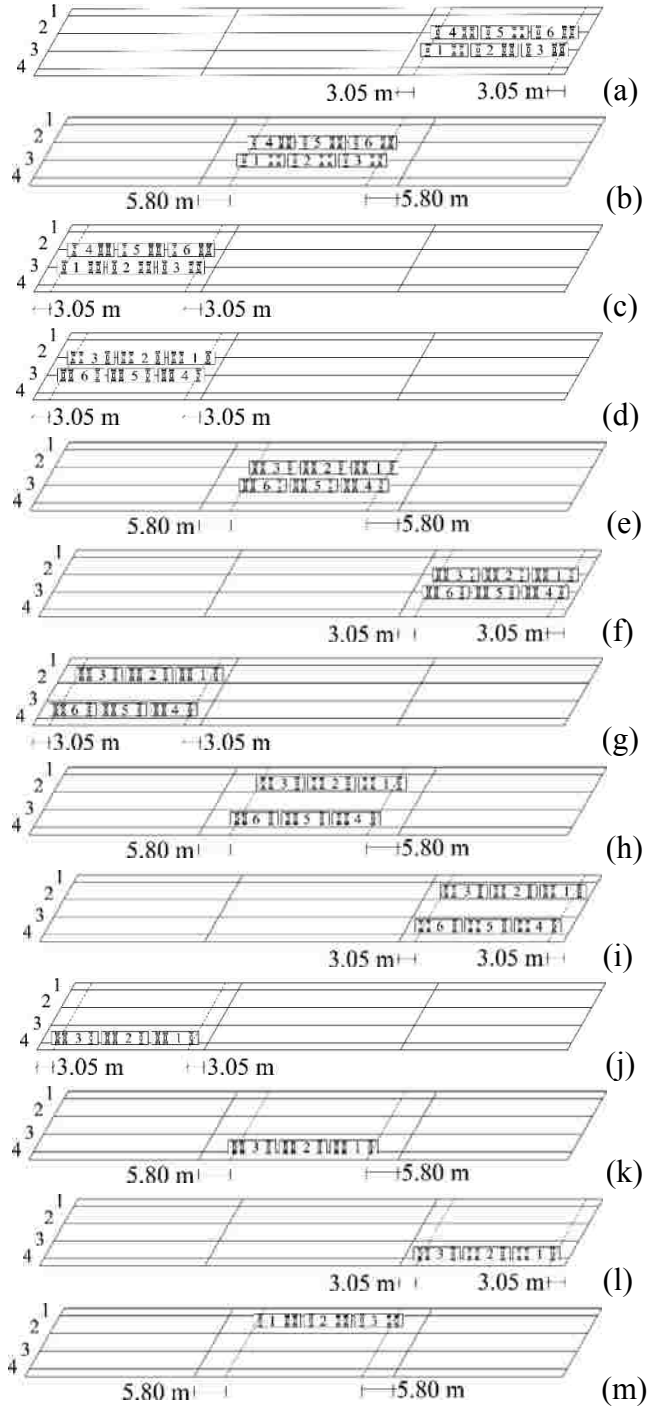

Figure 6. Static load test configurations.
Conversion factor: 1 m = 3.28 ft.

Figure 6 presents the thirteen static load configurations employed to obtain the maximum static vertical deflection of the bridge when a single lane or two lanes were loaded. For these first six load configurations, the center of the trucks' exterior wheels was separated 3.25 m (10.67 ft) from the safety barrier's edge [Figure 7(a)]. For stops 7–9, the trucks' exterior axles were placed at 0.60 m (2ft) from the safety barrier's edge [Figure 7(b)]. For the last for load stops, the trucks were located at 0.60 m (2 ft) from the barrier's edge [Figure 7(c)]. During the static load tests, the vertical deflection of the target prisms was obtained. The section locations are shown in Figure 4. Table 1 lists the vertical deflections estimated for the static load configurations described in Figure 6.

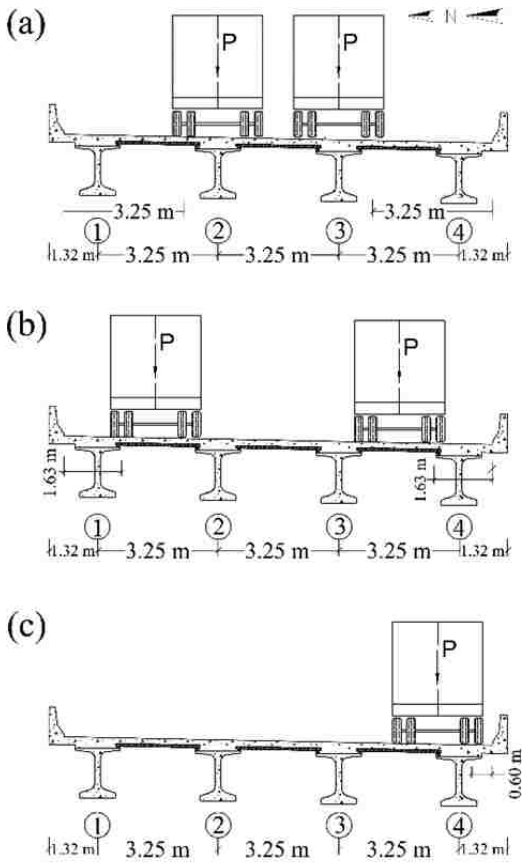

Figure 7. Trucks' distance to safety barrier.
(a) Stops 1–6; (b) stops 7–9; (c) stops 10–13. Conversion factor: 1 m = 3.28 ft.

The maximum deflections were obtained for midspan 2—the longest span. Larger deflections were obtained at midspan for the exterior and interior girders located near the applied load. For the load configurations loading the superstructure close to the safety barriers (stops 7-9), the load was distributed more uniformly, and the midspan deflections were comparable for the girders of the same span. The girders' bottom flange strain, collected with the VWSG instrumentation described in Figure 2, are reported in Table 2 ((Hernandez and Myers 2016b)). These values correspond to the two-lane and one-lane load configurations described in the previous section.

Table 1. Experimental vertical deflections (mm).

Stop	Span	Δ_{G1}	Δ_{G2}	Δ_{G3}	Δ_{G4}
Two lanes loaded					
1	3	4.2	7.1	6.9	4.6
2	2	6.3	9.7	9.5	6.2
3	1	5.1	6.9	6.7	4.9
4	1	4.2	6.7	6.9	4.4
5	2	6.4	9.8	10.1	6.4
6	3	4.9	8.4	7.8	5.2
7	1	4.9	5.1	5.5	5.7
8	2	7.3	7.8	8.1	7.6
9	3	4.4	5.5	5.9	5.9
One lane loaded					
10	1	0.1	1.3	3.5	5.0
11	2	0.8	2.0	4.9	7.7
12	3	1.2	2.1	3.5	5.4
13	2	8.6	5.4	2.6	1.0

Note: Experimental measurements were truncated to the accuracy of the ATS (Hernandez and Myers 2015a, 2018a). Conversion factor: 1 in. = 25.4 mm.

3.3.2. Dynamic Load Test. Dynamic tests were conducted by driving a truck at different speeds that ranged from 16 km/h (10 mi/h) to 97 km/h (60 mi/h). For each test, the truck speed was constant starting with 16 km/h (10 mi/h). Then, the speed was increased at a rate of 16 km/h (10mi/h) until the maximum speed of 96 km/h (60 mi/h)

was attained for the last test. Experimental data was recorded with the RSV-150 [Figure 3(b)] at a sampling rate of 120 Hz. The truck was driven in both directions, separated 0.60 m (2 ft) from the safety barrier's edge as illustrated in [Figure 7(c)]. The test procedures and load configurations used during the diagnostic test program have been reported by the authors elsewhere (Hernandez and Myers 2016c, 2016b, Hernandez and Myers 2017, Hernandez and Myers 2018a). The maximum dynamic and static deflections recorded at the centerlines of midspans 1 and 3 are reported in Table 3.

Table 2. Experimental longitudinal strains (με).

Stop	Span	ε_{G1}	ε_{G2}	ε_{G3}	ε_{G4}
Two lanes loaded					
1	3	45	83	89	48
2	2	55	95	92	54
3	1	46	84	87	49
4	1	49	87	84	46
5	2	54	92	95	55
6	3	48	89	83	45
7	1	-	-	73	65
8	2	-	-	80	75
9	3	-	-	67	58
One lane loaded					
10	1	-	-	44	64
11	2	4	17	51	78
12	3	-	-	43	65
13	2	78	51	17	4

Table 3. Static and dynamic vertical deflections.

Speed (km/h)	16	32	48	64	80	96
D_{dyn}^{max} (mm)	1.77	1.79	1.79	1.77	2.03	2.08
D_{sta}^{max} (mm)	1.77	1.77	1.77	1.77	1.77	1.77

Conversion factor: 16 km/h = 10 mi/h.

4. ANALYTICAL EVALUATION OF BRIDGE A7957

4.1. LOAD RATING OF BRIDGES (AASHTO LRFR)

The rating factor of a bridge component in LRFR format is obtained (Minervino et al. 2004, AASHTO 2010) by

$$RF = \frac{C - \gamma_{DC}DC - \gamma_{DW}DW \pm \gamma_P P}{\gamma_L LL(1 + IM)} \quad (1)$$

where RF = rating factor; C = capacity = $\varphi\varphi_c\varphi_s R_n \geq 0.85\varphi R_n$ (strength limit states); C = f_R (service limit states); f_R = allowable stress specified in LRFD specifications (Minervino et al. 2004, AASHTO 2012); φ = LRFD resistance factor; φ_c = condition factor; φ_s = system factor; R_n = nominal member resistance; DC = dead load effect due to structural components and attachments; DW = dead load effect due to wearing surface and utilities; P = permanent loads other than dead loads (e.g., post-tensioning); LL = live load effect; IM = dynamic load allowance (impact factor); γ_{DC} = LRFD load factor for structural component and attachments; γ_{DW} = LRFD load factor for wearing surfaces and utilities; γ_P = LRFD load factor for permanent loads other than dead loads; and γ_L = evaluation live load factor.

4.2. BRIDGE A7957 ANALYTICAL PARAMETERS

4.2.1. Girder Distribution Factors (G*DF*). The AASHTO LRFD approach (AASHTO 2012) approach was followed to estimate the interior and exterior girder distribution factors (GDF) for single and multiple loaded lanes. The GDF for an interior girder with two or more (multiple) design lanes loaded can be estimated by:

$$GDF_i^m = 0.075 + \left(\frac{S}{2900}\right)^{0.4}\left(\frac{S}{L}\right)^{0.2}\left(\frac{K_g}{Lt_s{}^3}\right)^{0.1} \quad (2)$$

where S = girder spacing (mm); L = span length (mm); t_s = deck thickness; K_g = stiffness parameter (mm^4); $K_g = n(I_g+e_g{}^2A_g)$; e_g = girder eccentricity (vertical distance from the girder's centroid to the slab's centroid); n = modular ration (E_{girder}/E_{slab}); E = modulus of elasticity of the concrete estimated as $0.043w^{1.5}(f'_c)^{0.5}$ (MPa); w = unit weight of concrete (kg/m^3); I_g = girder's moment of inertia (mm^4); and A_g = girder's cross-sectional area (mm^2). An interior girder's GDF with a single lane loaded was obtained by:

$$GDF_i^s = 0.06 + \left(\frac{S}{4300}\right)^{0.4}\left(\frac{S}{L}\right)^{0.3}\left(\frac{K_g}{Lt_s{}^3}\right)^{0.1} \quad (3)$$

the GDF of an exterior girder with two or more design lanes loaded was estimated with the following equations:

$$GDF_e^m = e(GDF_i^m) \quad (4)$$

$$e = 0.77 + \frac{d_e}{2800} \geq 1 \quad (5)$$

where d_e = horizontal distance from the barrier's edge to the exterior girder's centroid (mm). The simple static distribution method (lever rule), was used to estimate the GDF of an exterior girder subjected to a single-lane load as Equation (6) shows. This equation was written by assuming an internal hinge at an interior support (girder 3) and by summing moments, produced by the acting forces and girder's reactions, about girder 3 (support selected to estimate the GDF). For example, the forces acting to the left side of girder 3 are the girder 4's reaction and the load P producing moment about the girder 4 [Figure 7(c)].

$$GDF_e^S = m_p\left(\frac{S + d_e - 1524}{S}\right) \quad (6)$$

where m_p = multiple presence factor (1.2 for a single lane loaded). The skew modifying factor was determine using Equations 7–8.

$$SF = 1 - C_1(\tan\theta)^{1.5} \quad (7)$$

$$C_1 = 0.25\left(\frac{K_g}{Lt_s{}^3}\right)^{0.25}\left(\frac{S}{L}\right)^{0.5} \quad (8)$$

where *SF* = skew correction factor; and θ = skew angle. Table 4 lists the design parameters used to calculate the GDF of the exterior and interior girders of each span (Hernandez and Myers 2016b).

Table 4. Bridge design parameters.

Variable	Spans 1, 3	Span 2
Ag (mm^2)	$479.9x10^3$	$479.9x10^3$
Ig (mm^4)	$1.2383x10^{11}$	$1.2383x10^{11}$
Kg (mm^4)	$702.207x10^9$	$785.936x10^9$
d_e (mm)	914	914

4.2.2. Dynamic Load Allowance (*IM*). The current AASHTO LRFD Specifications (AASHTO 2012) presents a very simplistic method and recommends a DLA (impact factor) equal to 0.33 for bridge components other than deck joints (Barker and Pucket 2013). Table 5 lists the GDF values determined following the AASHTO LRFD procedure described above. The distribution factor of an exterior or interior girder correspond to the maximum value obtained for the two-lane and one-lane load cases.

Table 5. AASHTO LRFD GDFs.

Span	Case (lanes loaded)	*GDFi* (corrected)	*GDFe* (corrected)
1, 3	≥ 2	0.783	0.861
1, 3	1	0.533	0.932
2	≥ 2	0.756	0.832
2	1	0.507	0.936

Note: Skew factors were used to modify the GDFs.

4.2.3. Analytical Load Rating of Bridge A7957. Bridge A7957's rating fac- tor information is presented in Table 6. Rating factors' calculations are omitted for the sake of brevity; however, Table 7 summarizes Bridge A7957's analytical rating factors for the interior and exterior girders in each span.

Table 6. Bridge A7957 theoretical moments and load rating parameters.

Parameter	Span 1	Span 2	Span 3
Mn_A (kN-m)	11,116.0	13,606.8	11,122.0
M_{DC} (kN-m)	3,299.7	4,654.0	3,299.7
M_{DW} (kN-m)	309.4	280.7	309.4
M_{LL} (kN-m)	2,839.7	2,935.0	2,839.7
Theoretical parameters (AASHTO LRFD)			
GDF_i	0.783	0.756	0.783
GDF_e	0.932	0.936	0.932
IM	0.33	0.33	0.33

Conversion factor: 1 kN-m. = 0.7376 kip-ft.

Table 7. Bridge A7957 analytical rating factors.

Rating factor	Span 1	Span 2	Span 3
Interior member	1.26	1.43	1.26
Exterior member	1.06	1.15	1.06

5. EXPERIMENTAL EVALUATION OF BRIDGE A7957

5.1. LOAD RATING OF PRESTRESSED CONCRETE BRIDGES USING SITE-SPECIFIC PARAMETERS

The conservatism of an analytical load rating may be reduced by including site-specific parameters estimated from experimental data recorded during a diagnostic load test. Hernandez and Myers (2018b) proposed a systematic approach that permits isolating and estimating the contribution of these parameters.

In addition, this methodology permits removing unreliable contributing factors from the load rating of prestressed concrete bridges. The relation between the experimental and analytical rating factors can be obtained using the following expression (Hernandez and Myers 2018):

$$RT_E = \left[\rho_c \rho_g \rho_i \rho_k \rho_l \rho_b\right] RT_A \tag{9}$$

where RT_E = experimental bridge rating = $RF_E(RVW)$; RF_E = experimental rating factor; RVW = rating vehicle weight; RT_A = analytical rating = $RF_A(RVW)$; RF_A = analytical rating factor; ρ_c = contribution to experimental load rating from capacity (takes into consideration differences between experimental and nominal material strength properties); ρ_g = contribution factor due to lateral distribution; ρ_i = contribution from dynamic load allowance (impact factor); ρ_k = contribution from additional stiffness; ρ_l = contribution factor from longitudinal distribution moment; and ρ_b = bearing restraint force effects.

5.2. QUANTIFICATION OF SITE-SPECIFIC PARAMETERS

The quantification of the site-specific parameters necessary to apply Equation (11) in an experimental strength evaluation of a PC bridge can be summarized as follows (Barker 1999):

- Inspect the bridge to determine the actual dimensions, properties, and dead load.
- Use NDT technology to collect the mechanical properties of the different bridge's components. Compressive strength of concrete (f'c), modulus of elasticity of concrete (Ec), and modulus of rupture of concrete (fr) are obtained from the field data.
- Estimate the experimental girder distribution factor (DF_E).
- Estimate the experimental dynamic load allowance (IM_E).
- Determine the bearing restraint forces and moment (M_{BR}).
- Remove axial stress from critical section stress profile.
- Calculate the experimental total moment (M_T).
- Calculate the elastic moment (M_E) at the critical section.
- Calculate the elastic longitudinal adjustment moment at the critical section (M_{LE}).

5.2.1. Experimental Mechanical Properties. The experimental mechanical properties of the different bridge components were obtained the same day the diagnostic tests were conducted.

Table 8. Compressive strength of Bridge A7957's components.

Component	f'_c (MPa)
Span 1	72.46
Span 2	78.48
Span 3	63.58
Deck	38.33

Conversion factor: 1 MPa = 145 psi.

Table 8 lists the different bridge component's average compressive strength values (Hernandez and Myers 2015b, Myers et al. 2016). Table 9 lists the average modulus of elasticity of the different Bridge A7957's components.

Table 9. Modulus of elasticity of Bridge A7957's components.

Component	E_c (GPa)
Span 1	38.8
Span 2	39.3
Span 3	38.7
Deck	30.5

Conversion factor: 1 GPa = 145 ksi

5.2.2. Experimental Load Distribution Factor. The experimental distribution factors were estimated with deflection values recorded at the girders' midspan. The experimental distribution factor values were estimated with the following expression (ACI 2016, Hernandez and Myers 2016b):

$$LDF_E = n\frac{\delta_{Gi}}{\sum_{i=1}^{k}\delta_{Gi}} \tag{10}$$

where LDF_E = experimental distribution factor of *ith* girder obtained from strain values ,*n* = number of lanes loaded; and *k* = number of girders; and δ_{Gi} = vertical deflection of the *ith* girder at mid-span. Table 10 lists the DF_E values for all the exterior and interior girders (Hernandez and Myers 2016c).

5.2.3. Experimental Dynamic Load Allowance. The experimental dynamic load allowance was estimated with Equation (11):

$$IM_E = \frac{D_{dyn}^{max} - D_{sta}^{max}}{DLA_{sta}^{max}} \tag{11}$$

where IM_E = experimental dynamic load allowance; D_{dyn}^{max} = maximum dynamic (measured) vertical deflection (mm); and D_{sta}^{max} = maximum static deflection obtained from passing the test truck at a crawl speed (mm).

Table 10. Experimental LDFs (estimated with deflection measurements).

Stop	Span	$LDF^E_{\delta 1}$	$LDF^E_{\delta 2}$	$LDF^E_{\delta 3}$	$LDF^E_{\delta 4}$
Two lanes loaded					
1	3	0.368	0.623	0.605	0.404
2	2	0.397	0.612	0.599	0.391
3	1	0.432	0.585	0.568	0.415
4	1	0.378	0.604	0.622	0.396
5	2	0.391	0.599	0.618	0.391
6	3	0.373	0.639	0.593	0.395
7	1	0.462	0.481	0.519	0.538
8	2	0.474	0.506	0.526	0.494
9	3	0.406	0.507	0.544	0.544
One lane loaded					
10	1	0.010	0.131	0.354	0.505
11	2	0.052	0.130	0.318	0.500
12	3	0.098	0.172	0.287	0.443
13	2	0.489	0.307	0.148	0.057

Table 11 lists the bridge's maximum dynamic and static deflection recorded for the different speeds the truck passed over the bridge during the dynamic tests (rows 2 and 3, respectively).

Table 11. Experimental and analytical dynamic load allowance.

Speed (km/h)	16	32	48	64	80	96
D_{dyn}^{max} (mm)	1.77	1.79	1.79	1.77	2.03	2.08
D_{sta}^{max} (mm)	1.77	1.77	1.77	1.77	1.77	1.77
IM^E	0.000	0.010	0.010	0.000	0.150	0.175
IM^{A*}	0.33	0.33	0.33	0.33	0.33	0.33

*Value recommended by AASHTO LRFD Bridge Design Specifications (AASHTO 2012). Conversion factor: 16 km / h = 10 mi /h.

In addition, experimental values of IM^E, corresponding to different truck speeds passing over the bridge, are presented in row 4. The maximum experimental IM^E value was 0.175 corresponding to a truck speed of 96 km/h. (Hernandez and Myers 2017, Hernandez and Myers 2018a, 2018b). The analytical dynamic load allowance according to (AASHTO 2012) is reported in row 5.

5.2.4. Bearing Restraint Effects. The bearing restraint effect is provided by a bearing force causing a moment about the center of gravity of the girders' cross section. The bearing force (Figure 8) at the interior supports (piers) is obtained by using the recorded strains at both sides of the bearing and is estimated by

$$BF = \frac{(\sigma_{bfj} - \sigma_{bfi})A_{bf}}{2} \tag{12}$$

where BF = bearing force; A_{bf} = area of the bottom flange at the bearing; and σ_{bfj} = stress at the right face of the support; and σ_{bfi} = stress at the left face of the support.

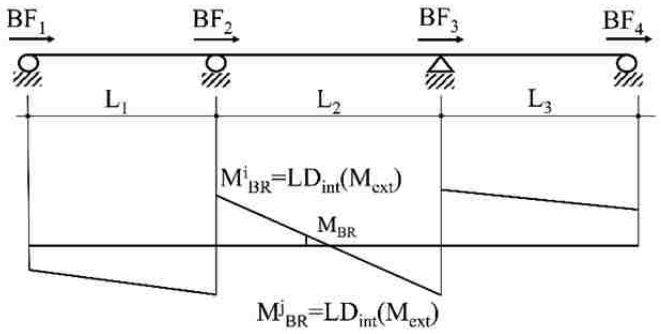

Figure 8. Bearing restraint moments.

The equivalent external applied moment (M_{ext}) caused by the bearing restraint effect at a support is estimated by

$$M_{ext} = BF * y_b \tag{13}$$

where y_b = distance from the neutral axis to bottom flange layer. The moment distribution method can be employed to distribute the external moment to each face of a support. If the main load-carrying member stiffness can be assumed to be constant throughout the span, the distribution can be obtained by (Barker 1999)

$$LD_{int} = \frac{\left(\frac{1}{L_i}\right)}{\sum\left(\frac{1}{L_i}\right)} \tag{14}$$

where LD_{int} = longitudinal moment distribution factor at pier i; and Li = span length of the ith span on each face of the support (Figure 8). For a critical section located at the midspan, the bearing restraint moment effect is computed by

$$M_{BR} = \frac{\left(M_{BRi} + M_{BRj}\right)}{2} \tag{15}$$

where M_{BR} = bearing restraint moment at a midspan critical section (Figure 8); M^i_{BR} = bearing restraint moment at the first pier location; and M^j_{BR} = bearing restraint moment at the second pier location.

5.2.5. Axial Stress. Strain gauges were installed throughout the depth of the member to record the longitudinal strains across the section. A strain profile (Figure 9) was constructed with the experimental data recorded by the strain gauges and the girder modulus of elasticity reported in Table 9. A best fit line was obtained to estimate the values of the stresses at the bottom flange of the girders. From this graph, the following relation can be written as

$$\sigma = \frac{1}{m}(y_b - d_i) \tag{16}$$

where σ = stress within girder section including axial bearing restraint stress; d_i = distance from bottom fiber to the ith layer where the strain gauge is installed; m = slope of the stress profile = y_b / ($\varepsilon_b E_c$); ε_b = strain at the bottom flange; and E_c = Modulus of elasticity of concrete (obtained experimentally the same day a load test is conducted).

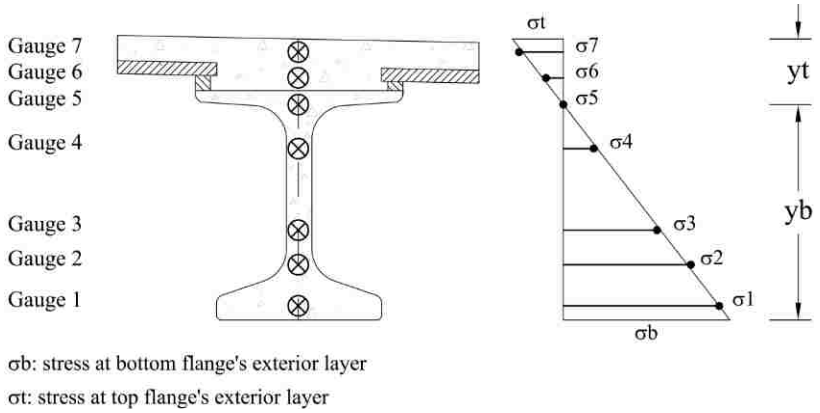

Figure 9. Girder stress profile at critical section.

The overall bearing force (axial force) acting at a section was found by summing the horizontal forces acting in the free body diagram of the critical section. The additional axial stress due to the bearing force can be computed and removed from the stress profile using the following expression:

$$\sigma_{BF} = \frac{BF}{A_{comp}} \tag{17}$$

where A_{comp} = equivalent concrete composite area = A_{conc} + $n_{slab}(A_{slab})$; A_{conc} = Area of concrete; A_{slab} = Effective slab area; and n_{slab} = modular ratio (E_{slab} / E_c). A section stress profile with the bearing axial force removed can be found as follows:

$$\sigma_m = \frac{1}{m}\left(y_b - \frac{d_i}{2}\right) - \sigma_{BF} \tag{18}$$

5.2.6. Total Experimental Moment. The total experimental moment in a pre-stressed concrete section (Figure 10) was estimated with the following expression:

$$M_T = \frac{2}{3}(y_b + y_t)\frac{\varepsilon_b E_c}{2}A_{tens} \tag{19}$$

where A_{tens} = area of the cross section subjected to tension; and y_t = distance from the neutral axis to the top flange layer.

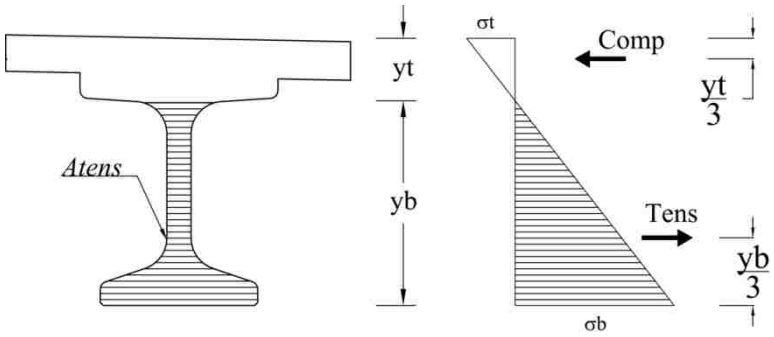

Figure 10. Total experimental moment.

5.2.7. Experimental Elastic Moment. The elastic moment with axial and bearing moment effects removed was computed at each critical section as follows (Barker 1999):

$$M_E = M_T - M_{BR} \tag{20}$$

5.2.8. Longitudinal Distribution Moment. The static moments were found using the following set of equations (Barker 1999):

$$M_A^{Stat} = M_{A2} - (1-\alpha)M_{A1} - \alpha M_{A3} \tag{21}$$

$$M_E^{Stat} = M_{E2} - (1-\alpha)M_{E1} - \alpha M_{E3} \tag{22}$$

where M_A^{Stat} = static moment for the analytical load truck moment; M_E^{Stat} = static moment for experimental data; M_A = analysis load truck moment at the critical sections

(i=1, 2 and 3) within the interior span (1 = left, 2 = maximum, and 3 = right location); M_E = experimental moment at the critical sections (i=1, 2 and 3) within the interior span (1 = left, 2 = maximum, and 3 = right location); and α = percentage of length to point of maximum moment.

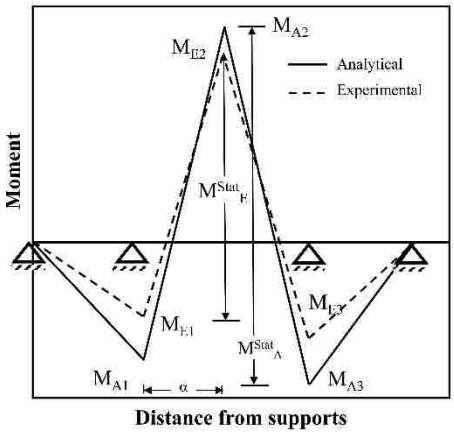

Figure 11. Analytical and experimental moment diagrams.

The experimental elastic moment adjusted for longitudinal distribution were computed by

$$M_{LE} = \frac{M_E^{Stat}}{M_A^{Stat}} M_{A2} \tag{23}$$

5.3. EXPERIMENTAL LOAD RATING RESULTS

Table 12 lists a summary of the experimental results of the interior and exterior girders of the middle span 2 when the maximum load was placed in span 2 (load stop 2 in Figure 6). Row 2 presents the interior and exterior experimental load distribution factors estimated with Equation (10) (see Table 10), and row 3 reports the experimental dynamic load allowance computed with Equation (11) (Table 11). Information about the longitudinal distribution of the bridge can be obtained by comparing ML_E and M_E.

Similarly, information about the contribution from the bearing restraint effects can be obtained by comparing the M_E and M_T.

Table 12. Experimental properties estimated from field test results.

Parameter	Midspan 2	
	Interior Girder	Exterior Girder
DF_E	0.639	0.544
IM_E	0.175	0.175
Mn_E, kN-m (kip-ft)	14,319.2 (10,561.3)	14,242.8 (10,505.0)
M_T, kN-m (kip-ft)	536.1 (726.8)	399.1 (294.4)
M_E, kN-m (kip-ft)	743.2 (548.2)	410.8 (303.0)
M_{LE}, kN-m (kip-ft)	-1,587.0 (1170.5)	709.4(523.2)
M_{TRK}, kN-m (kip-ft)	3,586.6 (2,645.3)	3,042.1 (2,243.8)

5.3.1. Contribution from Capacity. The contribution capacity factor was estimated using Equation (24):

$$\rho_c = \frac{c_E - \gamma_{DC} M_{DC} - \gamma_{DW\_E} M_{DW}}{c_A - \gamma_{DC} M_{DC} - \gamma_{DW} M_{DW}} \tag{24}$$

where C_E = experimental capacity = $\varphi\varphi_C\varphi_S Mn_E \geq 0.85\varphi Mn_E$ (strength limit states); Mn_E =experimental flexural resistance (estimated with mechanical properties collected in the field as shown in Tables 7–8); *DC* = dead load effect due to structural components and attachments; *DW* = dead load effect due to wearing surface and utilities; γ_{DC} = LRFD load factor for structural component and attachments; γ_{DW} = LRFD load factor for wearing surfaces and utilities [for strength limit state *DW* may be taken as 1.5 or 1.25 (if the wearing surface has been field measured)]; C_A = analytical capacity = $\varphi\varphi_C\varphi_S Mn_A \geq 0.85\varphi Mn_A$ (strength limit states); and Mn_A =analytical (nominal) flexural resistance. For illustration, the value of *DW* was assumed equal to 1.25 when the experimental flexural capacity was computed. The reason to do that was that during a field inspection, previous

to a load test, information related to the wearing surface thickness can be recorded and the AASHTO MBE allows this reduction. The estimated contribution from the capacity parameter (ρ_c) increases 10.6% and 9.6 % the experimental load rating capacity of the interior and exterior girder, respectively (Table 14, row 1).

5.3.2. Contribution from Lateral Load Distribution. The contribution capacity factor was estimated using the following expression:

$$\rho_g = \frac{DF_A}{DF_E} \tag{25}$$

where DF_A = analytical girder distribution factor obtained according to (AASHTO 2012) (Table 10); DF_E = experimental load distribution factor obtained as the maximum value (Table 9) for an interior and exterior girder . The experimental lateral load distribution factors resulted in less conservative values compared to the ones obtained following the equations proposed in AASHTO (2012). The contribution of the lateral load distribution for the interior girder was 18.3% and for the exterior girder 72.7%. The lateral load contribution in the case of an exterior girder with a single lane load is quite conservative because its value is obtained by applying the lever rule method. This is an example of the benefits that come with load test; a more precise estimation of an exterior girder's distribution factor that avoid underestimation of an exterior girder's remaining flexural capacity.

5.3.3. Contribution from Dynamic Load Allowance. The contribution capacity from dynamic load allowance was estimated with Equation (26).

The values of *IMA* and *IME* are reported in Table 11. The experimental dynamic load allowance represents an increment in the load rating of 13.2%.

$$\rho_i = \frac{(1 + IM_A)}{(1 + IM_E)} \tag{26}$$

5.3.4. Contribution from Additional Stiffness. The contribution from the additional stiffness is due to the presence of secondary elements that benefit the service response of the structure. The contribution from the additional stiffness was estimated using Equation (27):

$$\rho_K = \frac{(M_{TRK} DF_E)}{(ML_E)} \tag{27}$$

where M_{TRK} = analytical test truck moment; and M_{LE} = experimental elastic moment adjusted for longitudinal distribution (Table 12). The additional stiffness enhanced the analytical load rating of the middle span's interior girder in 44.4%. In the case of the exterior girder the increment of the load analytical load rating was 174%. It is obvious the additional contribution transmitted to the girder stiffness by the parapet in the case of the exterior girder. Although this parameter is not difficult to visualize and estimate, it is difficult to explain its source and to rely on its availability for high levels of service load. For this reason, some bridge owners may prefer to remove this parameter from the experimental load rating.

5.3.5. Contribution from Longitudinal Distribution Moment. The contribution from the additional stiffness was estimated using Equation (28):

$$\rho_l = \frac{(ML_E)}{(M_E)} \tag{28}$$

where M_E = experimental elastic moment with bearing restraint effect removed (Table 12). The longitudinal distribution increased the experimental load rating capacity 135% and 72.7% of the interior and exterior girders, respectively. This parameter suggests that the interior supports are stiffer than they are idealized by the models used in design and analytical evaluation of Bridge A7957. More research is necessary to estimate the real contribution and impact of the support rigidity.

5.3.6. Contribution from Bearing Restraint Force Effects. The contribution of the bearing restraint effects was estimated by

$$\rho_b = \frac{(M_E)}{(M_T)} \tag{29}$$

The bearing restraint contribution improved the rating capacity approximately 2% and 3% for the interior and exterior girders. This contribution can be neglected from the experimental load rating due to its low value. More research is necessary to quantify the real and impact of this parameter in an experimental load rating. It might not be worth the extra number of calculations to compute its value.

6. ACCEPTABLE EXPERIMENTAL LOAD RATING CAPACITY

Table 13 lists the site-specific parameters that enhance the experimental load rating capacity of Bridge A7957. The estimation of these parameters allows bridge owners to (1) reduce the conservatism of an analytical load rating; (2) isolate the contribution of each in-situ beneficial parameter to the load rating; (3) remove the contribution of the unreliable parameters, which are not present at higher service load levels, from the experimental load rating capacity; and (4) make a proper estimation of

the remaining flexural strength capacity of the main carrying member of this prestressed concrete bridge.

Table 13. Experimental site-specific contributing parameters.

Parameter	Midspan 2	
	Interior Girder	Exterior Girder
Member strength, ρ_c	1.106	1.096
Lateral distribution factor, ρ_g	1.183	1.727
Dynamic load allowance, ρ_i	1.132	1.132
Additional stiffness, ρ_k	1.444	2.740
Longitudinal distribution, ρ_l	2.135	1.727
Bearing restraint effect, ρ_b	1.023	1.029
Total product (LR_E/LR_A)	4.671	10.432

If the bridge owner does not accept the contribution from any of the site-specific parameters' contribution to the experimental load rating, the load rating can be adjusted by dividing out the unreliable parameters. For illustration purposes, two adjustments were made to Bridge A7957's experimental load rating factor (LR_{E_I} and LR_{E_I} in Table 14). The first adjustment (LR_{E_I}) was made by dividing out the contribution from the additional stiffness and bearing restraint contribution.

Table 14. Bridge A7957 adjusted experimental load rating capacity.

Parameter	Midspan 2	
	Interior Girder	Exterior Girder
Analytical load rating (strength I, inventory level), LR_A	1.43	1.15
Experimental load rating, LR_E [Equation (9)]	6.68	12.00
LR_{E_I} (ρ_k and ρ_b removed)	4.52	4.25
LR_{E_II} (ρ_k, ρ_l and ρ_b removed)	2.12	2.46

The second adjustment (LR_{E_II}) was attained by removing the longitudinal distribution in addition to the adjustments made to LR_{E_I}. The experimental load rating strength have been reduced to an acceptable level as shown in Table 14 (rows 4 and 5). It

can be noted that these experimental results indicate that Bridge A7957 possess a larger strength capacity than predicted by the theoretical approach proposed by the current evaluation code (AASHTO 2010). This difference can be explained by the fact that (1) a diagnostic load test reflects an as-built, in-service response of a bridge structure; and (2) this type of tests incorporates in-situ parameters that are beneficial to a bridge's service response and load rating capacity factor.

7. SUMMARY AND CONCLUDING REMARKS

The first series of static and dynamic diagnostic load tests was successfully performed on the superstructure of Bridge A7957 to corroborate some design and analysis assumptions, and to perform an experimental evaluation of a bridge's superstructure.

An experimental methodology to conduct strength evaluation of prestressed concrete bridges through load testing in LRFR format has been developed in this research study. The experimental evaluation presented herein proved that Bridge A7957' main supporting members possess a larger strength capacity than the predicted by the AASHTO Manual for Bridge Evaluation.

The evaluation by quantifying site-specific parameters allows isolating and estimating the contribution of each field parameter increasing the theoretical reported strength capacity (load rating) of a bridge. In addition, this systematic approach allows the removal of unreliable contributing parameters that may not be active after certain level of service load from the load rating of a bridge. This experimental alternative of strength evaluation will enable monitoring and updating changes in Bridge A7957's

remaining flexural capacity at the different stages of its service life. Moreover, this systematic methodology will allow bridge owners and evaluators make rational decisions related to maintenance, load posting, rehabilitation, and demolition of existing prestressed and reinforced concrete bridges.

ACKNOWLEDGEMENTS

The authors would like to acknowledge the Missouri Department of Transportation (MoDOT) and the Tier 1 University Transportation Center RECAST at Missouri S&T for sponsoring this research study. The staff support from the Dept. of Civil, Architectural & Environmental Engineering (CArEE) and Center for Infrastructure Engineering Studies (CIES) at Missouri S&T is also greatly appreciated.

REFERENCES

American Association of State Highway and Transportation Officials. (AASHTO). (2010). The Manual for Bridge Evaluation (2nd Edition) with 2011, 2013, 2014 and 2015 Interim Revisions, Washington, DC.

American Association of State Highway and Transportation Officials. (AASHTO). (2012). LRFD Bridge Design Specifications (6th Edition), Washington, DC.

American Concrete Institute. (ACI). (2016). "Report on Flexural Live Load Distribution Methods for Evaluating Existing Bridges." ACI 342R-16, Farmington Hills, MI.

Barker, M. G. (1999). "Steel girder bridge field test procedures." Const. Build. Mater., 13 (4). 229-239.

Barker, M. G. (2001). "Quantifying field-test behavior for rating steel girder bridges." J Bridge Eng, doi:10.1061/(ASCE)1084-0702(2001)6:4(254), 6 (4). 254-261.

Barker, R. M., and Pucket, J. A. (2013). Design of Highway Bridges: An LRFD Approach, John Wiley & Sons, 3rd Edition, Hoboken, N.J. USA.

Cai, C. S., and Shahawy, M. (2003). "Understanding capacity rating of bridges from load tests." Pract Period Struct Des Constr, 10.1061/(ASCE)1084-0680(2003)8:4(209), 209-216.

Domone, P. L. (2006). "Self-compacting concrete: An analysis of 11 years of case studies." Cement Concrete Comp., 28 (2). 197-208.

Hernandez, E. S., and Myers, J. J. (2015a). "In-situ field test and service response of Missouri Bridge A7957." 16th European Bridge Conference (EBC16), Edinburgh, Scotland, UK.

Hernandez, E. S., and Myers, J. J. (2015b). "Use of self-consolidating concrete and high volume fly ash concrete in Missouri Bridge A7957." Sustainable Performance of Concrete Bridges and Elements Subjected to Aggressive Environments: Monitoring, Evaluation and Rehabilitation, ACI SP 304 (6). 85-100.

Hernandez, E. S., and Myers, J. J. (2016a). "Initial in-service response and lateral load distribution of a prestressed self-consolidating concrete bridge using field load tests." Proc., The Fifth International Symposium on Life-Cycle Civil Engineering (IALCCE 2016), CRC Press, Delf, The Netherlands. 1072-1079.

Hernandez, E. S., and Myers, J. J. (2016b). "Monitoring the initial structural performance of a prestressed self-consolidating concrete bridge." Proc., 8th International RILEM Symposium on Self-Compacting Concrete (SCC2016), RILEM Publications SARL, Washington, DC. 401-411.

Hernandez, E. S., and Myers, J. J. (2017). "Dynamic load allowance of a prestressed concrete bridge through field load tests." SMAR 2017 Fourth Conference on Smart Monitoring, Assessment and Rehabilitation of Civil Structures, Zurich, Switzerland.

Hernandez, E. S., and Myers, J. J. (2018a). "Diagnostic test for load rating of a prestressed SCC bridge." Evaluation of Concrete Bridge Behavior Through Load Testing - International Perspective, ACI SP 323 (13).

Hernandez, E. S., and Myers, J. J. (2018b). "Strength evaluation of prestressed concrete bridges by dynamic load testing." Proc., Ninth International Conference on Bridge Maintenance, Safety and Management (IABMAS 2018), CRC Press, Melbourne, Australia.

Keske, S. D., Miller, D. E., Barnes, R. W., and Schindler, A. K. (2014). "Live-load response of in-service bridge constructed with precast, prestressed self-consolidating concrete girders." PCI Journal, 59 (4). 63-76.

Khayat, K. H., and Mitchell, D. (2009). "Self-consolidating concrete for precast, prestressed concrete bridge elements." National Cooperative Highway Research Program Report 628, NCHRP 628, Transportation Research Board, Washington, DC, 2009, pp. 99.

McSaveney, L., Papworth, F., and Khrapko, M. (2011). "Self compacting concrete for superior marine durability and sustainability." Concrete in Australia, 37 (2). 59-64.

Merkle, W. J., and Myers, J. J. (2004). "Use of the total station for load testing of retrofitted bridges with limited access." Proc., Smart Structures and Materials 2004 - Sensors and Smart Structures Technologies for Civil, Mechanical, and Aerospace Systems, San Diego, CA. 687-694.

Minervino, C., Sivakumar, B., Moses, F., Mertz, D., and Edberg, W. (2004). "New AASHTO guide manual for load and resistance factor rating of highway bridges." J Bridge Eng, doi:10.1061/(ASCE)1084-0702(2004)9:1(43), 43-54.

Myers, J. J., and Bloch, K. (2011). "Accelerated construction for pedestrian bridges: A comparison between high strength concrete (HSC) and high-strength self consolidating concrete (HS-SCC)." Proc., Design, Construction, Rehabilitation, and Maintenance of Bridges, GeoHunan 2011, American Society of Civil Engineers, Hunan, China. 129-136.

Myers, J. J., Hernandez, E. S., Alghazali, H., Griffin, A., and Smith, K. (2016). "Self-consolidating concrete (SCC) and high-volume fly ash concrete (HVFAC) for infrastructure elements: implementation." cmr 16-011, Missouri University of Science and Technology, Rolla, Missouri, Jun. 2016, pp. 725.

Myers, J. J., Volz, J., Sells, E., Porterfield, K., Looney, T., Tucker, B., and Holman, K. (2012). "Self-consolidating concrete (SCC) for infrastructure elements." cmr 13-003_A, Missouri University of Science and Technology, Rolla, Missouri, Aug. 2012, pp. 219.

Ouchi, M., Sada-aki, N., Thomas, O., Hallberg, S.-E., and Myint, L. (2003). "Applications of self-compacting concrete in Japan, Europe and the United States." ISHPC, ISHPC, US Federal Highway Administration. Office of Bridge Technology.

Stallings, J. M., and Yoo, C. H. (1993). "Tests and ratings of short□span steel bridges." J Struct Eng, doi:10.1061/(ASCE)0733-9445(1993)119:7(2150), 2150-2168.

Transportation Research Board. (TRB). (1998). "Manual for Bridge Rating through Load Testing" Research Results Digest No. 234, Washington, D.C.

WsDOT (2009). "Design Memorandum on the Use of SCC in Structural Applications." <http://www.wsdot.wa.gov/eesc/bridge/designmemos/15-2009.htm>. (September 1, 2016).

SECTION

3. SUMMARY, CONCLUSION, ORIGINAL CONTRIBUTION AND RECOMMENDATIONS

3.1. SUMMARY OF RESEARCH WORK

This study aimed at (1) presenting a load test protocol using robust and reliable measurement devices (including noncontact laser technology) to record Bridge A7957's response; (2) obtaining the initial spans' performance to analyze and evaluate the acceptability and predictability of SCC girder behavior when subjected to service loads; (3) comparing differences between the spans' initial performance (particularly the first and third spans that have the same geometry and target compressive strength, but whose girders are fabricated with concrete mixtures of different rheology); and (4) proposing a methodology to conduct strength evaluation of bridges through load testing presented in LRFD/LRFR format that allows isolating and quantifying the contribution of in-situ parameters that increase the reported strength capacity (load rating) of a bridge. The proposed research study consisted of seven tasks necessary to attain the objectives. The tasks are listed next:

- Task 1: Literature Review
- Task 2: Development of Bridge Instrumentation and Load Testing Program
- Task 3: Precast, Prestressed Concrete and Cast-in-place Elements Fabrication
- Task 4: Hardened Properties of Plant and Field Produced Concrete

- Task 5: Bridge Load Testing and Monitoring
    - Task 5a: Static Load Tests
    - Task 5b: Dynamic Load Tests
- Task 6: Evaluation of Experimental Load Testing Results and Refined Finite Element Analysis Simulations
    - Task 6a: Evaluation of Experimental Load Testing Results
    - Task 6b: Refined FEA Simulations
- Task 7: Strength Evaluation of Bridge Superstructure through Load Testing

Conclusions and recommendations based on the research programs results are presented in the following sections.

3.2. CONCLUSIONS

The Missouri Department of Transportation executed the first full-scale structure implementation of high-volume fly ash concrete (HVFAC) and high-strength self-consolidating concrete (HS-SCC) and normal-strength self-consolidating concrete (NS-SCC) on Bridge A7957. High volume fly ash concrete, a sustainable material, was employed at a 50% replacement level within one of the bridge's interior supports. Coupled with the use of SCC, Bridge A7957 is expected to have a longer service life than traditional prestressed and reinforced concrete structures.

Proper selection of material constituents and proper proportion is fundamental to ensure that SCC mixtures perform as expected and similarly to their conventional concrete mixtures counterparts. A performance-based specification may be warranted when specialized advanced concrete materials are used, such as high-strength self-

consolidating concrete, to ensure certain design parameters are met (i.e., modulus of elasticity, aggregate interlock, shrinkage and creep).

The instrumentation phase of the project was conducted effectively. Maturity studies were performed on the different concrete mixtures utilized in Bridge A7957. These studies were used to compare the differences among the mechanical properties development including: creep, shrinkage, thermal gradients, time dependent behavior and serviceability in the long term.

The first series of diagnostic tests was successfully conducted on Bridge A7957. Static tests were performed to (1) compare the end spans' in-service response; (2) establish the baseline response and strength capacity of the different spans; (3) validate design assumptions made during the design stage of the bridge (such as lateral load distribution and dynamic load allowance); and (4) to obtain an experimental load rating baseline of Bridge A7957. These results can be employed to monitor any trend or change in the future structure's behavior.

The structural service performance of conventional concrete (span 1) and normal-strength self-consolidating concrete (span 3) girders was comparable, suggesting that the short-term (i.e., less than one year) service performance of the normal- and high-strength SCC mixtures, employed in this study, should not hinder its implementation in infrastructure projects.

Lateral load distributions were estimated from field measurements (LDFs) and using the AASHTO LRFD approach (GDFs). The AASHTO LRFD GDFs resulted in larger values compared to experimental LDFs. These differences may be attributed to several causes. The AASHTO LRFD equations were developed to be applied to different

types of bridges with a wide range of span lengths, girders spacing, and stiffness. LDFs, obtained from field tests, implicitly consider field conditions such and unintended support restraints, skew angle, contribution of secondary members, and multiple presence factors, which may contribute to improve the bridge's in-service structural performance.

Finite element models of Bridge A7957 were developed and calibrated using experimental data collected during the different static load stops. The finite element models could represent the bridge's static response with an acceptable level of accuracy. The magnitude of the LDFs estimated from FEM simulations was very close to the magnitude of LDFs estimated from field measurements.These refined models will be used to predict the bridge's behavior in future diagnostic tests by performing "virtual" load tests on the structure. This will allow to identify load configurations that produce the absolute maximum static response of the structure, and thus, variations in the lateral distribution factors.

The first series of dynamic load tests were conducted on Bridge A7957 to experimentally establish a baseline dynamic response. The dynamic load allowance of Bridge A7957 was successfully obtained from field measurements and estimated by using three design specifications (OMTC 1983, AASHTO 1992, 2012). The dynamic load allowance estimated using the design specifications resulted in larger values compared to the field values. This disparity might be attributed to the presence of in-situ factors not considered by the theoretical methods proposed in current design and evaluation codes. More importantly, the variation between the experimental and analytical DLA values may have repercussions in the rating factor of existing bridge structures. Further research is needed to understand the source of these variations.

In the long term, the static and dynamic response of Bridge A7957's spans will vary as the prestressed concrete girders, fabricated with conventional concrete and SCC, age or are subjected to overloads. The load test protocols followed in this study is a useful tool that can be employed to update the dynamic load allowance and lateral distribution factors at different ages of the bridge service life.

An experimental approach to conduct strength evaluation of prestressed concrete bridges through load testing in LRFR format has been developed in this research study. To achieve this goal, a systematic methodology proposed by Barker (1999, 2001) was employed to isolate the contribution of field factors that improve a bridge's in-service performance and thus its load rating capacity. Baker's approach was modified to be applied to prestressed concrete bridges according to the current AASHTO LRFD/LRFR evaluation guidelines. The proposed procedure allows isolating and quantifying the contribution of in-situ beneficial parameters and permits removing the contribution from those parameters that might not be present at certain levels of service load yielding a more precise load rating capacity of the prestressed concrete bridges.

The experimental evaluation protocol presented herein proved that Bridge A7957's main supporting members possess a larger flexural strength capacity than the predicted by the AASHTO Manual for Bridge Evaluation. This evaluation approach will enable monitoring and updating changes in the remaining flexural capacity at the different stages of its service life. Moreover, this systematic methodology will allow bridge owners and evaluators make rational decisions related to maintenance, load posting, rehabilitation, and demolition of existing prestressed and reinforced concrete bridges.

3.3. ORIGINAL CONTRIBUTION

The instrumentation and load testing program presented in this study will allow monitoring Bridge A7957's serviceability and structural performance at different stages of the structure's lifetime. Initial values of the flexural strength of Bridge A7957's main carrying members will be compared to future experimental load ratings to quantify the degradation of these members as well as changes in the structure behavior during its 75-year design lifetime. Furthermore, this monitoring program represents a unique opportunity to showcase the use of SCC in infrastructure projects. For this project, the in-service behavior of prestressed self-consolidating concrete members was proven successful, it is expected that this study's results will encourage the implementation of self-consolidating concrete in future highway infrastructures, thereby benefitting the residents of Missouri and other states.

The experimental strength evaluation protocol of prestressed concrete bridges presented in LRFR format is first introduced in this study and was successfully tested. This evaluation protocol advanced the state-of-the-art load rating of prestressed concrete bridges by means of load testing, which is a significant outcome of this work. Specifically, the proposed adapted systematic methodology will enable bridge owners to make rational and reliable decisions regarding maintenance, load posting, rehabilitation, and demolition of other existing (steel, reinforced and prestressed concrete) bridge structures. In addition, this implementation project provided information about the service performance of prestressed self-consolidating concrete members to help fill the gap in current design specifications that do not present any guidance on the use of self-consolidating concrete in infrastructure projects.

The refined finite element simulations of Bridge A7957's superstructure performed with this study will permit the realization of "virtual diagnostic load tests" on the superstructure of Bridge A7957. These simulations will be used in future studies to advance the understanding of differences between the lateral distribution factors employed in bridge design and evaluation as adopted by AASHTO LRFD guidelines for consideration of refinements using new concrete technology.

3.4. RECOMMENDATION FOR FUTURE RESEARCH

The research conducted in this dissertation has yielded significant results and conclusions that can serve as the basis for further research. The following recommendations for future research are suggested:

- Development of standard guidelines to conduct static and dynamic load tests.
- Conduct an analytical and numerical parametric study on the sensitivity that geometric factors have on the lateral and longitudinal distribution of prestressed concrete bridges.
- Conduct an analytical and numerical study to observe how the lateral load distribution factors change when one or more of the main carrying members undergo inelastic deformations.
- Conduct non-deterministic analysis to verify the accuracy of the live load factors employed on the evaluation of prestressed concrete bridges.
- This study showed that it is necessary to continue investigating the source and availability of certain site-specific parameters such as the longitudinal and additional stiffness contribution. It seems easy to visualize and quantify these parameters'

contribution; however, the difficulty to pinpoint their origin and availability at high levels of service loads, makes it difficult to accept their beneficial contribution in the load rating capacity. Further research should be conducted to evaluate the real source and availability of these contributions.

BIBLIOGRAPHY

American Association of State Highway and Transportation Officials. (AASHTO). (1970). *Manual for Maintenance Inspection of Bridges*, Washington, D.C.

American Association of State Highway and Transportation Officials. (AASHTO). (1992). Standard Specifications for Highway Bridges, Washington, DC.

American Association of State Highway and Transportation Officials. (AASHTO). (1994). *Manual for Condition Evaluation of Bridges*, Washington, DC.

American Association of State Highway and Transportation Officials. (AASHTO). (2003). *Manual for Condition Evaluation and Load and Resistance Factor Rating (LRFR) of Highway Bridges*, Washington, DC.

American Association of State Highway and Transportation Officials. (AASHTO). (2010). The Manual for Bridge Evaluation (2nd Edition) with 2011, 2013, 2014 and 2015 Interim Revisions, Washington, DC.

American Association of State Highway and Transportation Officials. (AASHTO). (2012). LRFD Bridge Design Specifications (6th Edition), Washington, DC.

American Concrete Institute. (ACI). (2007). "Self-Consolidating Concrete." *ACI 237*, Farmington Hills, MI.

American Concrete Institute. (ACI). (2014). "Building Code Requirements for Structural Concrete and Commentary." *ACI 318-14*, Farmington Hills, MI.

American Concrete Institute. (ACI). (2016). "Report on Flexural Live Load Distribution Methods for Evaluating Existing Bridges." *ACI 342R-16*, Farmington Hills, MI.

American Society for Testing and Materials. (ASTM). (2010). ASTM C469/C469M-10 "Standard Test Method for Static Modulus of Elasticity and Poisson's Ratio of Concrete in Compression", West Conshohocken, PA.

American Society for Testing and Materials. (ASTM). (2012a). ASTM C39/C39M-12a "Standard Test Method for Compressive Strength of Cylindrical Concrete Specimens.", West Conshohocken, PA.

American Society for Testing and Materials. (ASTM). (2012b). ASTM C617/C617M-12 "Standard Practice for Capping Cylindrical Concrete Specimens", West Conshohocken, PA.

Bakht, B., and Pinjarkar, S. G. (1989). "Dynamic testing of highway bridges. A review." Transportation Research Record 1223, TRB, Washington, D.C., 93-100.

Barker, M. G. (1999). "Steel girder bridge field test procedures." Const. Build. Mater., 13 (4). 229-239.

Barker, M. G. (2001). "Quantifying field-test behavior for rating steel girder bridges." J Bridge Eng, doi:10.1061/(ASCE)1084-0702(2001)6:4(254), 6 (4). 254-261.

Barker, R. M., and Pucket, J. A. (2013). *Design of Highway Bridges: An LRFD Approach*, John Wiley & Sons, 3rd Edition, Hoboken, N.J. USA.

Bhide, S. (2004). "Material Usage and Condition of Existing Bridges in the U.S." Portland Cement Association (PCA), Skokie, IL, pp.

Cai, C. S., and Shahawy, M. (2003). "Understanding capacity rating of bridges from load tests." Pract Period Struct Des Constr, 10.1061/(ASCE)1084-0680(2003)8:4(209), 209-216.

Chajes, M., Shenton III, H., and O'Shea, D. (2000). "Bridge-Condition Assessment and Load Rating Using Nondestructive Evaluation Methods." Transportation Research Record: Journal of the Transportation Research Board, 10.3141/1696-48, 1696 83-91.

Deng, L., Yu, Y., Zou, Q., and Cai, C. S. (2015). "State-of-the-art review of dynamic impact factors of highway bridges." J Bridge Eng, 10.1061/(ASCE)BE.1943-5592.0000672, 20 (5). 04014080.

Domone, P. L. (2006). "Self-compacting concrete: An analysis of 11 years of case studies." Cement Concrete Comp., 28 (2). 197-208.

FHWA (2017). "National Bridge Inventory (NBI)." <http://www.fhwa.dot.gov/bridge/nbi/no10/defbr15.cfm>. (February 26, 2018, 2016).

Ghosn, M., Moses, F., and Gobieski, J. (1986). "Evaluation of steel bridges using in-service testing." Transportation Research Record 1072, Transportation Research Board, Washington, D.C., 71-78.

Harris, D. K. (2010). "Assessment of flexural lateral load distribution methodologies for stringer bridges." Eng Struct, 10.1016/j.engstruct.2010.06.008, 32 3443-3451.

Harris, D. K., Cousins, T., Sotelino, E. D., and Murray, T. M. (2010). "Flexural lateral load distribution characteristics of sandwich plate system bridges: parametric investigation." J Bridge Eng, 10.1061/(Asce)Be.1943-5592.0000105, 684-694.

Hernandez, E. S., Griffin, A., and Myers, J. J. (2014). "Balancing extended service life and sustainable concrete material usage in Missouri Bridge A7957." *Proc., Struct. Faults & Repair: European Bridge Conference (SF&R)*, London, England, UK.

Hernandez, E. S., and Myers, J. J. (2015a). "In-situ field test and service response of Missouri Bridge A7957." 16th European Bridge Conference (EBC16), Edinburgh, Scotland, UK.

Hernandez, E. S., and Myers, J. J. (2015b). "Use of self-consolidating concrete and high volume fly ash concrete in Missouri Bridge A7957." Sustainable Performance of Concrete Bridges and Elements Subjected to Aggressive Environments: Monitoring, Evaluation and Rehabilitation, ACI SP 304 (6). 85-100.

Hernandez, E. S., and Myers, J. J. (2016a). "Field load test and girder distribution factors of Missouri Bridge A7957." *Proc., 2016 PCI Convention and National Bridge Conference*, Nashville, TN.

Hernandez, E. S., and Myers, J. J. (2016b). "Initial in-service response and lateral load distribution of a prestressed self-consolidating concrete bridge using field load tests." *Proc., The Fifth International Symposium on Life-Cycle Civil Engineering (IALCCE 2016)*, CRC Press, Delf, The Netherlands. 1072-1079.

Hernandez, E. S., and Myers, J. J. (2016c). "Monitoring the initial structural performance of a prestressed self-consolidating concrete bridge." *Proc., 8th International RILEM Symposium on Self-Compacting Concrete (SCC2016)*, RILEM Publications SARL, Washington, DC. 401-411.

Hernandez, E. S., and Myers, J. J. (2017). "Dynamic load allowance of a prestressed concrete bridge through field load tests." SMAR 2017 Fourth Conference on Smart Monitoring, Assessment and Rehabilitation of Civil Structures, Zurich, Switzerland.

Hernandez, E. S., and Myers, J. J. (2018a). "Diagnostic test for load rating of a prestressed SCC bridge." Evaluation of Concrete Bridge Behavior Through Load Testing - International Perspective, ACI SP 323 (13).

Hernandez, E. S., and Myers, J. J. (2018b). "Strength evaluation of prestressed concrete bridges by dynamic load testing." *Proc., Ninth International Conference on Bridge Maintenance, Safety and Management (IABMAS 2018)*, CRC Press, Melbourne, Australia.

Keske, S. D., Miller, D. E., Barnes, R. W., and Schindler, A. K. (2014). "Live-load response of in-service bridge constructed with precast, prestressed self-consolidating concrete girders." PCI Journal, 59 (4). 63-76.

Khayat, K. H., and Mitchell, D. (2009). "Self-consolidating concrete for precast, prestressed concrete bridge elements." *National Cooperative Highway Research Program Report 628*, NCHRP 628, Transportation Research Board, Washington, DC, 2009, pp. 99.

Kim, S., and Nowak, A. S. (1997). "Load distribution and impact factors for I-girder bridges." J Bridge Eng, doi:10.1061/(ASCE)1084-0702(1997)2:3(97), 97-104.

McSaveney, L., Papworth, F., and Khrapko, M. (2011). "Self compacting concrete for superior marine durability and sustainability." Concrete in Australia, 37 (2). 59-64.

Merkle, W. J., and Myers, J. J. (2004). "Use of the total station for load testing of retrofitted bridges with limited access." *Proc., Smart Structures and Materials 2004 - Sensors and Smart Structures Technologies for Civil, Mechanical, and Aerospace Systems*, San Diego, CA. 687-694.

Minervino, C., Sivakumar, B., Moses, F., Mertz, D., and Edberg, W. (2004). "New AASHTO guide manual for load and resistance factor rating of highway bridges." J Bridge Eng, doi:10.1061/(ASCE)1084-0702(2004)9:1(43), 43-54.

Myers, J. J., and Bloch, K. (2010). "Innovative Concrete Bridging Systems for Pedestrian Bridges: Implementation and Monitoring." CIES Report for City of Rolla, Missouri University of Science and Technology, Rolla, Missouri, December, 2010, pp. 294.

Myers, J. J., and Bloch, K. (2011). "Accelerated construction for pedestrian bridges: A comparison between high strength concrete (HSC) and high-strength self consolidating concrete (HS-SCC)." *Proc., Design, Construction, Rehabilitation, and Maintenance of Bridges, GeoHunan 2011*, American Society of Civil Engineers, Hunan, China. 129-136.

Myers, J. J., and Carrasquillo, R. (1998). "Production and Quality Control of High Performance Concrete in Texas Bridge Structures." University of Texas at Austin, Austin, Texas, pp.

Myers, J. J., Hernandez, E. S., Alghazali, H., Griffin, A., and Smith, K. (2016). "Self-consolidating concrete (SCC) and high-volume fly ash concrete (HVFAC) for infrastructure elements: implementation." cmr 16-011, Missouri University of Science and Technology, Rolla, Missouri, Jun. 2016, pp. 725.

Myers, J. J., Volz, J., Sells, E., Porterfield, K., Looney, T., Tucker, B., and Holman, K. (2012). "Self-consolidating concrete (SCC) for infrastructure elements." cmr 13-003_A, Missouri University of Science and Technology, Rolla, Missouri, Aug. 2012, pp. 219.

Naik, T. R., Ramme, B. W., Krauss, R. N., and Siddique, R. (2003). "Long-term performance of high-volume fly ash concrete pavements." ACI Mater J, 100 (2). 150-155.

Ontario Ministry of Transportation and Communications (OMTC). (OMTC). (1983). Ontario Highway Bridge Design Code (2nd Edition), Downsview, ON, Canada.

Ouchi, M., Sada-aki, N., Thomas, O., Hallberg, S.-E., and Myint, L. (2003). "Applications of self-compacting concrete in Japan, Europe and the United States." *ISHPC*, ISHPC, US Federal Highway Administration. Office of Bridge Technology.

Paultre, P., Chaallal, O., and Proulx, J. (1992). "Bridge dynamics and dynamic amplification factors: a review of analytical and experimental findings." Can J Civ Eng, 19 (2). 260-278.

Simulia (2012) Abaqus Analysis User's Manual. Version 6.12. Providence, RI. USA, Dassault Systèmes Simulia Corp.

Stallings, J. M., and Yoo, C. H. (1993). "Tests and ratings of short□span steel bridges." J Struct Eng, doi:10.1061/(ASCE)0733-9445(1993)119:7(2150), 2150-2168.

Transportation Research Board. (TRB). (1998). "Manual for Bridge Rating through Load Testing" *Research Results Digest No. 234*, Washington, D.C.

Volz, J. S., Myers, J. J., Richardson, D. N., Arezoumandi, M., Beckemeier, K., Davis, D., Holman, K., Looney, T., and Tucker, B. (2012). "Design and evaluation of high-volume fly ash (HVFA) concrete mixes." Report cmr 13-008, Missouri University of Science and Technology, Rolla, Missouri, October 2012, pp. 40.

Wang, T. L., and Huang, D. (1992). "Cable stayed bridge vibration due to road surface roughness." Journal of Structural Engineering, doi:10.1061/(ASCE)0733-9445(1992)118:5(1354), 118 (5). 1354-1374.

WsDOT (2009). "Design Memorandum on the Use of SCC in Structural Applications." <http://www.wsdot.wa.gov/eesc/bridge/designmemos/15-2009.htm>. (September 1, 2016).

VITA

Eli Saul Hernandez Ramos received his B.S. in Civil Engineering in May 1996 from Universidad de Los Andes, Mérida, Venezuela. In May 2002, he also received his M.S. in Structural Engineering from Universidad de Los Andes, Venezuela, where he completed his thesis "*Influence of Geometric Non-linearity on the Development of Local Buckling of Steel Frames*".

As a doctoral student Mr. Hernandez acted as a graduate teaching and research assistant at the Missouri University of Science and Technology. During his last year as a doctoral student, he was instructor of the course "Structural Analysis I" of the Civil, Architectural and Environmental Engineering Department at Missouri University of Science and Technology. Mr. Hernandez is associate member of ACI Committee 435 "Deflection of Concrete Building Structures" and ACI Committee 342 "Evaluation of Concrete Bridges and Bridge Elements". He has been a member of the Prestressed Concrete Institute since September 2012, member of the American Concrete Institute since April 2006, and member of the American Society of Civil Engineers since 2005.

Prior work experiences included approximately twelve years of experience as Structural Engineer in Venezuela. Mr. Hernandez worked as an Assistant Professor at the School of Engineering of Universidad de Los Andes, Mérida, Venezuela, for one and half year (2006-08). He also worked as a teaching assistant at the School of Architecture of Universidad of Los Andes during the last year of his undergraduate studies.

Mr. Hernandez received his Ph.D. in Civil Engineering from Missouri University of Science and Technology in May 2018.